AD-A038 413 PENNSYLVANIA STATE UNIV UNIVERSITY PARK IONOSPHERE R--ETC F/G 4/1
STUDY OF D-REGION IONOSPHERE USING RADIO WAVE INTERACTION TECHN--ETC(U)
FEB 77 H S LEE, A J FERRARO N00014-75-C-0178
UNCLASSIFIED PSU-IRL-FR-77/1 NL

1 OF 2
AD A038413

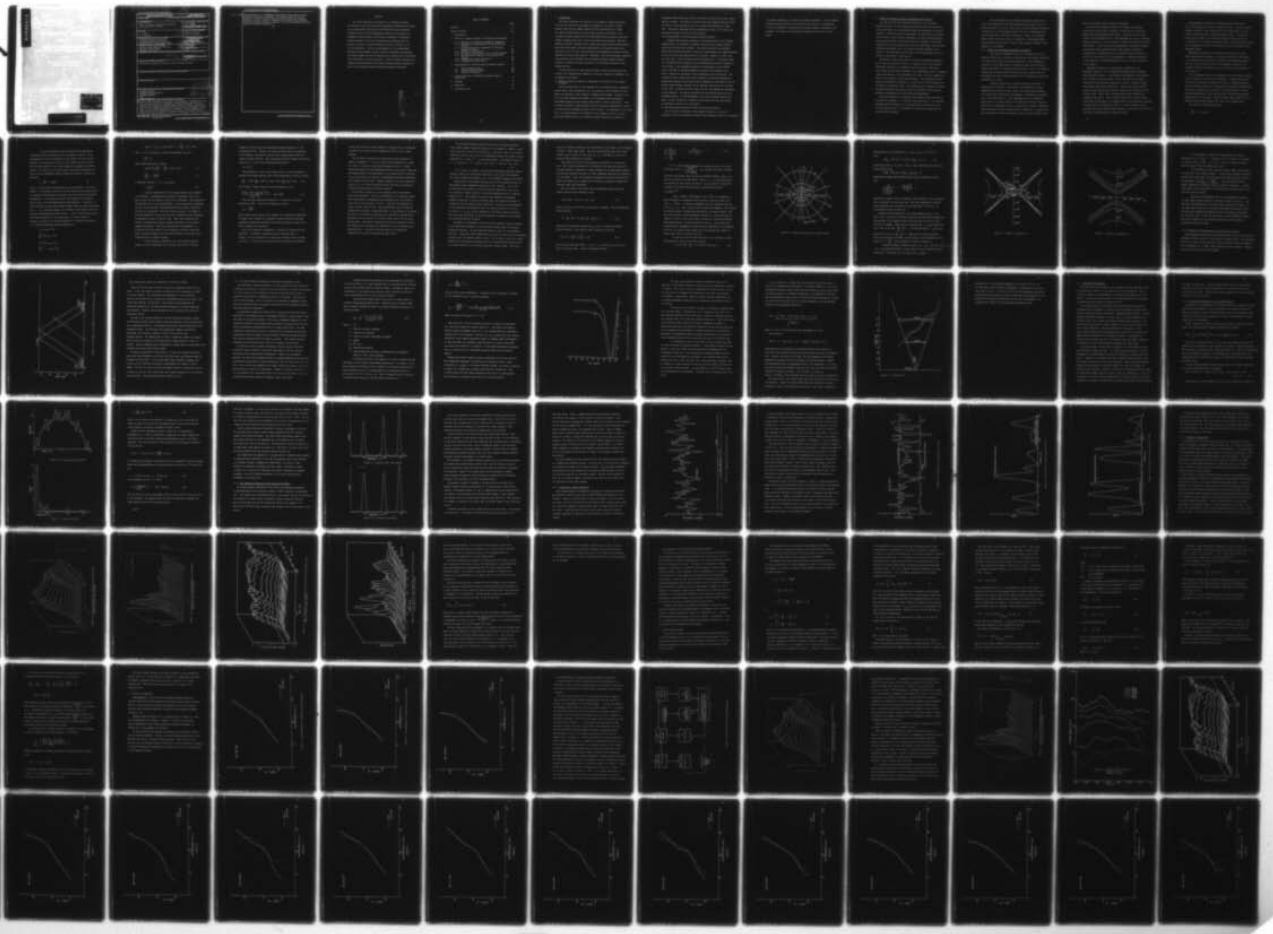

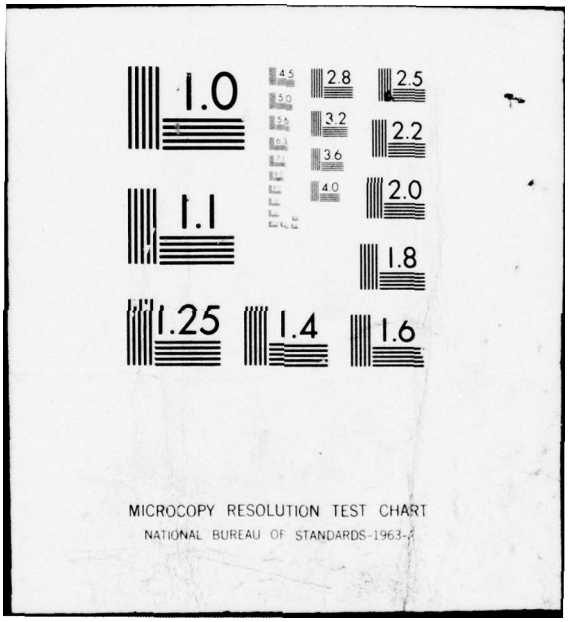
1.0
1.1
1.25
1.4
1.6
1.8
2.0
2.2
2.5
2.8
3.2
3.6
4.0
4.5
5.0
5.6
MICROCOPY RESOLUTION TEST CHART
NATIONAL BUREAU OF STANDARDS-1963-A

The

(14) PSU-IRL-FR-77/1

(10)

SECURITY CLASSIFICATION OF THIS PAGE (When Data Entered)

REPORT DOCUMENTATION PAGE

READ INSTRUCTIONS BEFORE COMPLETING FORM

1. REPORT NUMBER: PSU-IRL-FR-77/1	2. GOVT ACCESSION NO.
3. RECIPIENT'S CATALOG NUMBER	
4. TITLE (and Subtitle): Study of D-Region Ionosphere Using Radio Wave Interaction Technique	5. TYPE OF REPORT & PERIOD COVERED: Final Report. 1 Oct 75-30 Sep 76
6. PERFORMING ORG. REPORT NUMBER	
7. AUTHOR(s): H. S. Lee; A. J. Ferraro	8. CONTRACT OR GRANT NUMBER(s): N00014-75-C-0178
9. PERFORMING ORGANIZATION NAME AND ADDRESS: Ionosphere Research Laboratory, The Pennsylvania State University, University Park, Pennsylvania 16802	10. PROGRAM ELEMENT, PROJECT, TASK AREA & WORK UNIT NUMBERS: 61153N; RR032-08; RR032-08-01; NR089-063
11. CONTROLLING OFFICE NAME AND ADDRESS: Office of Naval Research (Code 461), 800 North Quincy Street, Arlington, VA 22217	12. REPORT DATE: 18 Feb 1977
	13. NUMBER OF PAGES: 102
14. MONITORING AGENCY NAME & ADDRESS (if different from Controlling Office)	15. SECURITY CLASS. (of this report): Unclassified
	15a. DECLASSIFICATION/DOWNGRADING SCHEDULE: N/A

16. DISTRIBUTION STATEMENT (of this Report)

Distribution unlimited; cleared for public release and sale.

17. DISTRIBUTION STATEMENT (of the abstract entered in Block 20, if different from Report)

18. SUPPLEMENTARY NOTES

19. KEY WORDS (Continue on reverse side if necessary and identify by block number)

Atmospheric Waves;
D-Region Electron Density;
Synthesis Methods;
VLF;
Cross-Modulation

20. ABSTRACT (Continue on reverse side if necessary and identify by block number)

This report describes the outcome of an ionospheric D-region study made with the wave interaction experimental technique mainly using the all-digitalized facilities at The Pennsylvania State University. Theoretical basis and the experimental evidence of the presence of atmospheric gravity waves in the D-region ionosphere are presented. Spectral analysis of the wave interaction data indicated that the presence of waves with periods ranging from tens of minutes to few hours are possible. Critical → next page

DD FORM 1 JAN 73 1473 EDITION OF 1 NOV 65 IS OBSOLETE
S/N 0102-014-6601

SECURITY CLASSIFICATION OF THIS PAGE (When Data Entered)

188150

cont →

intercomparison of two independently-developed electron-density profile inversion techniques are presented. The results showed that the two methods led to similar profile indicating their reliability in profile inversion. Finally, temporal variations in D-region electron densities are presented showing diurnal variations as well as the variability between normal and anomalous conditions.

Abstract

This report describes the outcome of an ionospheric D-region study made with the wave interaction experimental technique mainly using the all-digitalized facilities at The Pennsylvania State University. Theoretical basis and the experimental evidence of the presence of atmospheric gravity waves in the D-region ionosphere are presented. Spectral analysis of the wave interaction data indicated that the presence of waves with periods ranging from tens of minutes to few hours are possible. Critical intercomparison of two independently-developed electron-density profile inversion techniques are presented. The results showed that the two methods led to similar profile indicating their reliability in profile inversion. Finally, temporal variations in D-region electron densities are presented showing diurnal variations as well as the variability between normal and anomalous conditions.

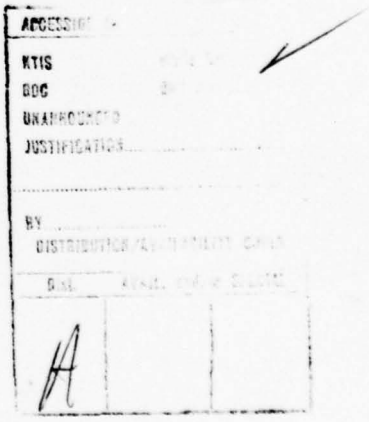

TABLE OF CONTENTS

1. Introduction

This report describes the outcome of an ionospheric D-region study made with the wave interaction experimental technique for the Office of Naval Research under Contract Number N00014-75-C-0178, Modification No. P00001. The research program used in part the wave interaction facilities of the Ionosphere Research Laboratory at The Pennsylvania State University which have reached a sophisticated level of data procurement and processing. Data were digitally recorded on magnetic tape covering 28 D-region heights simultaneously every 300 milliseconds; continuous measurements were frequently made over a time span of over 10 hours, with additional daily sampling of D-region electron densities at shorter time intervals. Matching to this data procurement capability is an elaborate and diversified data processing high-speed computer program tailored to individual research objectives to be described in detail in subsequent sections.

The main objectives of this research program, which have been carried out relying on the sophisticated capability of the wave interaction experiment, can be summarized as follows:

(a) Effects of Dynamic Processes of Atmospheric Wave Motions in the D-Region Ionosphere -

Various perturbations in the ionosphere due to infrasonic waves, atmospheric gravity waves, tidal oscillations, etc. can account for the variability in the phase and amplitude of radio signals in communication systems. In spite of the fact that these phenomena are present in the ionosphere most experimental measurements neglected these effects being unable to detect such effects. With the high resolution in time and height the wave interaction experiment is capable of identifying the atmospheric waves in the D-region. Such knowledge not only will add to the understanding of the dynamics of the D-region, but also to better model the chemistry since it is needed in properly removing the influence of

atmospheric waves from data in order to correctly account for the solar control upon the D-region. The effects of gravity waves were observed using Penn State facilities at State College as well as at Arecibo NAIC Observatory, Puerto Rico. Theoretical background and the experimental results on the subject are described in detail in Section 2 of this report.

(b) Intercomparison of Electron Density Synthesis Methods -

A reliable data reduction technique is an essential part of this research program since it is desirable to produce accurate electron density profiles from wave interaction data profiles. The profile inversion (or synthesis) method which IRL has been using is based on an overdeterministic scheme developed by Dale in 1973 and has been proven to be reliable. However, in view of the fact that another profile inversion method developed by C. H. Shellman at NELC for processing VLF data happened to have considerable similarities compared to that of Dale, it was considered important to intercompare the two methods jointly with NELC to determine whether the methods could complement each other to improve the reliability of the synthesized electron densities. This cooperative effort started with initial exchange of technical informations, studying and testing of each others method independently, and wound up with two parties closely working together with Mr. Shellman visiting IRL for two weeks in June 1976. In spite of the fact that there are some fundamental differences in their approach, the results produced by the two methods were found to be strikingly similar. It was satisfying to find the two methods confirm each other in their reliability. Details of these methods and the test results are described in Section 3 of this report.

(c) Continued Routine Operation of Wave Interaction Facilities -

One of the major objectives of this research program is to take full advantage of IRL's all digitalized sophisticated experimental facility to determine

its ultimate capability in studying the D-region ionosphere. For this purpose continued routine operation of the facility was conducted to determine and to show its capability in observing and resolving temporal variations of the D-region. The results of this effort are described in Section 4 of this report.

2. Effects of Dynamic Processes of Atmospheric Wave Motions

For some years the Wave Interaction Facility of the Ionosphere Research Laboratory at The Pennsylvania State University has been used to study the D-region of the ionosphere through the measurement of electron densities. During this period, improvements have been made in the experimental facility, data collection techniques, and data processing methods. As the resolving power of the whole system has increased, it has become apparent that certain fluctuations in the data, which might once have been considered undesirable noise, are caused by dynamic processes in the D-region. Those processes, and how they may be studied using wave interaction are the subject of this section.

Specifically, this section shows how the wave interaction experiment may be used in the study of gravity, or buoyancy, waves in the D-region . These waves, believed to be generated near the surface of the Earth, carry energy into the upper atmosphere, and, surprisingly, what is considered a small perturbation in the troposphere, will grow and have a significant effect on the dynamics of the upper atmosphere. This characteristic and others are discussed in subsection 2.1, which gives a brief discussion of the theory of atmospheric waves. This subsection also considers the means by which atmospheric fluctuations result in detectable electron density variations as measured by the wave interaction experiment.

The second subsection 2.2 describes the methods by which the data is collected and processed. It is divided into three parts: 2.2.1 discusses appropriateness of methods, 2.2.2 discusses Fourier analysis as a tool for data analysis, and 2.2.3 describes the interactive program used for data analysis and display.

The third subsection 2.3 presents preliminary results found by the means described in the second subsection and relates them to the theory discussed in the first. The need for further additional techniques to reveal more of the information held by the data is demonstrated and some on-going work in this area is described. Finally, the knowledge gained in this research is used in a discussion of improvements which could be made in the facility to obtain a more complete knowledge of the dynamics of the D-region.

2.1.1 Theory of Low Frequency Atmospheric Propagation

The theory of atmospheric waves is an application of fluid mechanics, which has its basis in the derivation of microscopic properties of a medium which should be treated statistically. The atmosphere is composed of a very large number of molecules so that for all practical purposes the physics of individual particle motion leads to a statistical descriptions of overall behavior which is so nearly accurate that the statistical base may be dropped leaving a set of governing laws which are deterministic in nature.

Molecular motion may be classed according to the degree of organization or coherence. Wave motion in the atmosphere is a very organized kind of motion in that certain vector quantities describing wave motion may be predictable over hundreds, or thousands of kilometers. Heat, on the other hand, is a very disorganized form of atmospheric motion since it is random motion of the individual molecules and may be described on a macroscopic level by a single scalar variable, temperature. Then turbulence is a form of motion which is organized to a lesser degree than wave motion but more so than heat, since it may be described as the

more or less random motion of groups of molecules.

One reason why atmospheric waves are of interest is that they carry energy from one place to another, and they may do it much more rapidly than random thermal motion (heat). Energy may be also transferred from an organized form to a less organized one, that is, waves may generate turbulence, or heat, perhaps in a region far from where the wave was generated. Since the waves are represented by variables of average motions rather than individual motion, this transfer of energy is represented by a dissipation term in the equation of motion much as it would be in the equations for a sliding mass. In general, dissipation is very difficult to model mathematically and it is usually ignored if at all possible.

Mathematical modeling of the macroscopic properties of the atmosphere leads to a set of differential equations which in general have wave-like solutions. The variables and parameters in the equations may be divided into three classes: first, those which are directly derived from the microscopic properties of the gas: pressure, density, heat capacity and thermal conductivity. Second, those which describe external forces acting upon the gas as a whole, such as gravity and the Coriolis force. Third, those variables which directly describe the response of the medium. This is usually taken to be a velocity vector which gives the macroscopic or average velocity of the medium as a function of three position coordinates and time. It is also possible to use a position vector which describes the location of a particular bit of air as a function of time referred to an initial location.

The mathematical description of atmospheric waves involves the use of three equations: motion, continuity and state. Certain intuitive arguments leading to these equations will be discussed here; for more rigorous derivations refer to Gossard and Hooke (1975). The approach adopted here is known as the Eulerian in which the motion of the air is described by its velocity as indicated above. An equivalent description can be formulated in terms of the position vector; this is known as the Lagrangian system.

The equation of motion is a variation on the usual force equals mass times acceleration equation. The mass is replaced by the density, ρ, and obviously the force must be replaced by the appropriate quantity. The force per unit area on a wall in the atmosphere is given by the difference between the pressures on the two sides or by the gradient of the pressure, p.

The two external forces on the atmosphere are the vertically directed force of gravity and the Coriolis acceleration. Actually the rotation of the earth introduces two effects; the first is a latitude dependent upward acceleration which may be allowed for by adopting a modified value for $\vec{g}$, the acceleration due to gravity. The second effect is a force directed perpendicular to both the direction of motion and the angular momentum vector of the earth. The latter effect may be ignored for the waves with periods much shorter than a day to be considered here.

The equation of motion then becomes:

$$\rho \frac{\partial \vec{U}}{\partial t} = \rho \vec{g} - \text{grad } p \qquad 2.1$$

For static conditions, $\vec{U} = 0$, the equation becomes

$$\rho_0 g_0 = \frac{\partial p}{\partial z} \qquad 2.2$$

where the subscript zero indicates static unperturbed conditions, and z is the vertical coordinate. Elementary gas lows show that the density and pressure are proportional for steady conditions. The relationship may be stated as $p_0 = C^2/\gamma p_0$, where C is the speed of sound, about 300 m/sec, and γ is the ratio of constant pressure specific heat to constant volume specific heat. Substitutions and solution of the first order differential equation shows that both ρ_0 and p_0 are proportional to exp $(-\gamma gz/C^2)$. $C^2/\gamma g$ is defined as H, known as the 'scale height'.

The exact differential equations which results from the equations being considered is difficult to solve. Thus perturbations causing wave motions are assumed small, and the perturbed value is set equal to the static value plus a perturbation. This is substituted into the appropriate equation and only terms up to the first order are kept. Thus Equation 2.1 becomes

$$\rho_0 \frac{\partial \vec{U}}{\partial t} = \rho \vec{g} - \text{grad } p \qquad 2.3$$

where ρ and p are the perturbed values.

The continuity equation is an expression of the conservation of matter and thus relates the partial derivitive with respect to time of the density to the causes of density variation. First, if the density function has spatial changes, that is, a non-zero gradient, then velocity of the medium will cause a net transport of matter to or from any given location in space. Also if the velocity at a particular point has divergence then

there is a net accumulation or depletion of matter at this point. The equation, including only first order perturbation as described above is:

$$\frac{\partial \rho}{\partial t} + \vec{U} \cdot \text{grad } \rho_0 + \rho_0 \text{ div } \vec{U} = 0 \qquad 2.4$$

In the derivation above of the relationship between unperturbed density and pressure, thermal equilibrium was assumed. For wave-like perturbations, the pressure and density changes generally flow faster than heat, requiring a relationship which is obtained when there is no heat flow (adiabatic). Some simple thermodynamics (Gossard and Hooke, 1975) yields the relationship $\frac{dp}{dt} = C^2 \frac{d\rho}{dt}$. For the total derivative, we may substitute the partial derivative plus the term resulting from a non-zero gradient. Dropping the appropriate terms, to give first order perturbation only, gives

$$\frac{\partial p}{\partial t} + \vec{U} \cdot \text{grad } p_0 = C^2 \left[\partial \rho / \partial t + \vec{U} \cdot \text{grad } \rho_0 \right] \qquad 2.5$$

By algebraic manipulation of the three basic Equations 2.3 through 2.5, they may be modified to give a form for which a wave solution may be found. It is helpful, however, to first look at some of the simple motions possible in such a medium, and it is especially useful to look at what happens if some of the terms are ignored.

Consider a medium which has the unperturbed density and pressure variations of the atmosphere, but is composed of an incompressible fluid. Suppose a volume element of this fluid is given a downward initial velocity. This element, with density ρ_{01}, encounters an upward restoring force approximately proportional to its displacement since it moves into a region of increasing density. This causes the element to move back up and experiences oscillation about its initial position.

To find the frequency of this oscillation, the appropriate relationship must be substituted into the equation of motion. In an incompressible fluid, the divergence of the velocity is zero, and the gradient of the pressure is due only to two causes, the gravitational force and the movement of the volume element into regions of different density. The first of the two must cancel the $\rho\vec{g}$ term in Equation 2.3; this is how the exponential height variation was derived. Thus we are left with

$$\rho_o \frac{\partial \vec{U}}{\partial t} = -\text{grad } p' \qquad 2.6$$

where p' is the pressure perturbation due to the movement of the volume element. If the element always has the same density as the medium around it, equilibrium would never be disturbed, and there would be no pressure perturbation. If the density were zero, the pressure on the element would be due to the full unperturbed pressure gradient. In general, it will be given by the fractional density change times the pressure gradient, that is, the restoring pressure will increase as the element moves into regions of increasingly different density. Thus for small displacements, the pressure gradient per unit displacement on a volume element at altitude z is given by the density gradient at z divided by the density at z times the unperturbed pressure gradient at z.

$$\rho_o = A \exp ({}^{z}/H)$$

$$\frac{\partial \rho_o}{\partial z} = \frac{A}{H} \exp ({}^{z}/H)$$

$$p_o = \frac{C^2}{\gamma} A \exp ({}^{-z}/H)$$

$$\frac{\partial p_o}{\partial z} = \cdot A \exp ({}^{-z}/H)$$

$$\text{grad } p' = -\frac{1}{H}\, g\, A \exp(-z/H)\, z' = -\frac{g^2\gamma}{C^2}\, A \exp(-z/H) \cdot z$$

when z is the coordinate of vertical displacement such that

$$\frac{\partial z}{\partial t} = \vec{U}_z$$

Then, substituting into 2.6 gives

$$A \exp(-z/H) \frac{\partial^2 z'}{\partial t^2} = \frac{g^2\gamma}{C^2} A \exp(-z/H)\, z' \qquad 2.7$$

$$\frac{\partial^2 z'}{\partial t^2} = -\frac{g^2 \gamma z'}{C^2} \qquad 2.8$$

A sinusoidal solution $z' = B \sin \omega t$ gives

$$\omega = \frac{g\sqrt{\gamma}}{C} \qquad 2.9$$

Allowing compressibility in the medium modifies the frequency of oscillation. We assume that the process is adiabatic, that is, no heat is lost from the element of air as it is compressed. This simplifies the analysis and is a good approximation. If the process were isothermal, that is, heat flowed until thermal equilibrium was reached, then there would be no oscillations. We can see this by imagining an element of air moved downward so slowly that the rise in temperature from compression is negligible as heat is conducted away. Under these conditions the product of pressure and volume is constant and thus so is the ratio of pressure and density. Since the energy gained from compression is conducted away as heat there is none available to develop a restoring force; the volume element of air is always identical to and thus interchangeable with its ambient elements.

For the adiabatic compression case, the perturbed pressure gradient per unit displacement will be given by the ratio of density

gradient to density times the unperturbed pressure gradient as in the incompressible case. However, the density gradient must now be modified by the adiabatic compression received as the volume element moves into regions of higher pressure. When considering adiabatic changes from initial conditions p, ρ, and T the relationship which holds is

$$dp = C^2 \, d\rho$$

The application of this is very simple since it is only necessary to decrease the pressure gradient used in the incompressible case by an amount

$$\frac{d\rho}{dz} = (1/C^2) \frac{dp}{dz} = (1/C^2) \, g \, A \exp(-z/H) = \frac{1}{H\gamma} A \exp(-z/H) \qquad 2.10$$

The fractional density change per unit displacement is then

$$\frac{\frac{A}{H} \exp(-z/H) - \frac{A}{H\gamma} (\exp -z/H)}{A \exp(-z/H)} = (1/H)\left(\frac{\gamma-1}{\gamma}\right) \qquad 2.11$$

Thus the right hand side of Equation 2.7, and also 2.8, must be multiplied by $\frac{\gamma-1}{\gamma}$. Thus for the frequency we obtain

$$\omega_B = \frac{\sqrt{\gamma-1}\, g}{C} \qquad 2.12$$

This is known as the Vaisala-Brunt frequency (for temperature independent of height) and it appears as a parameter in most equations describing atmospheric motion when the density and pressure gradients caused by the force of gravity are considered.

That this frequency is independent of pressure and density may seem remarkable. It should be recognized that any resonance may be thought of as the interaction of a spring-like restoring force and mass or inertia. In this case, the physical forces governing the variations

in one, also control the other, leading to resonance which is independent of height to the extent that the temperature (hence C) and g remain constant.

The oscillation described here represents the free response of a small bit atmosphere. It is not a form of wave propagation, but might be a part of a process in which wave propagation occurs. If there exists some source of random atmospheric motion in the vertical direction, the maximum velocity and displacement in the response would be expected at ω_B if the energy of the source is approximately uniformly distributed with frequency in that range. However, whether or not wave propagation occurs at ω_B, or at other frequencies may be most easily determined by solving the three equations for wave solutions.

The equation of motion is a vector equation and thus represents three scalar equations. This may be simplified to two equations without loss of generality by assuming the wave propagation in the horizontal occurs only in one direction, say the x. The other two equations are scalar, giving a total of four. Some simplification may be gained by assuming zero divergence (incompressibility) in the equation of continuity. The loss of the spring-like restoring force provided by compressibility eliminates from the solution all acoustic waves, but not the so-called gravity waves. This would be expected from the above analysis in which the buoyancy force was shown to be modified by, but not dependent upon, compressibility. A solution for gravity waves in the absence of compressibility is given in Gossard and Hooke (1975).

For the scalar equations derived from the three original equations, Hines (1960) assumed a wave-like solution for the pressure p, density ρ, horizontal velocity U_x and vertical velocity U_z. Note that p and ρ are perturbed quantities, while p_0 and ρ_0 are the corresponding steady state values, and the quantities $(p - p_0)$ and $(\rho - \rho_0)$ are perturbations. The assumed solution is

$$P \cdot (p - p_0)/p_0 = R \cdot (\rho - \rho_0)/\rho_0 = U_x/X = U_z/Z = A \exp i(\omega t - k_x x - K_z z) \qquad 2.13$$

P, R, X and Z are complex, and give the relationships among the several variables, while A is an arbitrary amplitude, K_x and K_z are the horizontal and vertical complex wave numbers, and ω is the angular frequency of the wave.

Substitution of the assumed solution into the four equations yields four simultaneous linear homogeneous equations of four variables. It may then be shown that the solution is valid only when the quantities ω, K_x, and K_z are related in a manner which may be described mathematically by a quadratic equation of ω^2. This equation is known as the dispersion relationship; properly interpreted, it gives information about the possible directions of propagation, and the phase and group velocities. Given that the requirements of the dispersion relationship are met, the solution yields P, R, X, and Z in terms of ω, K_x, K_z, and the parameters in the three originial equations. These equations, which give the relative magnitude and phase of the variables are called polarization relations.

The absence of dissipation terms in the basic equations, and the constancy of the unperturbed variables in the horizontal direction make the following assumption plausible: the wave amplitude suffers no decay in the horizontal direction. Thus Hines (1960) assumed that K_x is real and found that the dispersion relation gives two possible classes of waves. One of these is that K_z is purely imaginary and thus energy propagates only in the horizontal direction and there is no phase variation in the vertical direction (surface waves). This class

was not of interest to Hines at the time although it does exist in the ionosphere (Valverde , 1958, Thome, 1968). The other mode describes those waves called internal gravity waves; for this class $K_z = k_z + i/2H$ where k_z is real, and vertical phase propagation is allowed.

This implies that the vertical amplitude is growing at an exponential rate. Thus a small perturbation at the surface of the earth may grow until at high altitudes it represents a large percentage of the unperturbed pressure. The equations presented here will no longer adequately describe the propagation for two reasons: first, the linearizing assumptions by which the higher order terms were dropped are no longer valid, and second, dissipation becomes very important under these conditions.

Since all waves in this class have the exponential growth factor the assumed solution may be modified to read

$$A \exp (z/2H) \cdot \exp i(\omega t - k_x x - k_z z) \qquad 2\text{-}14$$

where k_x and k_z are both real for this class of solution. Thus the dispersion relation becomes

$$(\omega^2 - \omega_a^2)\, \omega^2/C^2 - \omega^2\, (k_x^2 + k_z^2) + \omega_B^2\, k_x^2 = 0 \qquad 2\text{-}15$$

where ω_B has already been defined and $\omega_a = \gamma g/2C$ is called the acoustic cuttoff frequency. This equation may be rewritten in the form

$$k_z^2 = (\omega^2 - \omega_a^2)/C^2 + \left(\frac{\omega_B^2}{\omega^2} - 1\right) k_x^2 \qquad 2\text{-}16$$

which clearly shows that either $\omega < \omega_B$, or $\omega > \omega_a$, since both k_x and k_z are real for internal waves. Further rearrangement yields:

$$\frac{\dfrac{k_x^2}{(\omega^2 - \omega_a^2)/C^2}}{\left(1 - \dfrac{\omega_B^2}{\omega^2}\right)} + \frac{k_z^2}{(\omega^2 - \omega_a^2)/C^2} = 1 \qquad 2\text{-}17$$

If $\omega > \omega_a$ this equation describes an ellipse centered at the origin with major axis $a = 2\sqrt{\dfrac{(\omega^2-\omega_a^2)}{C^2(1-\omega_B^2/\omega_a^2)}}$. As ω becomes very large, the major and minor axis becomes equal, and the relationship between k_x and k_z is a circle, as expected for sound waves. When $\omega_B < \omega < \omega_a$, the equation does not describe any real figure, but when $\omega < \omega_B$, the result is a hyperbola centered at the origin with the slope of the asymtotes given by

$\pm (1-\omega_B^2/\omega^2)^{-1/2}$.

The k_x versus k_z relationship, with $T = \frac{2\pi}{\omega}$ as a parameter, is shown in Figure 2.1; parameters from the middle D-region are used (ω_B = .016, ω_a = .0195). It should be remembered that this represents the case $K_x = k_x$, $K_z = k_z + i/2H$, and that other solutions are possible. The ellipses are acoustic waves; the hyperbolas are gravity, or buoyancy, waves. Note that the direction of phase propagation is given by a line drawn from the origin to a point on one of the curves, and that for long period buoyancy waves this direction is almost constant for any k_z. This implies that the direction of propagation is almost entirely determined by the frequency, and also it is clear from the figure that the horizontal wave number is almost fixed, while the vertical may vary.

In order to look for other solutions, it is convenient to begin with Hines (1960) original dispersion equation.

$$\omega^4 - \omega^2 C^2 (K_x^2 - K_z^2) + (\gamma-1) g^2 K_x^2 + i\gamma g\omega^2 K_z = 0. \qquad 2.18$$

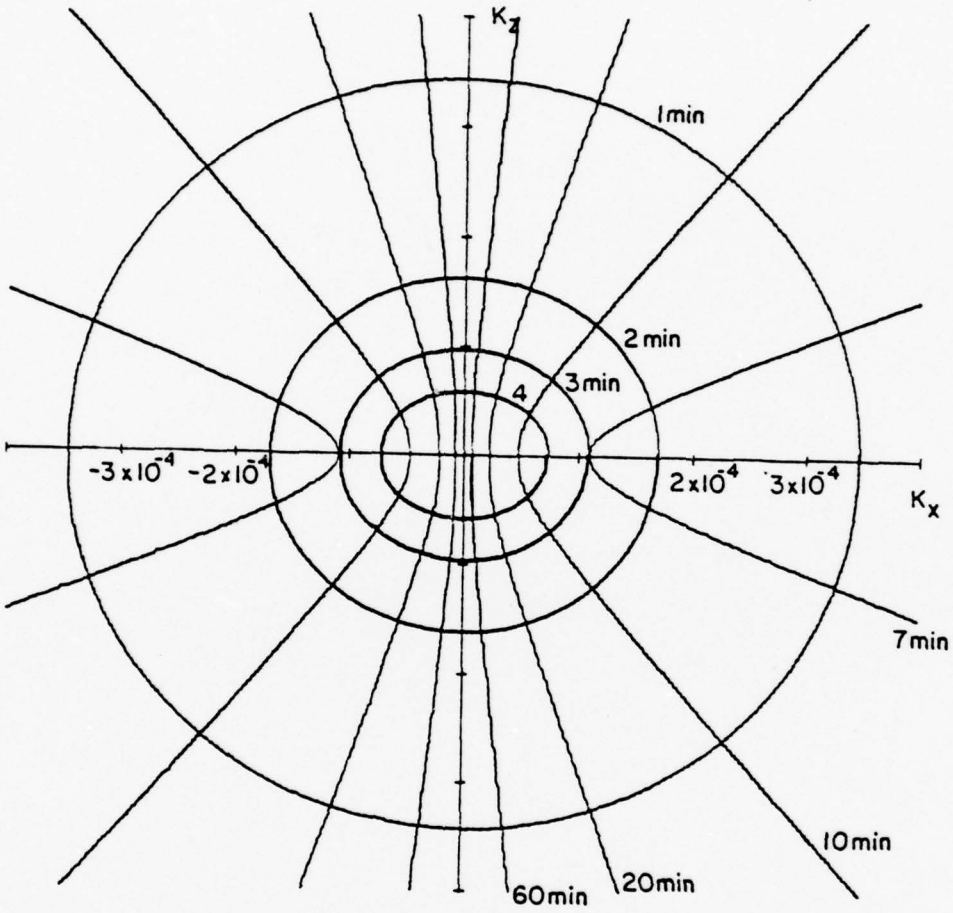

Figure 2.1 K-space for acoustic and buoyancy waves

Substituting in the relationships $\omega_a = \gamma g/2C$, and $\omega_B = (\gamma-1)^{1/2}\, g/C$ gives

$$(C^2\omega_B^2 - \omega^2C^2)\, K_x^2 - \omega^2\, C^2\, K_z^2 + i2C\omega_a^2 \quad K_z = -\omega^4 \qquad 2.19$$

Consider the case $K_x = k_x$ (real), and $K_z = im_z$; substituting this into the above equation gives

$$(C^2\omega_B^2 - \omega^2C^2)\, k_x^2 + \omega^2C^2m_z^2 - 2C\omega_a\omega^2m_z = -\omega^4$$

Completing the square and dividing through puts this equation in conic form:

$$\frac{k_x^2}{\dfrac{(\omega^2-\omega_a^2)/C^2}{(1-\omega_B^2/\omega_a^2)}} - \frac{(m_z-\omega_a/C)^2}{(\omega^2-\omega_a^2)/C^2} = 1$$

Note that for large ω this is a hyperbola, and for small ω it is an ellipse, just the opposite as in the last case. This case represents no vertical phase propagation and the waves are called Lamp waves, and the $k_x - k_z$ relationship is shown in Figure 2.2.

Consider next the possibility of K_x being imaginary, say $K_x = im_x$. Then, if $K_z = k_z - i/2H$ as for internal waves the only difference between this case and that of the internal waves is that the sign in front of the m_x^2 term will be changed. There will be no solution for $\omega < \omega_B$ since there can be no conic of the form $-\frac{x^2}{a^2} - \frac{y^2}{b^2} = 1$. On the other hand $\omega > \omega_a$ will give hyperbola of the form $-\frac{x^2}{a^2} + \frac{y}{b^2} = 1$. There will be vertical hyperbola rather than horizontal as before, and the slopes of the asymototes will be given by $\pm\,(1 - \frac{\omega_B^2}{\omega^2})$. This relationship is shown in Figure 2.3.

Finally, consider K_x complex, say $K_x = L_x + i\, M_x$. Since $K_x^2 = L_x^2 + 2i\, L_x\, M_x - M_x^2$ no relationship between K_x and K_z with only real coefficients may be established. Thus there can be no waves with K_x complex.

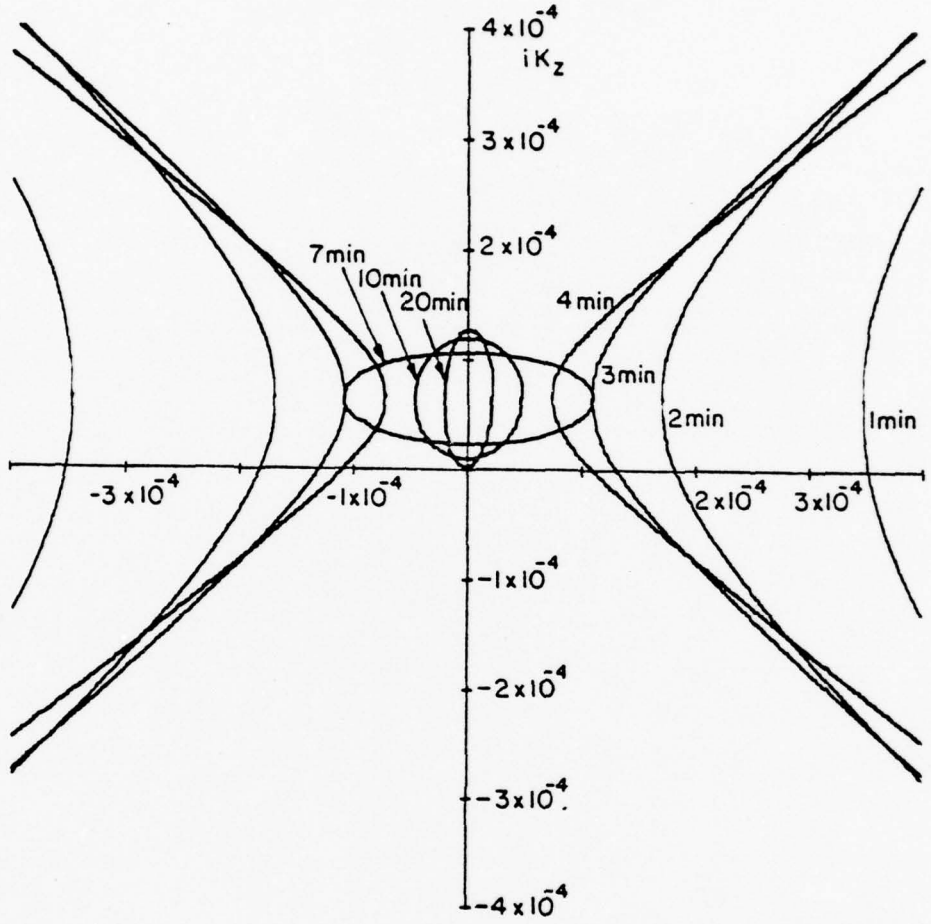

Figure 2.2 K-space for imaginary K_z

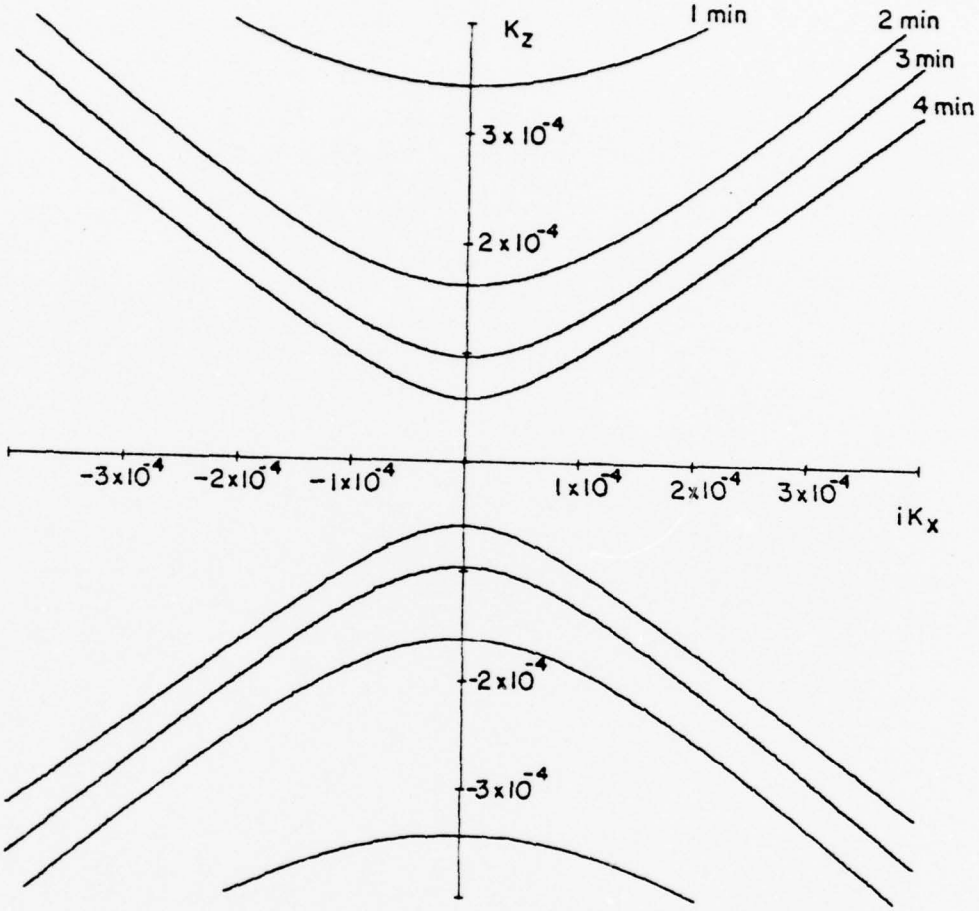

Figure 2.3 K-space for imaginary K_x

It is convenient to think of the medium having an index of refraction of one if $\omega/k = C$. In general, $\omega/k = C\,n$, where n is the index of refraction and $n_x = \frac{k_x C}{\omega}$, $n_z = k_z\, C/\omega$. Figure 2.4 shows the gravity wave and acoustic wave relationship for n_x-n_z.

For the internal gravity waves and acoustic waves, the direction of energy flow is not readily apparent. From the wave propagation theory it is known that it must be in the direction of the group velocity, which has the components $\left[\partial\omega/\partial k_x\right]_{k_x}$ and $\left[\frac{\partial\omega}{\partial k_z}\right]_{k_x}$. Thus the direction may be roughly determined by looking at the k_x-k_z curves of constant T. As Hines (1960) shows, this is equivalent to the direction of a normal drawn to the curve away from the origin.

The effect of dissipation will not be discussed here except to say that higher frequency waves are effected the most by viscosity. Thus very short wavelengths will be absorbed before reaching the D-region. On the other hand, waves with long vertical wavelength (low frequency) will be reflected by temperature gradients unless the horizontal wavelengths are also quite long. As will be shown later, the wave interaction experiment is not sensitive to the vertical structure of a wave unless the horizontal structure is large.

2.1.2 Description of Experimental and Data-Collecting Facility

The experimental and data-collecting facility used for the wave interaction experiment has been described in some detail by Swanson (1976). The description here will be brief, covering the basic method by means of which simultaneous data is generated over a height range covering the entire D-region. Sampling rate and data accuracy are also discussed.

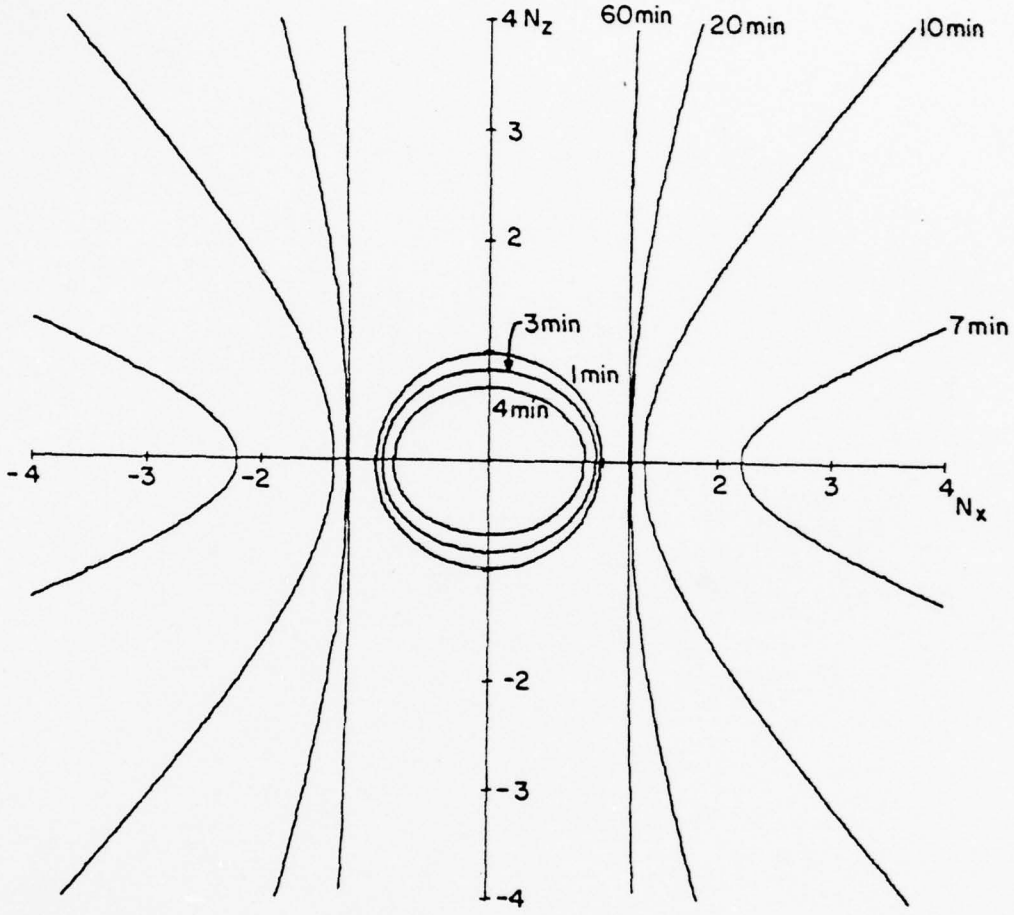

Figure 2.4 N-space for acoustic and buoyancy waves

Figure 2.5 shows the time versus height relationship for a conceptual version of the experiment involving two very narrow transmitted pulses, the W(wanted) and the D (disturbing). The W is relatively low power (5 kw peak, 2.4 MHz) and is transmitted at a rate of about 300/sec, while the D is about 11 MW ERP (4.55 MHz) and is transmitted at one-half the rate of W pulse. The W pulse reflects from the E-layer and meets the up-going D pulse at a height h_i which depends upon the relative time delay between the two pulses. The set of pulses (W_i) is a set of successively delayed W pulses, which meet the D pulse at successively higher h_i.

The experiment may be thought of as transmitting the set (W_i), followed by the D pulse, and then receiving the series of echos from the set (W_i). The amplitude of each of the W pulses is measured, and then the sequence is begun again, only this time after transmitting the set (W_i), no D pulse is transmitted. The amplitudes are measured for this undisturbed cycle and compared with those measured during the last cycle. Cycles continue to alternate in this manner, and the comparison between the two cycles is made in a device known as the wave interaction detector, which gives an average value of amplitude differences between cycles. Data is taken at 28 heights, requiring 28 detectors, followed by some method of storing the data.

The actual experiment differs somewhat from the above simplified description. Let each member of (W_i) be one kilometer wide with one kilometer spacing, thus creating a single wide rf pulse. This is what is actually transmitted and known as the W-pulse. The received echo is divided into the proper sections in the receiving equipment. In practice, h_i is determined from the delay between the D pulse and the leading edge of the R pulse, which is used to gate the returning echo. The W pulse is made somewhat wider than the absolute minimum (which is the width of the R pulse),

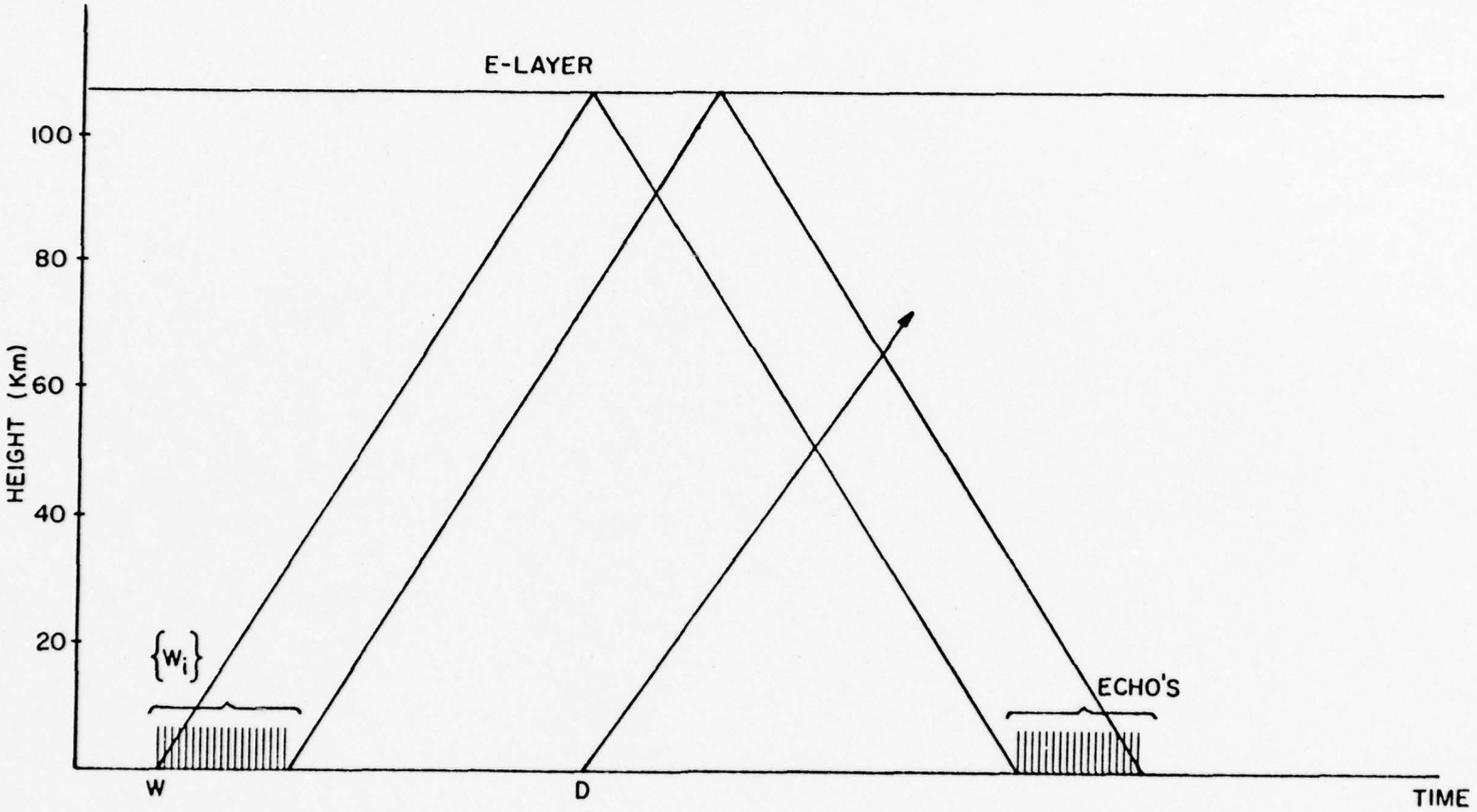

Figure 2.5 Time-height relationship for wave interaction experiment

thus allowing some leeway for variations in reflection height.

There are two more ways in which the practical experiment varies from the ideal. First, the D pulse is finite in width and is not rectangular in shape, but cosine squared. This complicates the mathematics of data reduction. Second, the received echo is divided into overlapping sections wider than 1 km, rather than distinct 1 km sections. This results in some smoothing and eliminates saturation in the wave interaction detectors, but also complicates data analysis. However, these variations are all accounted for in the wave interaction theory.

The data to be recorded consists of 28 wave interaction detector outputs, an AGC output (Automatic Gain Control; gives the amplitude of the received echo), and a signal derived from the D-transmitter monitoring circuitry which gives the transmitted power. The 30 signals are sequentially sampled, digitilized, serialized, and recorded on magnetic tape as a first step in the analysis process. The sampling rate is about 3 samples per channel per second, while the data is filtered at 20 db/decade with a time constant of about 10 seconds. Thus the sampling rate is sufficient to obtain highly accurate data since aliasing errors will be very small indeed.

The data is digitized to a resolution of one part per thousand full-scale. Since data values generally run no more than half scale, the resolution must be decreased by this factor. On the other hand, means obtained by summing many points will have resolution increased by approximately the number of points summed. This will be true as long as the sampled signal is sufficiently varying in nature so that the least significant digit changes frequently in the shortest observed period. This condition has been observed to hold.

2.1.3 The Wave Interaction Experiment for Detecting Atmospheric Waves

The experimental system described in the last subsection allows continuous recording of data which is related to electron densities, and their fluctuations. It is the purpose of this subsection to show that this data may be used to determine the existence of atmospheric waves in the D-region. There are two parts to this problem: first, the effect of the passage of atmospheric waves upon the electron density, and second, the detection of this effect by means of the wave interaction experiment.

As explained in Gossard and Hooke (1975), electrons move with the neutral particles in the D-region since the atmospheric density is great enough so that the region is collision dominated. This gives a tremendous simplicity to any analysis as compared to the plasma physics required in regions above, but also adds one significant complicating factor for longer period waves. The time constants for generation and decay of electrons in the D-region are such that longer period waves may modify the photo-chemical reactions, having an effect upon electron densities which is unknown at present. This problem is quite complicated in theoretical nature, and will be ignored in this report.

In principle, electron density fluctuation could be detected from wave interaction data by reducing a sufficient time period of data to electron densities and then searching for fluctuations. However, for preliminary analysis, the data values themselves serve the purpose adequately since they are approximately proportional to electron densities with the restriction that the data in its raw form does somewhat limit height resolution because of the finite pulse widths and nature of the experiment. However, the height resolution is not irretrievably lost, and methods which allow its recovery without the use of a complicated synthesis program are presently under development.

Although the wave interaction data are approximately proportional to electron density, it is also dependent upon the electron-neutral collision frequency which depends upon the neutral pressure. Atmospheric waves cause perturbations in the pressure and thus will cause variations in the data values through modification of the collision frequency.

The approximate significance of this effect can more readily be evaluated using Appleton-Hartee theory. Equation 2-36a of Weisbrod (1964) gives a quantity showing the effect of collision frequency variations at a particular height

$$T_{hA} = \frac{A}{h^2} \frac{\left[Z \ (1 \pm Y_L)^2 - Z^2\right]}{\left[(1 \pm Y_L)^2 + Z^2\right]^2} \qquad 2\text{-}20$$

where $Z = \frac{\nu}{\omega}$

ν = electron collision frequency

ω = angular wave frequency

A = constant virtually independent of height

h = height

$Y_L = \frac{\omega_H}{\omega} \cos \theta$

ω_H = angular gyrofrequency

θ = angle between the direction of propagation and the magnetic field ($\theta \approx 19^o$ at State College).

To evaluate this effect, and compare it to that of electron density variations, we must define an experimental sensitivity. For example, if the wave interaction coefficient $T(h_i)$ is assumed to be linearly proportional to electron densities since it is approximately so as mentioned earlier, it can be given by $T^*(h) = K(h) N_e(h)$. Then an acceptable form of definition of relative sensitivity S_N to electron density variations is

$$S_N = \frac{\frac{\delta T^*}{\delta N_e}}{T^*(h)} \cdot N_e = 1$$

giving a direct linear dependency. If similar form of definition is adopted for the sensitivity due to collision frequency

$$S_Z = \frac{\frac{\delta T_{hA}}{\delta Z} \cdot Z}{T_{hA}} = \frac{D - 3Z^2 - (D - Z^2)\, 4X^2/(D + Z^2)}{(D - Z^2)} \qquad 2\text{-}21$$

based on equation 2-20 where $D = (1 \pm Y_L)^2$

This turns out to be not as simple as S_N and it needs to be calculated as a function of height for typical values of ν. The results are shown in Figure 2.6 using an examplary value of D = .61, showing that S_Z is reasonably constant down to 65 kilometers. Defining $S_T = S_Z + S_N$ gives the total relative sensitivity, which remains reasonably useful to somewhat under 65 kilometers. At lower altitudes, the extremely large variation of S_T with h would make the results very difficult to interpret. As the quasi-longitudinal approximation is in effect here, the Sen-Wyller equations would give very similar results.

Another factor which requires careful consideration is the fact that the wave interaction experiment is affected by two classes of noise: first, interfering r.f. signals on the wanted frequency channel, and second, variations in wanted echo strength due to causes other than wave interaction. Both of these sources can have random components which have to be distinguished from variations in alternate pulse area due to wave interaction.

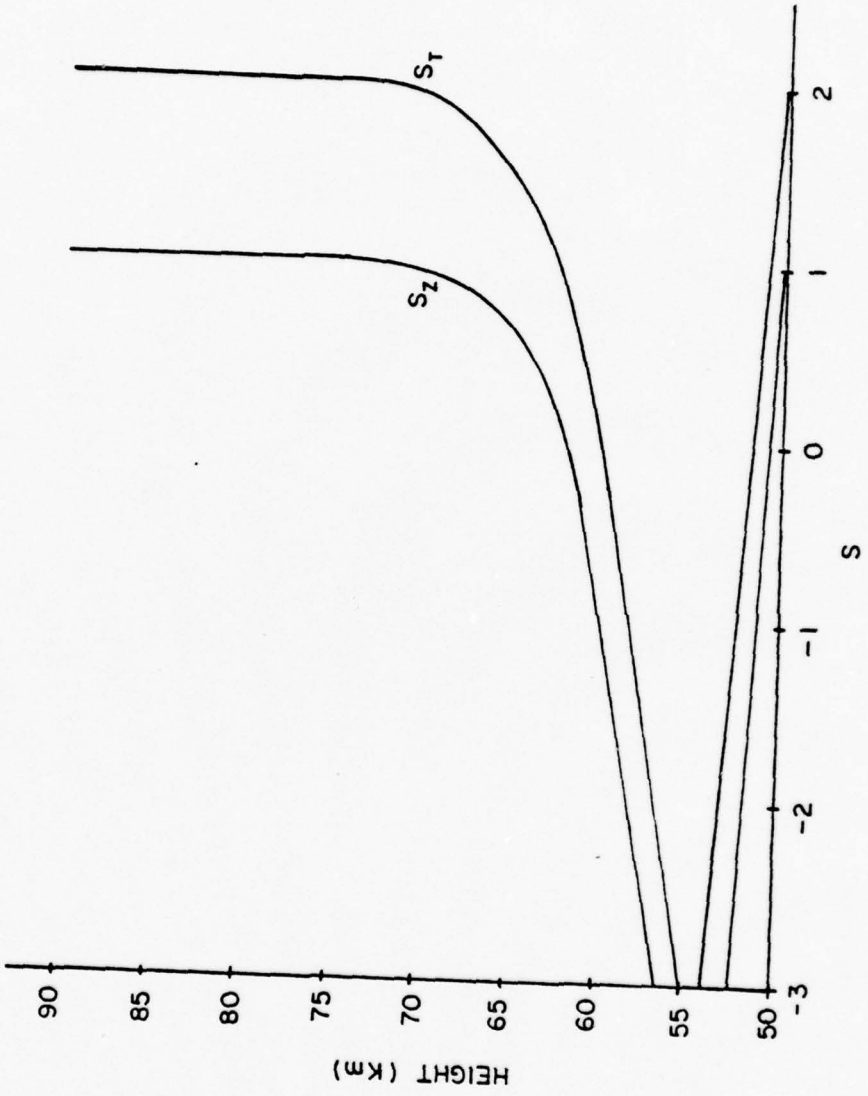

Figure 2.6 S_z and S_T versus height for typical ν

The first class consists of natural atmospheric noise such as lightening, noise spikes generated by power lines, and occassionally, man-made r.f.signals. This class of noise is significant only when the echo is weak, and thus tends to be somewhat more important at noon than in the morning or afternoon. Around sunset, however, noise may increase tremendously due to changing propagation conditions and is significant even when the echo is very strong.

The second class is mainly the result of ionospheric variations near the reflection height. Although such noise is present all the time, it is most important during the times the E-layer is forming or decaying, while the echo strength tends to be relatively constant around noon. Power line fluctuations and power supply ripple in the wanted transmitter contribute no significant noise since the former are removed by the AGC, and the latter are too far removed from the frequency of coherent detection to be significant. Variations in D-transmitter power are removed from the data by recording the actual transmitted power and then normalizing the data to a standard power.

It is essential to know if variations in data resulting from noise will mask variations from dynamic behavior. A very simple technique has been adopted to check this, which involves executing the experiment with the D-transmitter turned off. The W transmitter is operated normally and both classes of noise variations will be present. The resulting noise data is treated just as if it were real data, and a power spectrum is computed. This is compared to a power spectrum of real data, giving a signal to noise ratio as a function of wave frequency. In this manner, the useful frequency range of the experiment may be determined. This data will be presented later in the report.

If it is assumed for a moment that the D-transmitter uniformly heats a cone of the ionosphere with half-angle θ, as shown in Figure 2.7, then a wave propagating through the heated region with wave numbers K_x and K_z will perturb the electron density by an amount proportional to the amplitude of the wave. Since perturbations of data value at a particular height represent the integrated effect across the entire arc, the relative strength of the perturbation divided by the unperturbed condition is

$$P(z) = \frac{\int_{-l}^{l} (N(h) \cdot A \exp j\ (K_x x + K_z z - \omega t)\ )\ dx}{\int_{-l}^{l} N(h)\ dx}$$

where $l = Z \tan \theta$, and the arc has been approximated by a line.

This reduces to

$$|P(z)| = A \cdot \exp j\ (K_z z - \omega t) \quad (\sin[K_x z \tan \theta])/(K_x z \tan \theta)$$

which shows that the sensitivity to measuring vertical wave structure is affected by the horizontal structure, the altitude and the size of the heating cone. Actually, the cone is not abrupt, and the mathematical relationship governing its intensity should be included in the above integral. Despite this approximation and the approximation made in the integration, it is clear that small horizontal wavelength (large K_x) will cause the loss of sensitivity regarding the vertical structure. For very small K_x (large λ_x), $(\sin[K_x z \tan \theta])/(K_x z \tan \theta)$ approach unity and there is no loss of sensitivity.

As stated earlier, only certain waves reach the D-region, due to reflection or dissipation. Figure 6 in Hines (1960) shows that waves with a vertical wavelength of three or more kilometers could have a wide range of horizontal

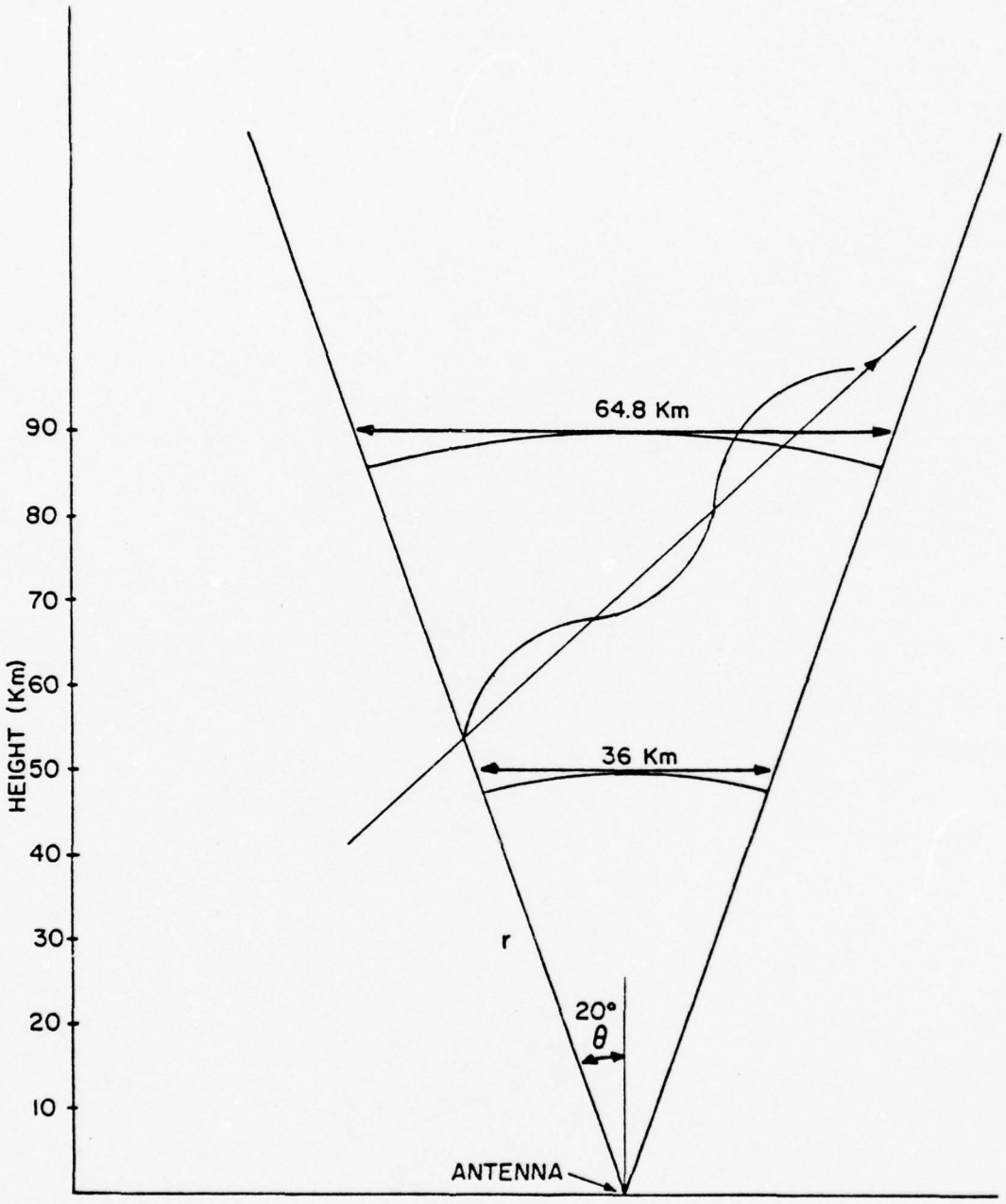

Figure 2.7 Heating cone

wavelength up to a few hundred kilometers at an altitude of 90 km. On the other hand, waves of vertical wavelengths of approximately up to 70 km could exist at 90 km. In view of the fact that the experimental capability in detecting wave structures is ideally around vertical wavelengths of a few kilometers and horizontal wavelengths over few tens of kilometers, it is considered well suited for studying D-region atmospheric waves.

2.2.1 Methods of Data Analysis

The first step in data analysis is to determine the power spectrum of data fluctuations and compare it to the spectrum of noise fluctuations. This is relatively simple but is indispensable in evaluating the significance of the results. The second and third parts of this subsection describe the analysis procedures while the results are presented in 2.3.

The previous section of this report has shown how the wave interaction experiment has the potential to explore the vertical dynamic structure of the D-region, with some inherent limitations. Demonstrating the existence of waves requires considerable analysis. The first step in a thorough analysis is to reduce the data so as to obtain the highest possible height resolution. The algorithm for this process is nearly complete, but will not be described here due to space limitations. The major limitation in the process is that a lower boundary condition must be assumed and the accuracy of the results does depend upon the suitability of the boundary condition. Although data is recorded every kilometer over much of the height range, the height resolution is estimated as two to three kilometers throughout the height range.

After this process, the data may be thought of as a two dimensional array, with variables of height and time. If a few strong waves present at discrete frequencies, the autocorrelation function with height as a variable would show them up. However, it is unlikely that such a simple situation pertains, since the spectrum is likely to be broad and continuous. Cross correlation functions between the data measured at different heights with time as a variable can enlighten such a spectrum. However, as pointed out in Gossard and Paulson (1968) the variations in phase speed will tend to destroy the significance of the cross-correlation in the three receiver experiment for detecting horizontal infrasound propagation. Similarly, the variations in vertical phase speed in this experiment

will have the same effect. For this reason Gossard relied on the so-called cospectrum, which may be loosely interpreted as a cross-correlation over a limited frequency range. Nevertheless, data analysis must proceed with extreme caution in a case such as this.

2.2.2 The Fourier Transform as a Tool for Data Analysis

The results to be presented in 2.3 of this report are the completion of the first step in the analysis of the data obtained by the means outlined above. They were obtained by means of Fourier analysis, and it is the purpose of this subsection to show how this technique may be used to reveal physically significant data in the ionosphere.

Given a signal X(t), meeting certain easily satisfied conditions, (Carlson, 1968), the following Fourier Transform integral may be defined

$$X(f) = \int_{-\infty}^{\infty} X(t)e^{-j\omega t}dt = \int_{-\infty}^{\infty} X(t) \cos \omega(t)\, dt - j\int_{-\infty}^{\infty} X(t) \sin \omega t\, dt \qquad 2\text{-}22$$

$|X(f)|^2$ is the power spectrum, and it is the intent here to show that the quantity may be interpreted in such a manner as to yield a quantitative picture of the periodic fluctuations which compose the signal X(t). Since the difficulties may not be immediately apparent, a few problems will be described here. The approach here will be practical in nature; the theory may be found in Blackman and Tukey (1959).

The most easily manageable situation would seem to be a signal composed of a few discrete sinusoidal waves, for example:

$$X(t) = \cos(17.5\ t) + .85 \cos(4.72\ t + .61) + .9 \cos(11.94\ t + 2.36)$$

$$0 \leq t \leq 2\pi \qquad 2\text{-}23$$

This function is shown in Figure 2.8, and its power spectrum in Figure 2.9.

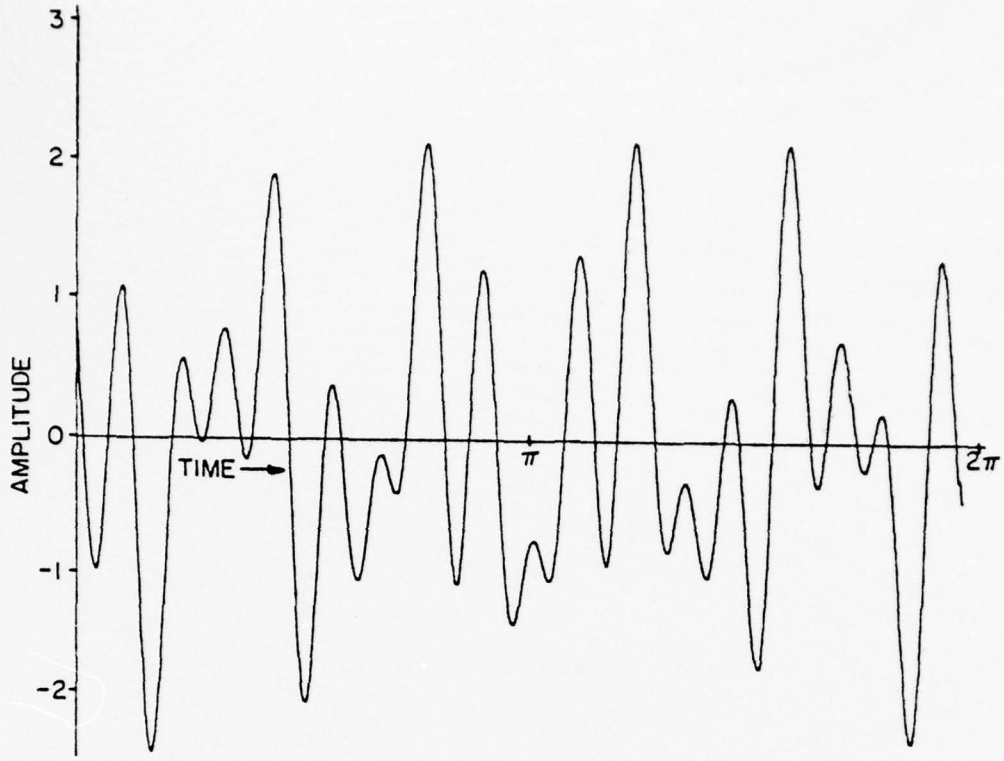

Figure 2.8 Test function

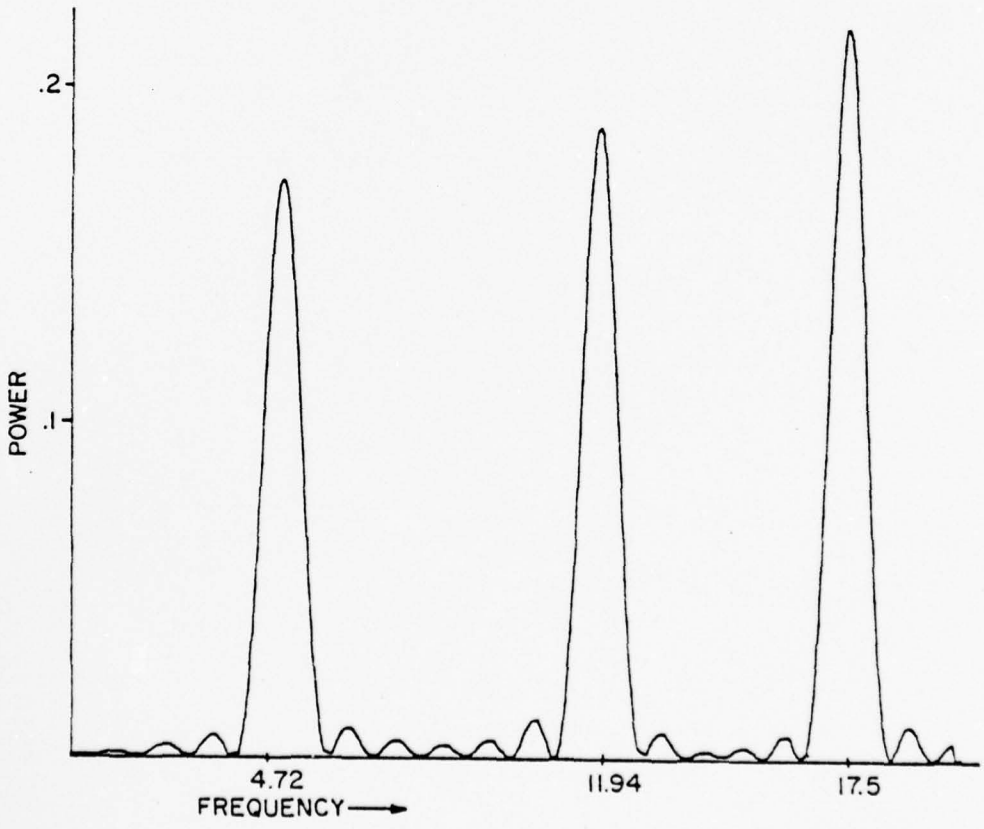

Figure 2.9 Spectrum of above

Although three peaks are clearly distinguishable, in a real situation there would be some question as to whether the smaller peaks represent real data or, as in this example, the samller lobes of three overlapping sinc functions ($\frac{\sin x}{x}$). It is thus desirable to modify the power spectrum so that a single period present in the data will yield a single peak, even if some resolution is lost in the process.

Physical data does not usually exist without a large amplitude, slow-varying essentially non-periodic part, which we shall denote as a trend. Such a trend has been added to the data of the last example, and the result is shown in Figure 2.10. As expected, the trend has a severe effect on the spectrum (Figure 2.11) as can be seen in the figure.

The second class of problems has to do with the integration. First, the function is not known continuously, but only at a set of discrete points, and second, even if it were, the integration would have to be performed numerically, and thus approximately, since no analytic representation is possible. These two limitations complement one another, and an error bound may be deduced readily.

Numerical integration is usually carried out by sampling the function at evenly spaced points, finding an analytic approximation between these points and adding together the approximated areas. The data collection process yields evenly spaced samples with spacing very much closer than the periods this work is concerned with here. As shown earlier, some averaging may be performed giving a set of high resolution, equally spaced points, with spacing much wider than the original data, but still very much less than periods of interest. This latter set of points is the one used for Fourier analysis.

The error in the power spectrum may now be related to the error inherent in the numerical integration. The routine used here employs trapezoidal integration, for which the error bound is given by

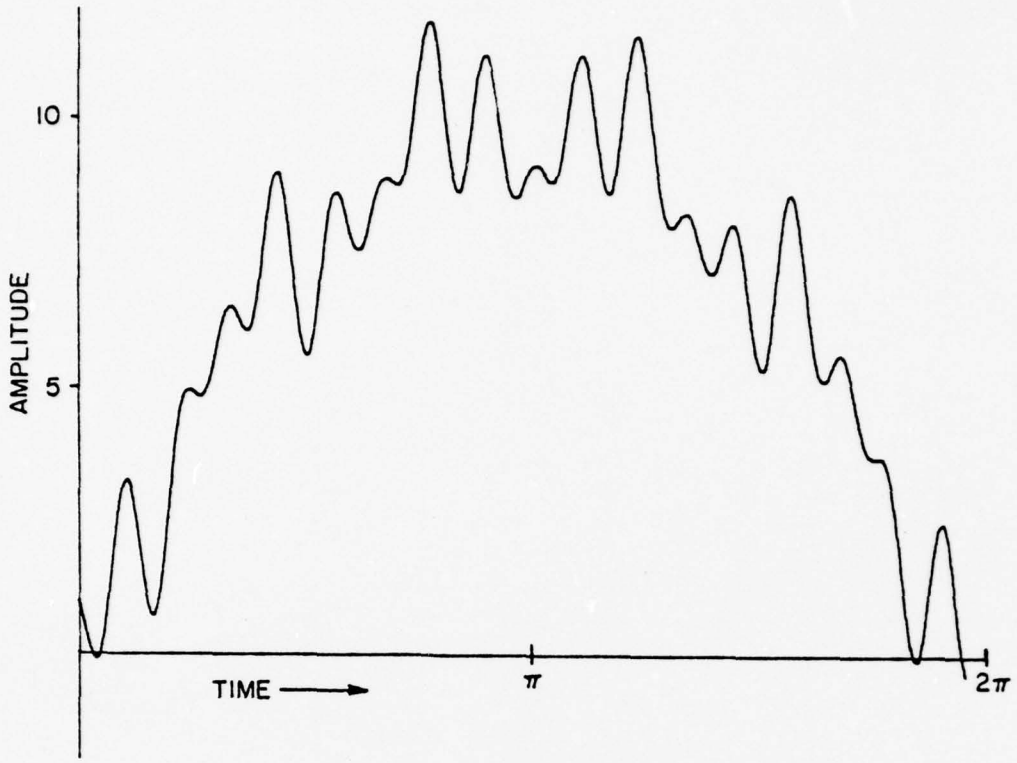

Figure 2.10 Test function with trend

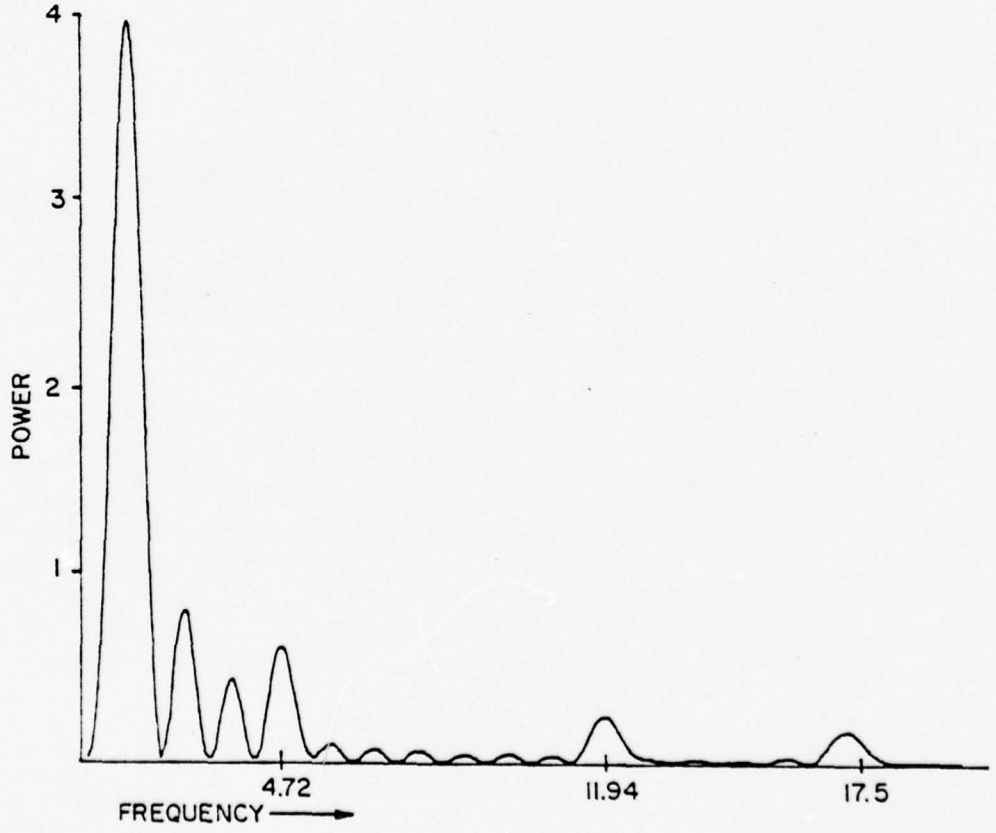

Figure 2.11 Spectrum of above

$$e \leq \frac{T^3}{12m} \quad (\max X'' (t)) \qquad 2\text{-}24$$

where T is the length of the interval of integration, m is one less than the number of points, and max X(t)"is the maximum value of the second derivative of the signal in the interval (Moursand and Davis, 1967).

Assume that the averaging has given a signal that is approximately bandlimited to ω_o. This is equivalent to saying that the signal changes much more slowly than a sine wave of amplitude approximately equal to the signal amplitude. The first derivative of the real part of the integrand of equation 2-22 is given by

$$X'(t) = - \omega X(t) \sin \omega t + \frac{d X(t)}{dt} \cos \omega(t)$$

In looking for the maximum, the second term will be negligible and may be dropped. Using the same approximation, the second derivative is given by $-\omega^2 X(t)\cos \omega(t)$, and

$$| - \omega^2 X(t) \cos \omega(t)| \leq | \omega^2 \max X(t) | \qquad 2\text{-}25$$

It is convenient to set T = 1, and so

$$e = \frac{\omega^2 \max X (t)}{12 m^2} \approx (f/m)^2 \max X(t) \qquad 2\text{-}26$$

Thus the relative error to the maximum of X(t) is just $(f/m)^2$ for the real part of the integrand. The imaginary part will have the same error; squaring and adding gives an error in the power spectrum of

$$2 (f/m)^4$$

Note that a frequency of 1 has one full period in the length of the data sample. As long as we have at least four points in the period of the highest frequency of interest the spectrum will be quite accurate since $2(f/m)^4 \leq .0078$. This is just the error inherent in the mathematics; the errors of interpretation due to leakage and trends described earlier must still be dealt with.

Slowly varying trends may be removed by fitting a polynomial to the data. For the data in this report a fourth order polynomial fitted by the least squared error method was chosen. The trend varies sufficiently rapidly that the diurnal variation of the atmosphere may be followed, but not so quickly that useful data will be filtered out. The spectrum of the data of Figure 2.10 is shown after trend removal in Figure 2.12. Note that it is very close to the spectrum obtained before the trend was inserted (Figure 2.9).

The leakage may be eliminated by a process known as "Hanning" which consists of replacing each coefficient in the real and imaginary part of the transform by a weighted average of neighboring coefficients. The theory of this operation is explained in Blackman and Tukey (1959). The effect is shown in Figure 2.13, where the bar indicates the range of significantly weighted averaging. Note that complete elimination of the minor lobes involves broadening of the major peak.

2.2.3 The Interactive Program for Data Analysis and Display

The Hybrid Computer Laboratory of the Electrical Engineering Department of The Pennsylvania State University operates a PDP-10 computer in time-shared mode. The computer has a high speed CPU and a large memory, as well as interfaces and software for various types of terminals, display screens and plotters. Used in conjunction with the PSU computation center's main computer, the IBM 370-168, the PDP-10 forms a powerful and versatile tool for data analysis and display.

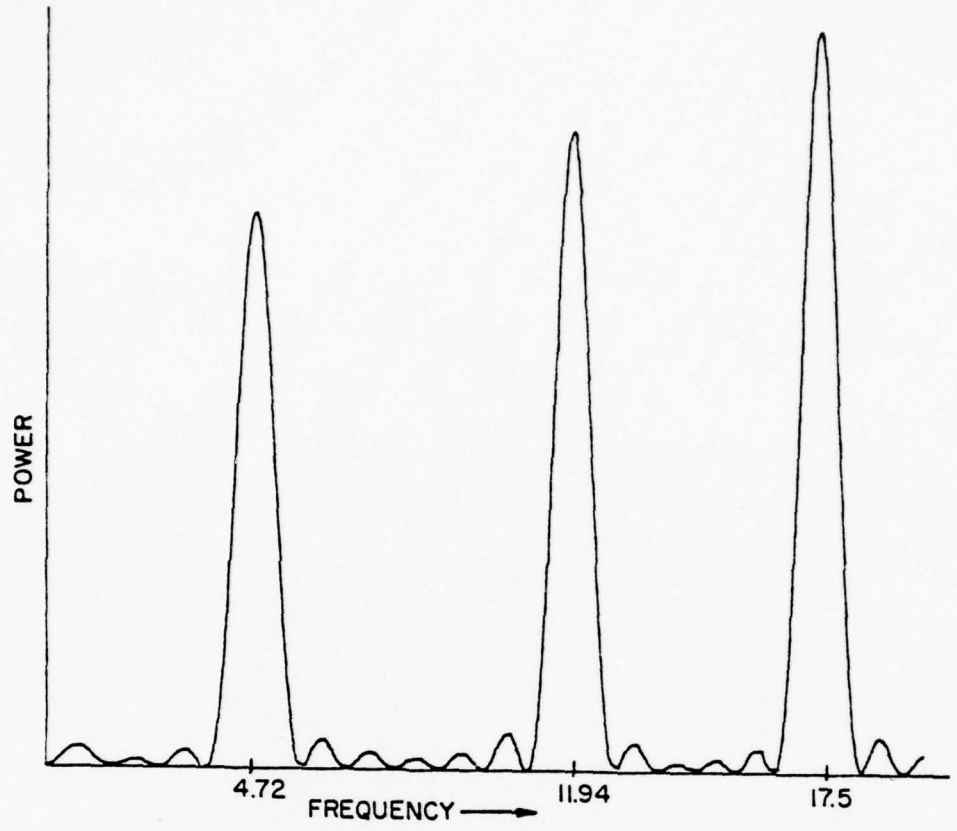

Figure 2.12 Spectrum after trend removal

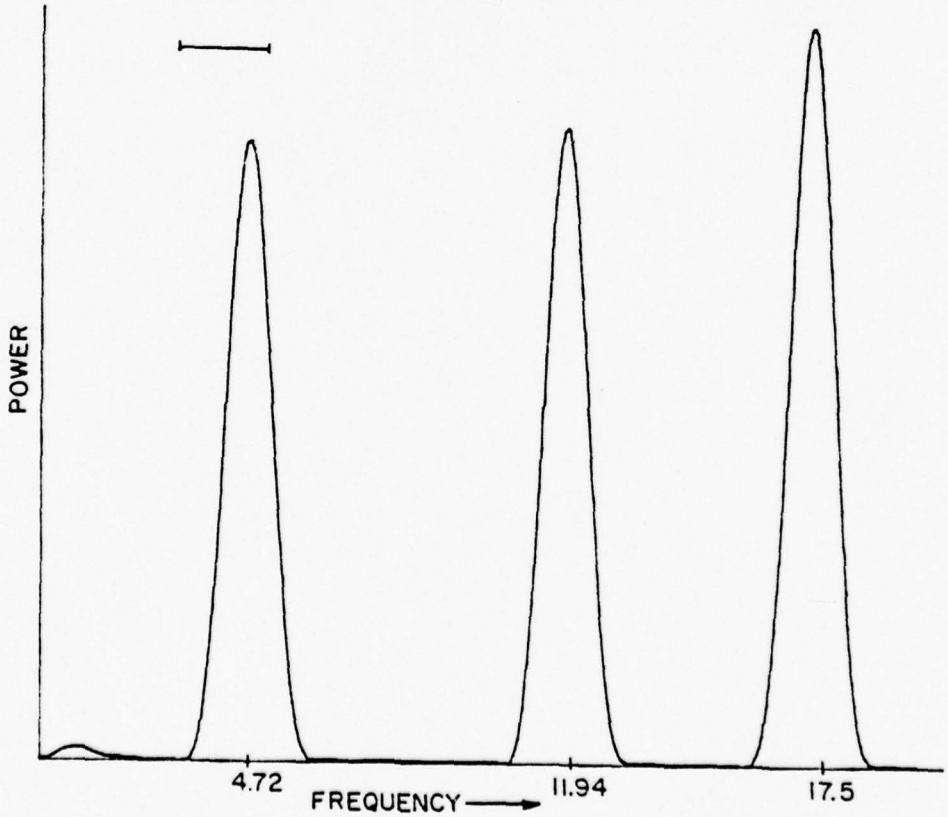

Figure 2.13 Spectrum after hanning

A full day's operation at the Scotia experimental facility produces about 4 million data points on a seven track magnetic tape. The 370-168 is used for the brute force averaging into sets of these points for permanent storage in condensed form and for transfer to the PDP-10 for further analysis. This subsection describes the interactive program used in this analysis.

There are several basic functions which the program must perform. These are the following: (1) the reading of data from tape or disk, (2) the processing of the data as described in the last subsection, and (3) writing out or displaying the data, both the final result, and at intermediate points to aid and direct further processing. The second category consists of various types of averaging and filtering and Fourier analysis, while the third category includes numerical printouts, display screen graphs, and plotter graphs.

The strength of a time shared computer system lies in the interaction between the operator and program during execution time, since the operator is able to look at intermediate results and make decisions which are beyond the capability of the machine. However, the program itself must be designed in a manner which increases the extent of this interaction by making the most information available to the operator in the most convenient manner.

The program is primarily intended to be operated from a Tektronix 4010 graphics display terminal, although many of its features may be used with any terminal. The program consists of a set of commands which may be executed from the terminal, and the software for executing these commands. These commands each perform in one of the three basic categories described above. When execution of a command is completed, the program asks for another command, unless instructed to stop.

A complete description of the program would be too long, and so a few examples will suffice here. The figures in the last subsection were produced by the

following method: first, a command denoted DATA was executed, computing a test function and loading it into an array for further processing. Using initial information regarding the frequency range of the function certain parameters are set using the command SPAR. If at any time during further processing the initial assumptions change, the parameters may be reset. Then the command AVER filter out unwanted high frequencies and reduces the number of points in a manner set by SPAR, to enable more efficient use of the plotting and analysis routines. The function is then plotted on the graphics terminal to check for possible errors, and finally the plot is made on the HP-7202A. In a similar manner commands for performing trend removal, Fourier analysis, Hanning, and so on are performed and the results are checked in the graphics terminal and then plotted.

The three-dimensional plots presented in the next subsection were produced by a somewhat more elaborate process. First the data is read and trial processing is performed and checked on the graphics terminal. When the proper parameters and procedures have been decided upon, the proper command sequence is stored and executed iteratively on successive records. The plot is not performed on line, but is stored on magnetic tape played back later into the plotter with the assistance of IRL's NOVA computer.

2.3.1 Presentation of Data and Results

Data presented here will demonstrate that the wave interaction experiment has sufficient signal to noise ratio to detect dynamic perturbations in the D-region. Figure 2.14 shows one hour of data taken August 2, 1976, at around noon time, at 82 km, and one hour of noise from the same recorder channel taken at a time when ionospheric conditions were almost the same as when the data were taken. Conditions were very good in both cases, based upon operator judgement regarding the stability of the echo and the absence of interfering signals.

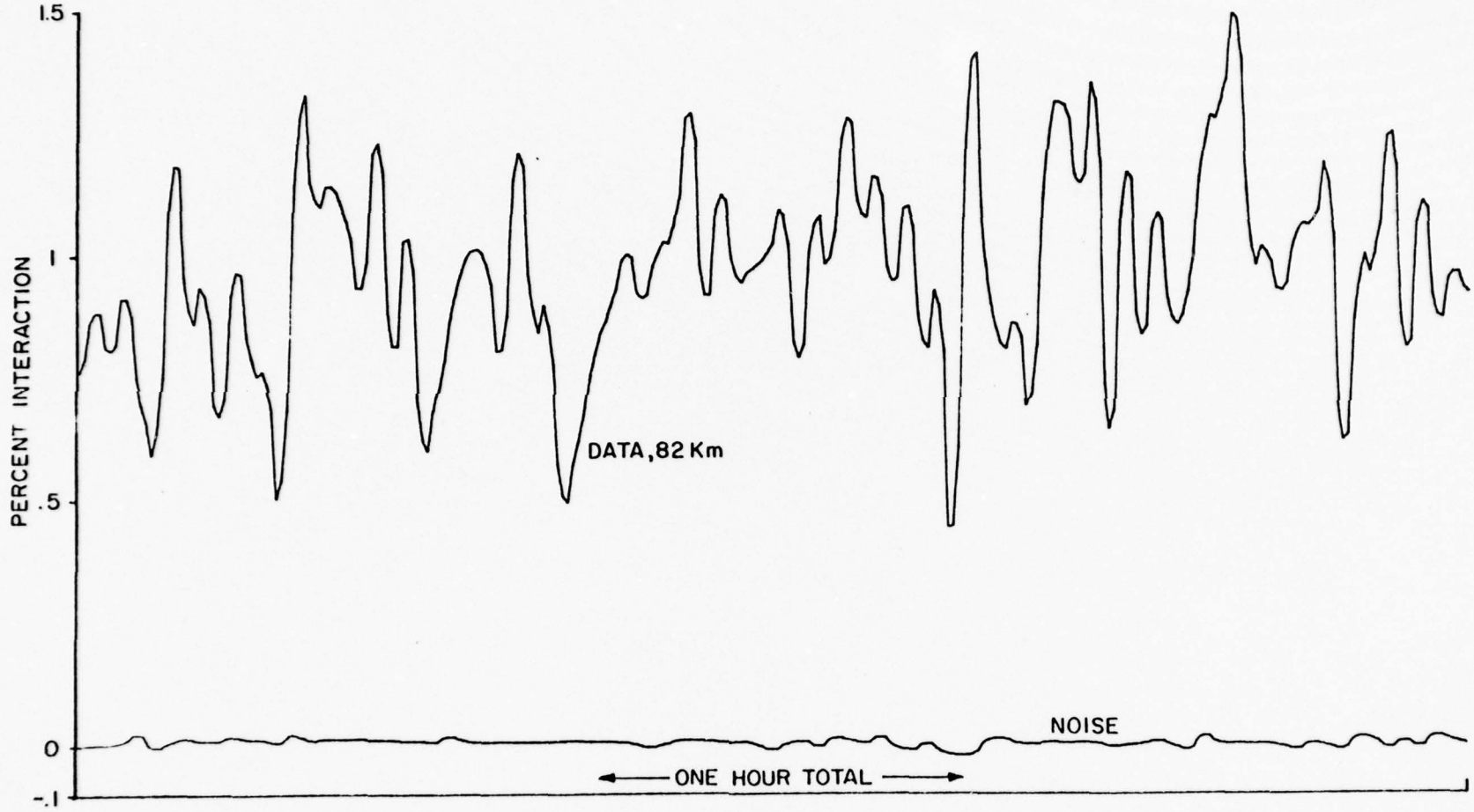

Figure 2.14 Comparison of data and noise at 82 km

The fluctuations in the noise curve are not due to system noise, but rather to ionospheric noise and echo fluctuations as described earlier. System noise is about another factor of five below the noise shown here and is thus totally insignificant. It is clear from Figure 2.14 that the fluctuations on the data are much greater than what may be explained by noise. Figure 2.15 shows the same comparison for data from 56 km, where the data is much smaller. The noise from that channel is approximately the same as in all channels, so the signal to noise ratio is not as good at low heights. Nonetheless, it is still adequate.

The power spectra for the two heights, data and noise, are shown in Figures 2.16 and 2.17. Since the power spectrum is proportional to amplitude squared, the signal to noise ratio is exaggerated and when the two are plotted on the same scale, the noise spectrum cannot be distinguished from the base line at 82 km, and is still quite small at 56 km. Conditions could deteriorate considerably before noise becomes a problem. Under certain unusual conditions, noise can be as much as 40 db greater in effect than shown here. Such conditions occur when the echo is both weak and unstable, and background noise is high. Such conditions are unusual, however, and the experiment usually operates with a satisfactory signal to noise ratio.

Power spectra cannot prove the existence of waves, but those presented here suggest there may be periods present which are significantly above the background level. It is possible that such periods are the results of waves, although gravity waves are expected on the average, to have a continuous spectrum without significant peaks. However, any specific sample could exhibit such peaks. It is interesting that the noise spectrum at 56 km shows a few significant peaks also. This can be explained as some sort of periodic behavior in the amplitude of the wanted echo. It is not known whether or not the cause is wavelike behavior in the E-region at the reflection height.

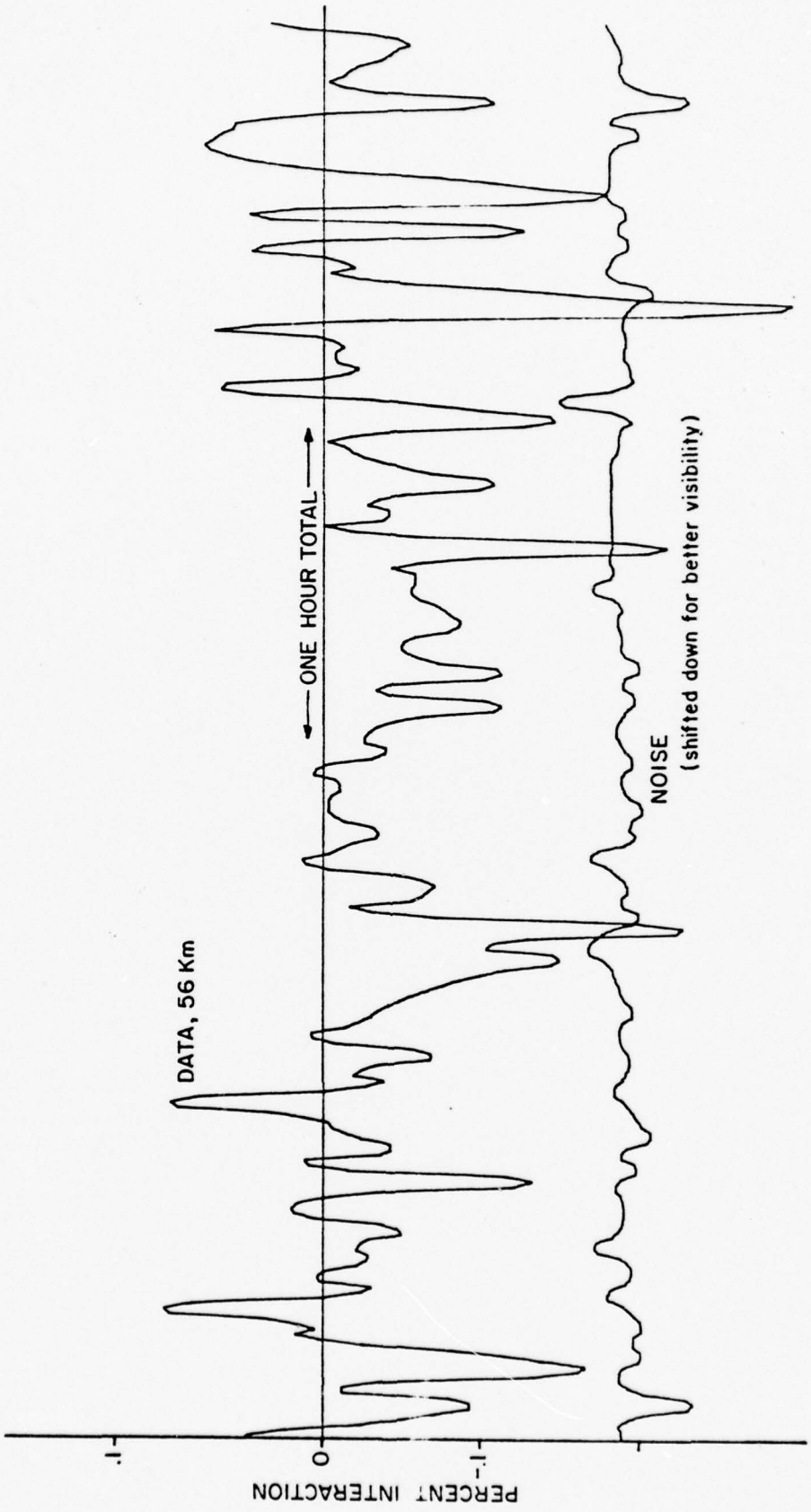

Figure 2.15 Comparison of data and noise at 56 km

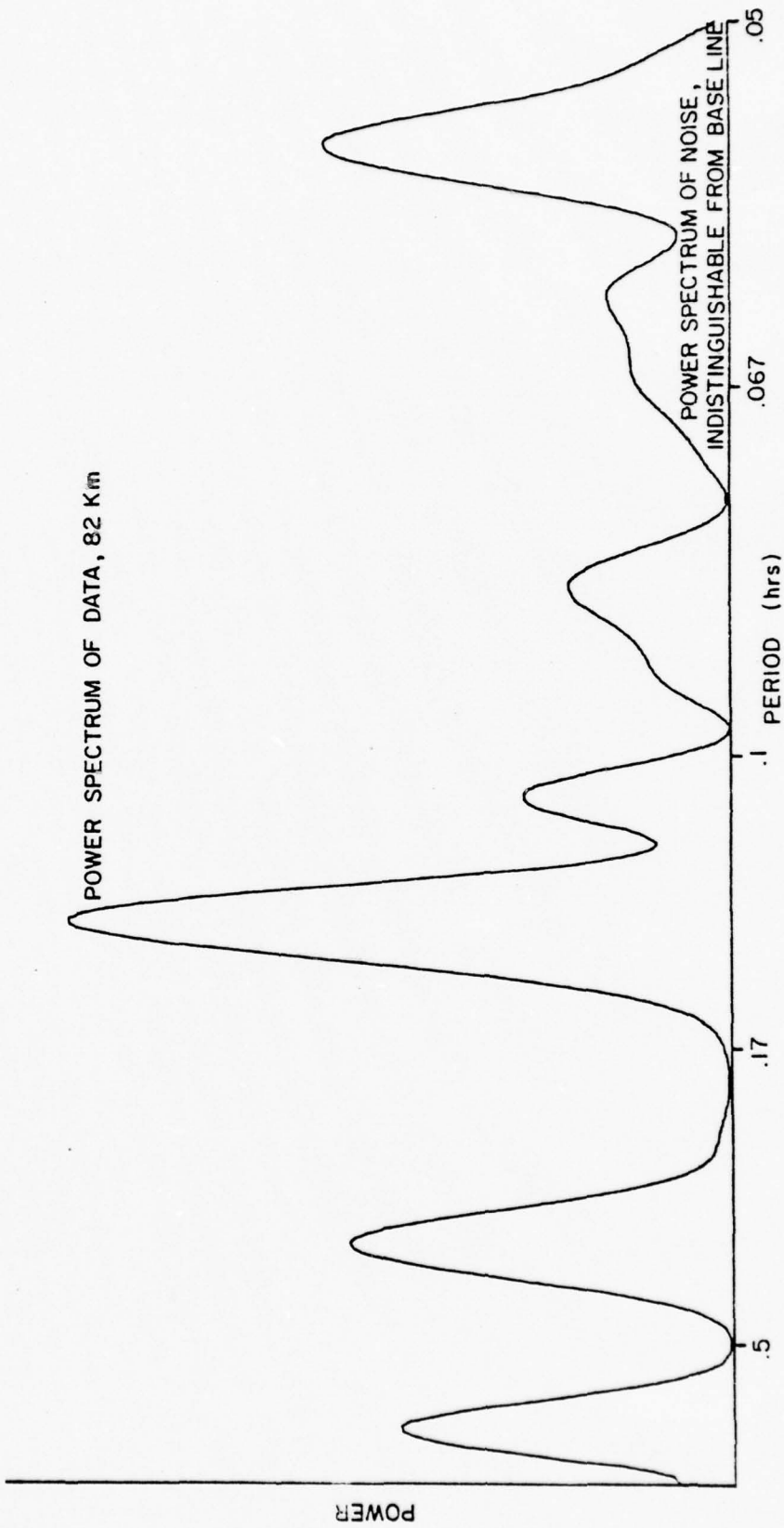

Figure 2.16 Power spectra of data and noise at 82 km

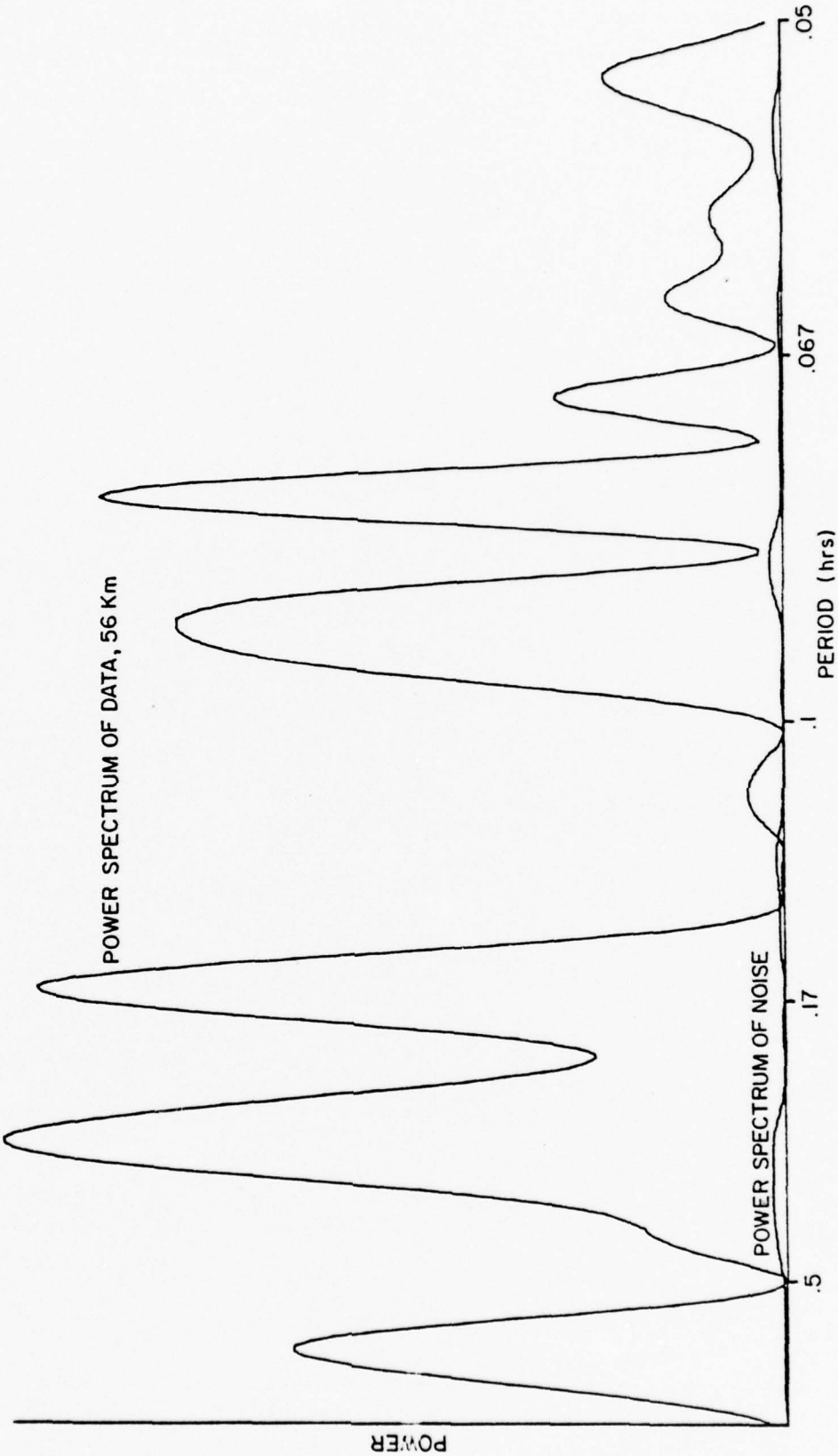

Figure 2.17 Power spectra of data and noise at 56 km

To illustrate the capabilities of the entire system several sets of data and spectra are shown in Figures 2.18 - 2.23. These represent data from what are known as all-day runs, since the period of data collection covers most or all of the daylight hours. The data and spectra curves indicate the possibility of wavelike behavior. The next subsection discusses the steps necessary for a more detailed analysis of this data.

2.3.2 A Summary of Present Work

As discussed in 2.1 of this report, data taken at a particular h_i is not a result of ionospheric parameters from that height alone. The range of influence extends from that height down to the base of the ionosphere, but a detailed study of the experiment shows that heights farther from h_i exert less influence. This is a result of the very rapid cooling times in the lower D-region. The range of influence also extends upward from h_i due to the finite widths of the pulses. None of this causes height resolution to be completely lost, but of course, it is not possible to fully recover the one kilometer resolution which is the absolute limit due to data spacing.

The technique for height resolution recovery, which has been developed and now being programmed is basically a deconvolution of finite wanted and disturbing pulse data into that of very narrow wanted and disturbing pulses. For such an approach, it is necessary to extend the data profile below the lowest altitude at which data has been taken by assuming that the data tapers rapidly to zero. This extrapolation agrees quite well with the actual physical situation because the increasing collision frequency at lower altitudes does cause the data values to decrease rapidly with height. It may be shown that the wave interaction coefficient at a designated height of a finite wanted pulse is the mean of the sum of the coefficients of a set of very narrow pulses with height range covering the finite pulse. The deconvolution process has to be applied to both the wanted

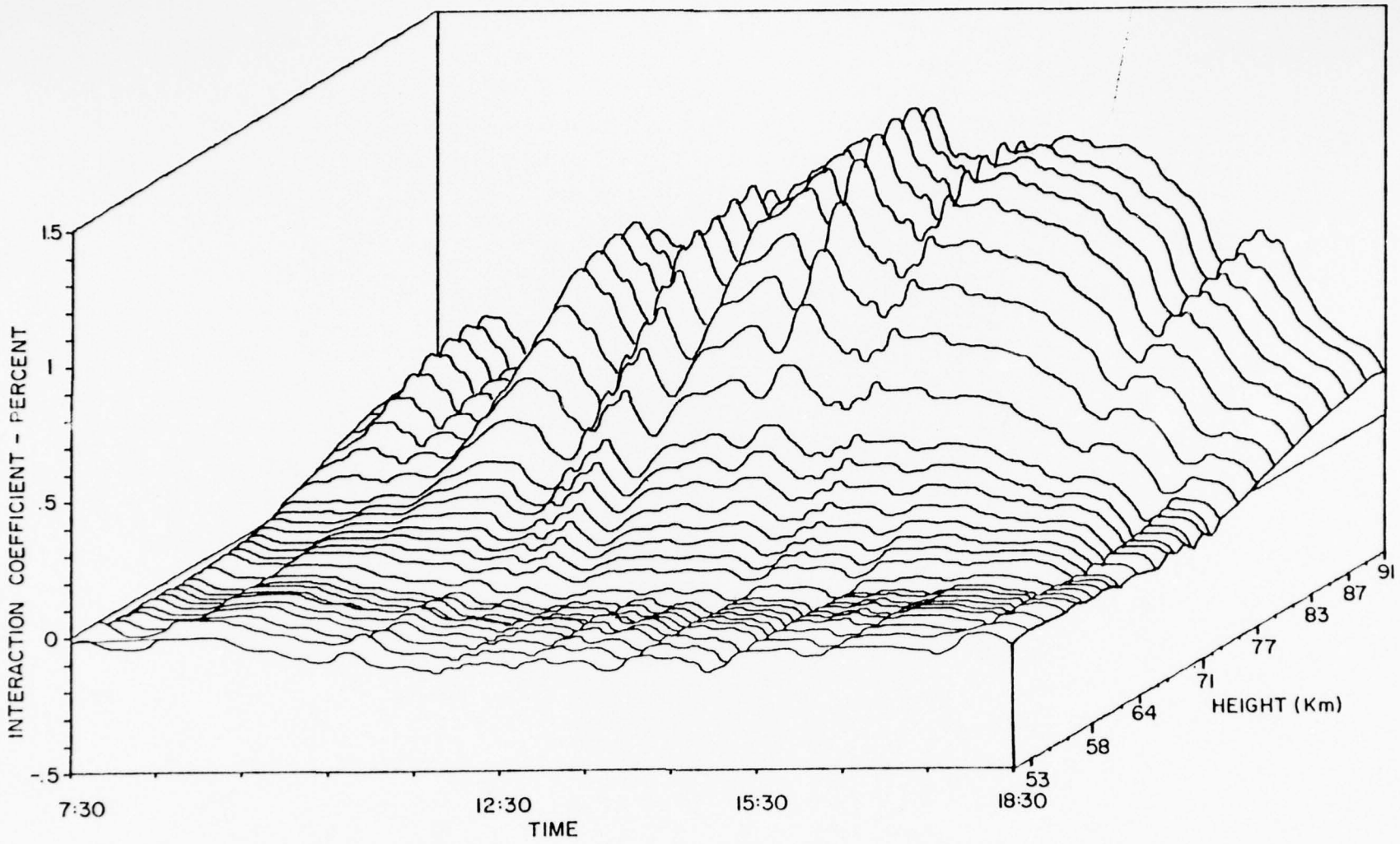

Figure 2.18 Three-dimensional wave interaction data (812176, NAIC, Arecibo, P.R.)

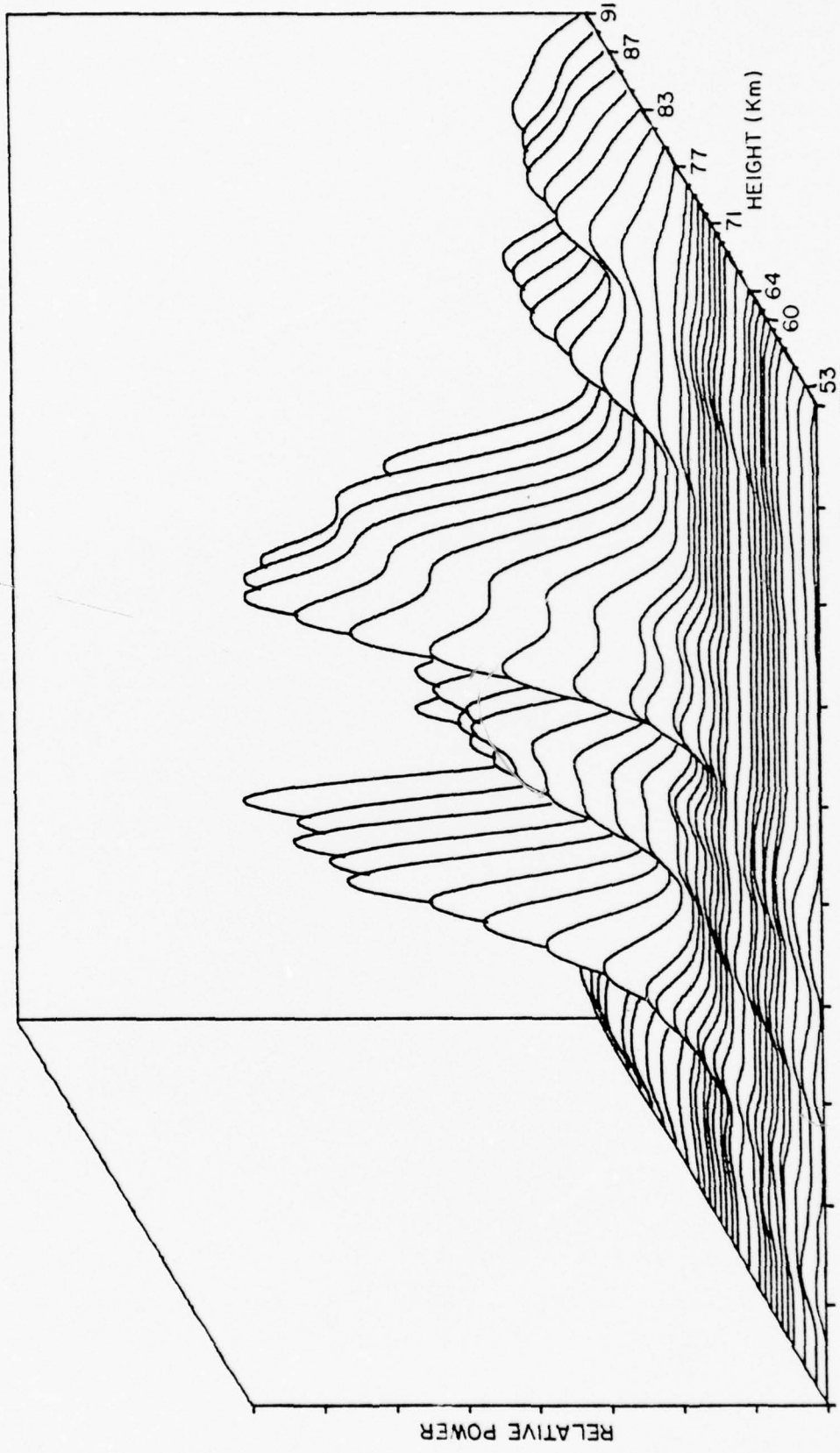

Figure 2.19 Power spectra of three-dimensional data (812176, NAIC, Arecibo, P.R.)

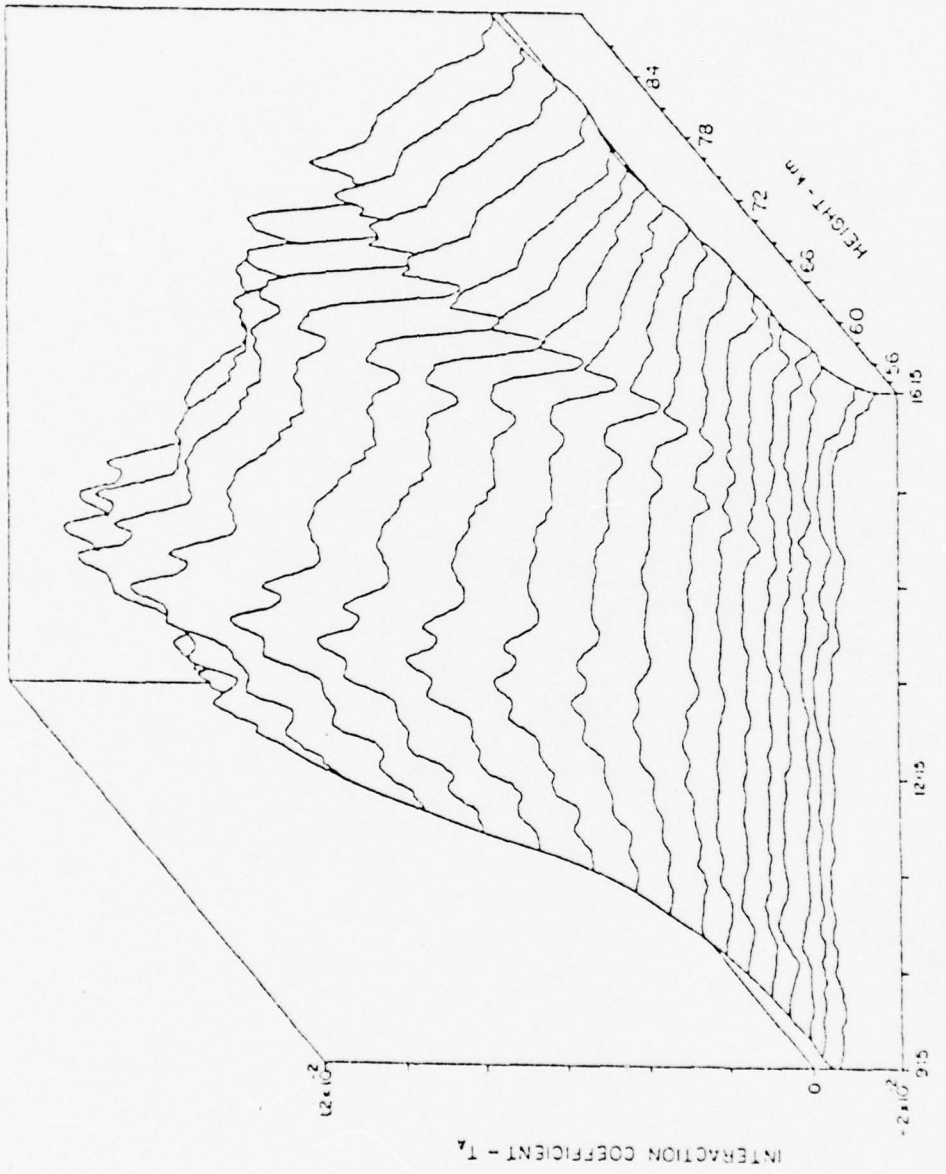

Figure 2.20 Three-dimensional wave interaction data (quiet day, January 31, 1976, State College)

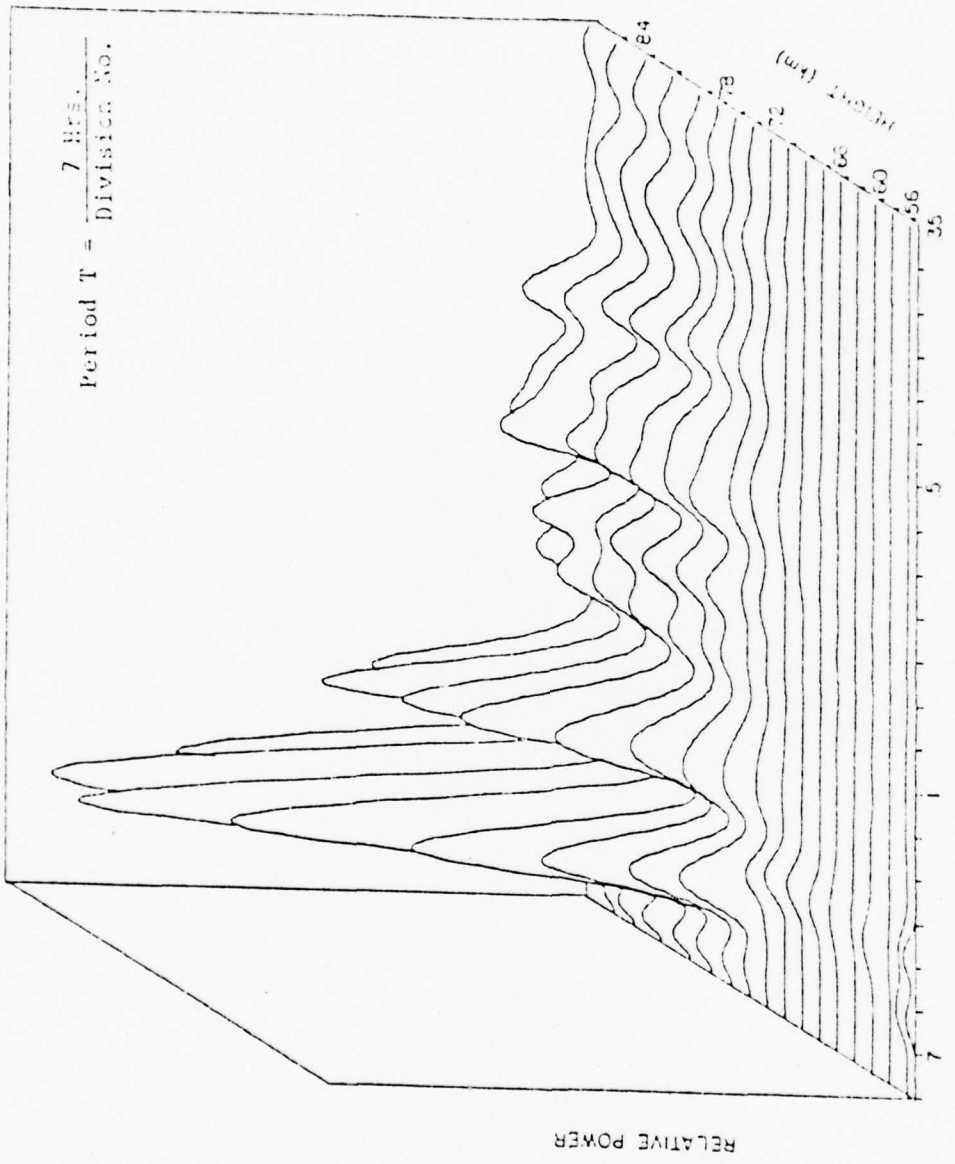

Figure 2.21 Power spectra of three-dimensional data (quiet day, January 31, 1976, State College)

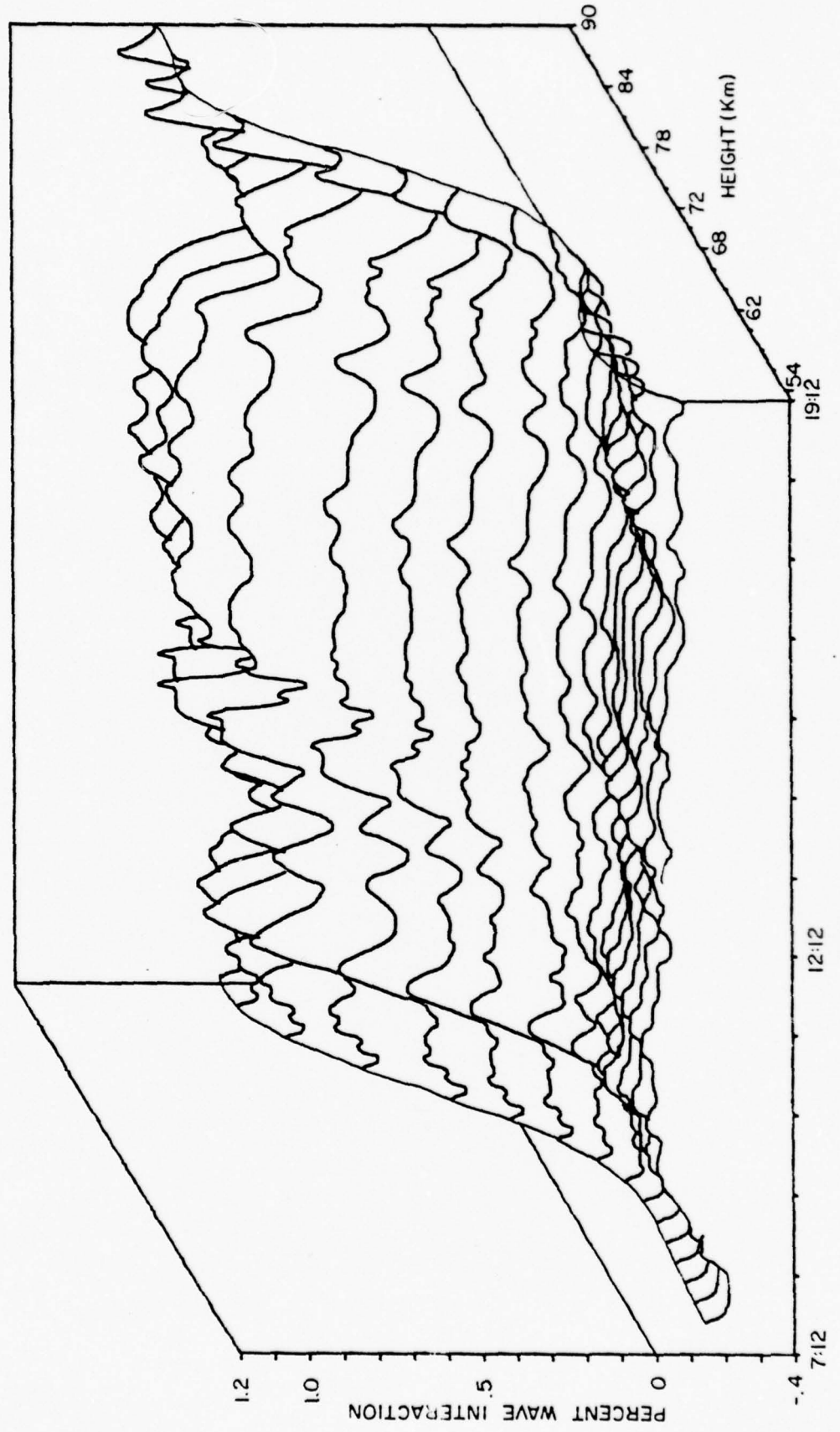

Figure 2.22 Three-dimensional wave interaction data (electron precipitation event, March 27, 1976, State College)

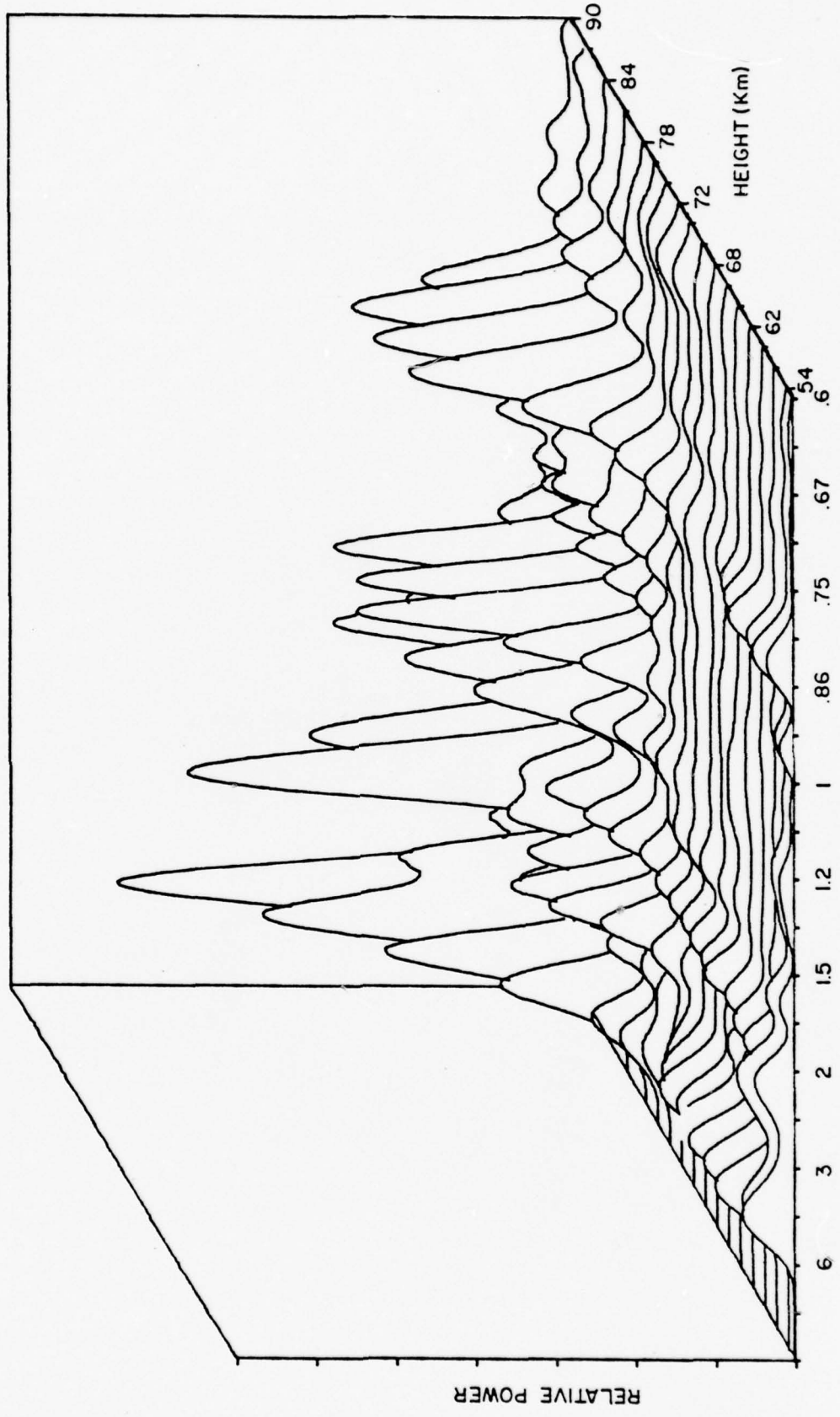

Figure 2.23 Power spectra of three-dimensional data (electron precipitation event, March 27, 1976, State College)

and the disturbing pulses. In the case of the wanted pulse if the finite pulse coefficients are known every kilometer, the coefficients for the narrow pulses may be found by starting at the base of the ionosphere where the coefficients are assumed to be zero and working upward.

The finite D pulse may be treated in a similar manner, and using a similar model tapering the data points to zero, the coefficients for narrow wanted and disturbing pulses may be recovered from those for narrow wanted and wide disturbing pulses. The accuracy of these two processes is limited by the accuracy of the assumed model at low heights, and also by the accuracy of the data points.

Now that the data has been processed into the form where it may be modeled by the conceptually simple narrow wanted, narrow disturbing pulse experiment, it is fairly simple to find a process for deriving quantities which are proportional to parameters at one height only. Letting the wave interaction coefficient for narrow pulses, at h_i be given by $T(h_i)$, it may be shown that

$$T(h_i) = \int_0^{h_i} W(h)\, J(h_i,h)\, dh \qquad 2\text{-}27$$

where W(h) is a quantity which depends only upon ionospheric parameters at h assuming that the power absorbed in the lower D-region from the D pulse transmission is negligible, and $J(h_i, h) = \exp\left(\frac{-2\, G\nu(h_i-h)}{c}\right)$ where ν is the electron-neutral collision frequency and G is the energy loss factor.

The above integral may be approximated by a summation with one kilometer steps. Making the same assumption as before with the data tapering to zero the quantity W(h) may be found for a given assumed height profile of $G\nu$. Note that each $T(h_i)$ is a sum of W(h)'s weighted by the appropriate J's. Beginning at low altitudes where the data values are zero and working up will yield a set of W's whose accuracy depends upon the accuracy of the assumed $G\nu$ profile. Since the

decay is rather rapid at low altitudes, some inaccuracy in the $G\nu$ profile can be tolerated while still achieving reasonably good height resolution.

The next step is to normalize the data so that changes can be expressed as fractional variations. Finally, cross-correlation and co-spectrum analyses may be performed.

3. Intercomparison of Electron Density Synthesis Methods

The difficulties of obtaining accurate electron density height profiles from groundbased experimental data profiles arise from the facts that the data profiles are usually an integral effect over a wide height range and the data are contaminated with noise. Therefore it is important to somehow enhance the reliability of synthesized electron density profiles through statistical means. The two methods, Dale's and Shellman's, to be compared in this section both have common aim of minimizing the afore-mentioned difficulties. As will be seen from the detailed discussions given in the following subsections, Dale's method achieves this aim by applying overdeterministic approach in which the data at larger number of heights are used compared to the number of heights where unknown electron densities are being determined. On the other hand Shellman's method achieves the same aim by balancing the trade-off between the smoothness of electron density profiles and the fit to the data as described later in this section.

Throughout this section the amplitude interaction coefficient T_A is used as an example and both methods assume all parameters, such as collision frequency, electron temperature, energy loss coefficient, etc., as known; thus treating electron densities as the only unknown. In subsection 3.1 and 3.2, theoretical bases for both methods are presented; whereas in 3.3, test results from the two methods are intercompared.

3.1 Dale Synthesis Method

Since the basic theory of the wave interaction experiment involved in this intercomparison has been well documented in previous papers, only the expressions appropriate for introducing synthesis method will be cited here. Detailed development of the theory can be found in Lee and Ferraro (1969) and Dale (1973).

As mentioned earlier, the so-called over-deterministic synthesis method is basically a method of inverting a data height profile to yield an electron density height profile using larger number of data points than the number of heights where electron densities are determined.

The amplitude and phase interaction effects, denoted from here on by T_A and T_ϕ, respectively, are simply expressed in terms of the perturbation of the imaginary (χ) and real (μ) parts of the Sen-Wyller refractive index for the wanted signal as

$$T = T_A + jT_\phi = \frac{R - R'}{R}$$

$$= j \int_o^{h_i} \Delta n\,(h)\, \beta \; dh$$

$$= j \int_o^{h_i} \beta \left[\frac{\partial \mu}{\partial \nu} - j \frac{\partial \chi}{\partial \nu} \right] \Delta\nu \; dh$$

or

$$T_A = \int_o^{h_i} \beta \frac{\partial \chi}{\partial \nu} \nu \frac{\Delta \nu}{\nu} \; dh \qquad 3\text{-}1$$

$$T_\phi = \int_o^{h_i} \beta \frac{\partial \mu}{\partial \nu} \nu \frac{\Delta \nu}{\nu} \; dh \qquad 3\text{-}2$$

where R' is the reflection coefficient of the disturbed sequence of wanted pulses and R is that of the undisturbed sequence of wanted pulses. β is the free space propagation constant for wanted pulses and ν is the most probable collision frequency of Sen-Wyller formula for index of refraction. A different definition of T, for example T = (R' - R)/R, will result in an opposite sign in the expressions of T_A and T_ϕ. However, as long as the polarity

of the quantities T_A and T_ϕ measured by the detecting system is made consistent with the definition, use of either definition is acceptable. It should be noted that the quantity $\frac{\partial \chi}{\partial \nu}$ can be either negative or positive depending on height range. It is typically in the case of the ordinary mode wanted wave, negative below around 65 km and positive above, thus creating a crossover height between the negative and positive amplitude interaction data. Both μ and χ involve the electron density, N_e, and the collision frequency, ν; and, in summary, Equations 3-1 and 3-2 can be expressed in the form of

$$T_{A,\phi}(h_i) = \int_{h_B}^{h_i} G_{A,\phi}(h,h_i)\, F(h)\, dh \qquad 3\text{-}3$$

where F(h) is the only term which contains the unknown electron density N_e. h_B is the base of the ionosphere and h_i is the height of interaction where the upgoing disturbing wave meets the downgoing wanted wave in the wave interaction experiment. Other variables of height such as collision frequency, which is contained in $G_{A,\phi}(h,h_i)$ and F(h) are considered to be known in this synthesis method. Subscripts A and ϕ denote amplitude and phase interaction respectively.

F(h) is the portion of the integrand that contains all the electron density terms in the form of

$$F(h) = N_e \exp\left\{\int_{h_B}^{h} N_e\, f(z)\, dz\right\} \qquad 3\text{-}4$$

where z is a dummy variable for height.

The general approach of the synthesis is to solve for F(h) using the system of simultaneous equations obtained by forming Equation 3-3 for each data point $T(h_i)$ where the number of $T(h_i)$ is larger than that of unknown F(h).

The first step of the technique is to solve for F(h). Since linear interpolation is used on F, as a function of height h, below to over-determine the system, it is desirable that the unknown function F(h) be fairly linear over the interpolated range. To accomplish this, an estimate of the electron density profile is made and substituted into 3-4. The resulting known function, referred to as $F_2(h)$, is multiplied by an unknown correction function, $F_1(h)$, and the product is made equal to F(h). That is,

$$F(h) = F_1(h)\, F_2(h) \qquad 3\text{-}5$$

This is substituted into 3-3. If the estimate is close to the actual profile the F(h) will be approximately linear over small height increments. Numerous tests indicated that such an indirect approach as using an initial estimate of an electron density profile improved the results over those found by solving for F(h) directly. Each of these F's are assumed constant over horizontal slabs of ionosphere. This reforms Equation 3-3 as

$$T(I) = \sum_K F_1(K)\, F_2(K) \int_{K^{th}\ \text{slab}} G(h, h_i)\ dh \qquad 3\text{-}6$$

It was found that integrating $G(h,h_i)$ over the slab gave much better results than assuming it to be constant over the slab.

Now, define the elements of a matrix (A^o) to be

$$A^o(I, K) = F_2(K) \int_{K^{th}\ \text{slab}} G(h,h_i)\ dh \qquad 3\text{-}7$$

where (A^o) has nonzero elements in positions consistent with the range of the sum in Equation 3-6 or the limits of the integral in Equation 3-3.

The system can now be expressed in matrix form as

$$[T] = [A^o] [F_1] \qquad 3\text{-}8$$

where

$[T]$ = (n x 1) matrix with n representing the number of data points

$[F]$ = (m x 1) matrix with m representing the number of heights where N_e is determined

$[A^o]$ = (n x m) matrix

In order to introduce over-deterministic feature, let F_1 be formed by the linear interpolation of the elements of R, where the ratio of the number of elements of F_1 to those of R is the degree of over-determination. This can be expressed as

$$[F_1] = [S] [R] \qquad 3\text{-}9$$

The system of equations to be solved is then

$$[T] = [A^o] [S] [R] \qquad 3\text{-}10$$

or, multiplying $[A^o]$ and $[S]$

$$[T] = [AS] [R] \qquad 3\text{-}11$$

Lastly, to eliminate possible negative values for the elements of $[R]$, define a new vector $[R']$ such that

$$R(J) = \exp \{R'(J)\} \qquad 3\text{-}12$$

where J is an index.

The system of equations defined by Equations 3-11 and 3-12 are now solved by a nonlinear, least square algorithm of Marquardt (1963, 1971), the result of which is the vector $[R']$. $[R]$ is formed using Equation 3-12 and in turn $[F_L]$ by Equation 3-9 and $[F]$ by Equation 3-5.

All that remains is to solve for N_e, knowing F and using Equation 3-4 which is rewritten in the form

$$N_e = \left[F \exp \left\{ - \int_{h_B}^{h} N_e \, f(z) \, dz \right\} \right] \qquad 3\text{-}13$$

This equation is solved using an induction method starting at the lowest slab and solving for the electron density at each skab using Wegstein iteration scheme (Lance, 1960 and Wegstein, 1960) which solves equations of the form $x = f(x)$.

The effect of a finite width wanted pulse in the wave interaction experiment can easily be included by using the convolution integral:

$$T_w(x) = \frac{2}{c\tau} \int_{c\tau/2} T(x') \, dx'$$

where τ is the width of the wanted pulse or receiver gate in seconds. This causes only a modification to the matrix $[A^o]$ and does not alter the basic technique. In this intercomparison, the effects of a finite width wanted pulse are fully taken into account.

The theory of synthesis method presented here is equally applicable to amplitude and phase interaction data T_A and T_ϕ. However, the intercomparison tests were conducted concentrated on T_A only.

3.2 Shellman Synthesis Method

Since basic wave interaction theory has been described in summary form in 3.1 along with the Dale synthesis method, only the key factors depicting the basic concept of the Shellman Synthesis Method will be summarized here. The details of the method could be found in Shellman (1973).

In this method, in order to parameterize the electron density profile, it is represented by a series of short exponential segments. The common logs of the electron densities at the heights, h_j, where the segments join, are taken to be the unknown parameters of the profile and are denoted by $\alpha_j = \log N_e(h_j)$, where $j = 1, 2, \ldots, n$.

Basic approach in minimizing experimental errors is to search for the smoothest possible electron density profile which provides exceptable fit to the experimentally measured data. The quantitative scheme of simultaneously satisfying the smoothness and the data fit is to minimize the quantity

$$f = c + \lambda s \qquad 3\text{-}14$$

where

$$c = \int \left(\frac{d^2 \alpha}{dz^2} \right)^2 dz \qquad 3\text{-}15$$

is the measure of curvature in the electron density profile with $\alpha = \log N_e$ and

$$s = \sum_{i=1}^{m} \left\{ \frac{t(h_i) - T(h_i)}{\sigma_i} \right\}^2 \qquad 3\text{-}16$$

is the measure of deviation of data value, $t(h_i)$, computed from the assumed electron density profile, from experimentally measured data $T(h_i)$ with σ_i as standard deviation. The equation 3-14 could take the form of

$$f = c + \tfrac{1}{2} \lambda^2 s$$

to simplify mathematical manipulations or the form of

$$f = c + d + \tfrac{1}{2} \lambda^2 s$$

in order to include a damping term d where

$$d = K_d \int \left[\Delta(\log N_e)\right]^2 dz$$

where K_d is some chosen constant and $\Delta(\log N_e)$ is the change in the profile at height z corresponding to the increment $\Delta\lambda$.

General steps taken in the search scheme is first to find the electron density profile corresponding to $\lambda = 0$, which is the best-fit exponential profile; and then find profiles for successively larger values of λ as details are added to the profile with the progress of search. The increments in λ depend on the linearity of the $t(h_i)$ with respect to α_j.

For the present intercomparison purpose, equation 3-14 was used while the damping term d is included only in the process of determining the best-fit exponential profile. The advantage in starting with the best-fit exponential profile is that the derivatives $\frac{\partial t(h_i)}{\partial \alpha}$ are better behaved for profiles of simpler form. This is an important factor, as can be seen from the search scheme described below.

The first step in obtaining a solution to Equation 3-14 is to differentiate this equation with respect to α_j's, yielding

$$\frac{\partial f}{\partial \alpha_j} = \frac{\partial c}{\partial \alpha_j} + \lambda \frac{\partial s}{\partial \alpha_j} = \frac{\partial c}{\partial \alpha_j} + \left[2 \sum_{i=1}^{m} \frac{\partial t(h_i)}{\partial \alpha_j} \lambda \sigma_i^{-2} \right.$$

$$\left. \cdot \left[t(h_i) - T(h_i) \right] \right] = 0$$

This expression, however, cannot be solved directly since $t(h_i)$'s are not known unless α_j's are known and since the derivatives $\frac{\partial t(h_i)}{\partial \alpha_j}$ are functions of α_j. Nevertheless, solution equations can be given for the α_j's in terms of the parameters $\alpha_j = \alpha_{j0}$ of some assumed starting profile, and the computed values $t(h_i) = t_0(h_i)$ and derivatives $\frac{\partial t(h_i)}{\partial \alpha_j}$, for the assumed profile. These solution equations can be used if the starting profile and solution profiles are sufficiently similar.

In application the curvature function c of Equation 3-15 is expressed in terms of summation over profile segments. This becomes

$$c = \sum_{j=2}^{n-1} \left[\frac{\frac{\alpha_{j-1} - \alpha_j}{h_{j-1} - h_j} - \frac{\alpha_j - \alpha_{j+1}}{h_j - h_{j+1}}}{(\Delta h)_j} \right]$$

where the expression in brackets represents a second derivative at height h_j and

$$(\Delta h)_j = (h_{j-1} - h_{j+1})/2$$

is the height increment over which the j-th second derivative is considered to apply. The slab summation form of c approaches the integral of Equation 3-15 as the slab is made sufficiently thin.

The search scheme described above has a tendancy to give successively smaller value of s, in the process of iteration, at a substantial rate until it reaches a threshold beyond which the rate of reduction in s become insignificant. The final electron density profile is chosen at this threshold point.

3.3 Results of Comparison

Intercomparison of the two electron density synthesis method was initially made with the data generated from known electron density profiles. Then as a final test the two methods were applied to real data obtained from the wave interaction experiment conducted at the Ionosphere Research Laboratory, PSU.

Eighteen samples obtained over a five-hour period on January 31, 1976 were synthesized by both methods. Figures 3.1 through 3.3 show three typical comparisons, while fifteen others are presented as Figures 1-A through 15-A in the appendix for reference.

As can be seen from the figures, the results of two different methods are in excellent agreement. However, the Dale synthesis method seem to give somewhat more detail in electron density profiles. This could be due to the fact that the Shellman Synthesis Method has a built-in feature of balancing the trade-off between the smoothness of profiles and the data fit which tends to give smoother profiles.

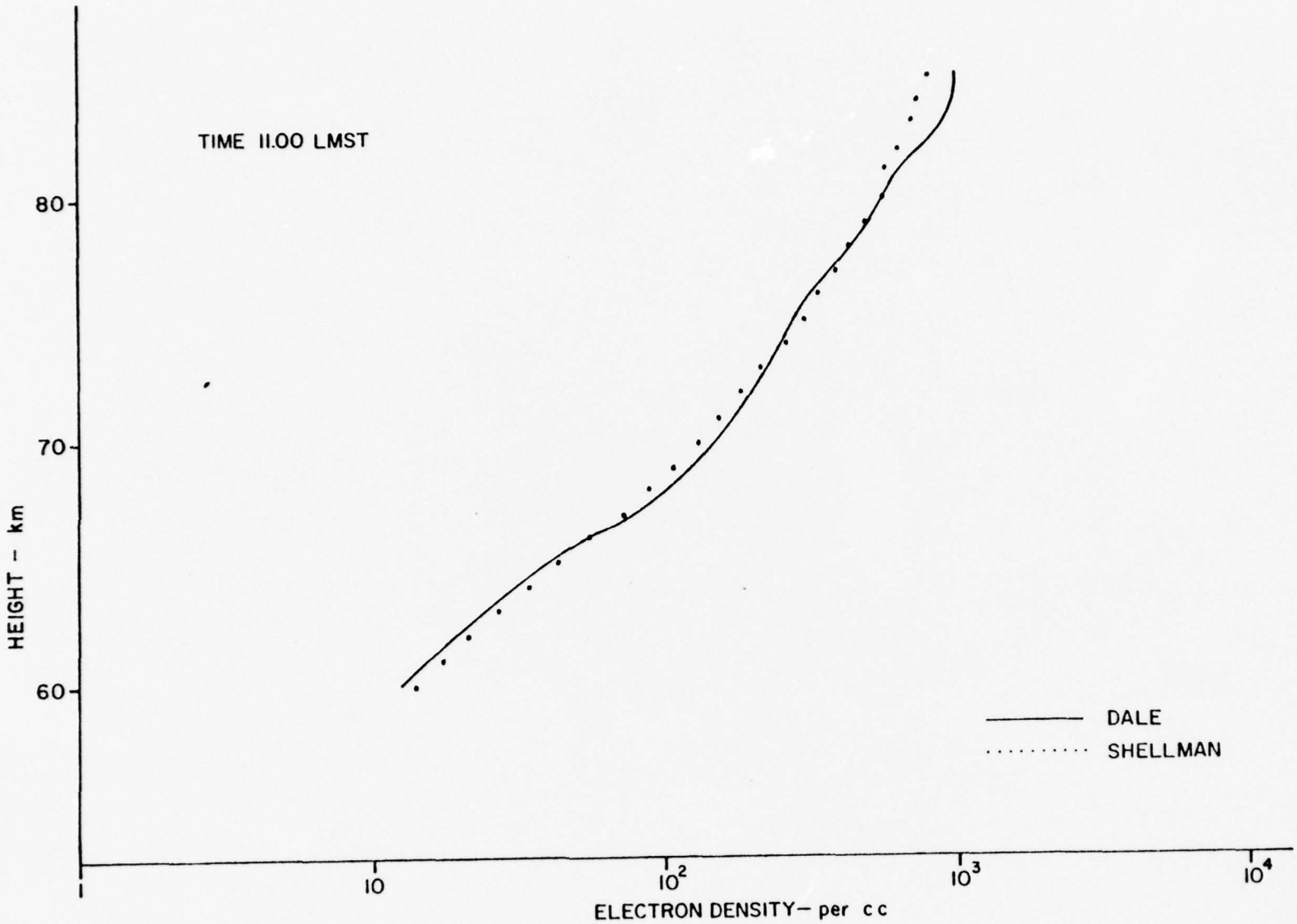

Figure 3.1 Intercomparison of synthesized electron densities

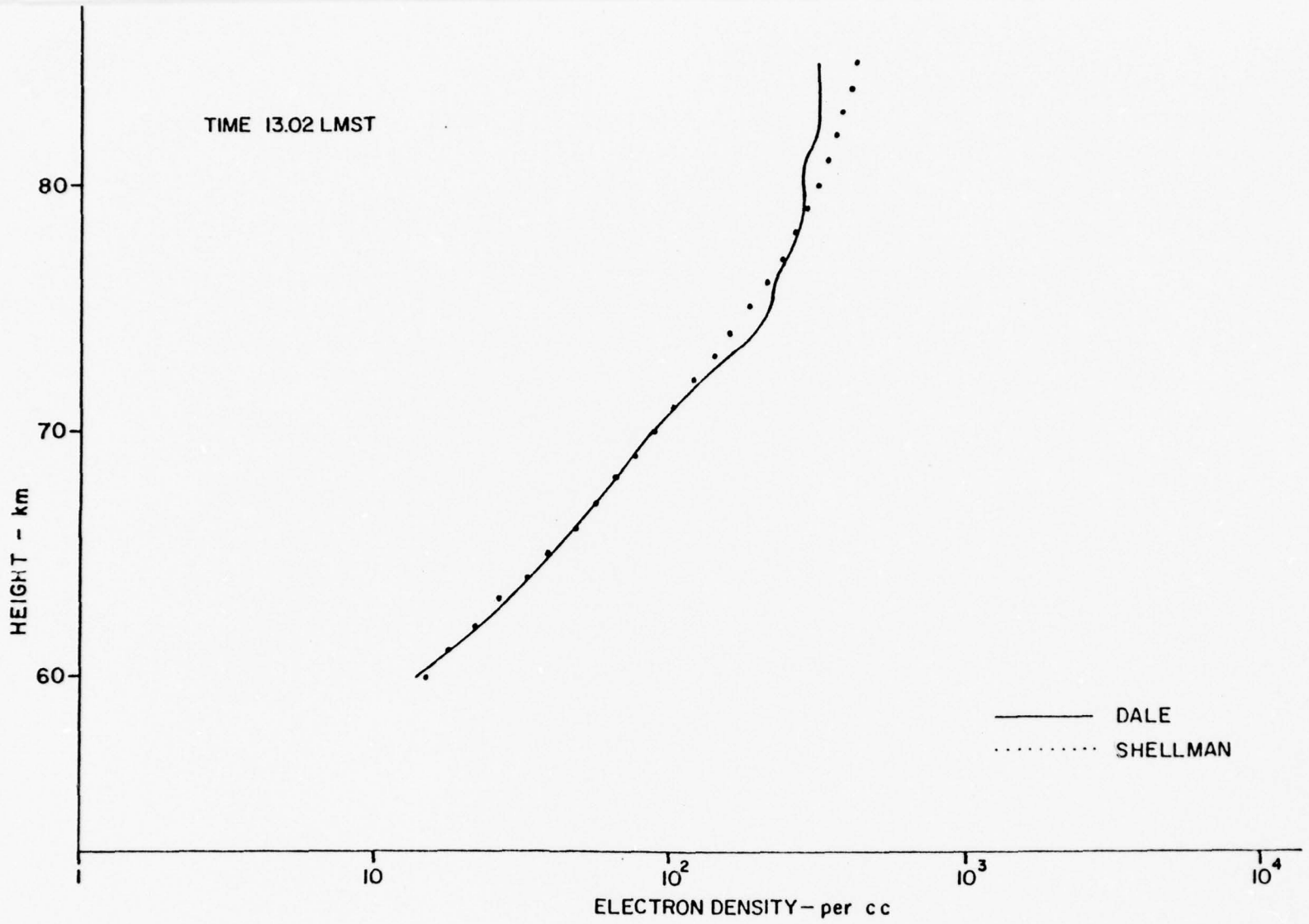

Figure 3.2 Intercomparison of synthesized electron densities

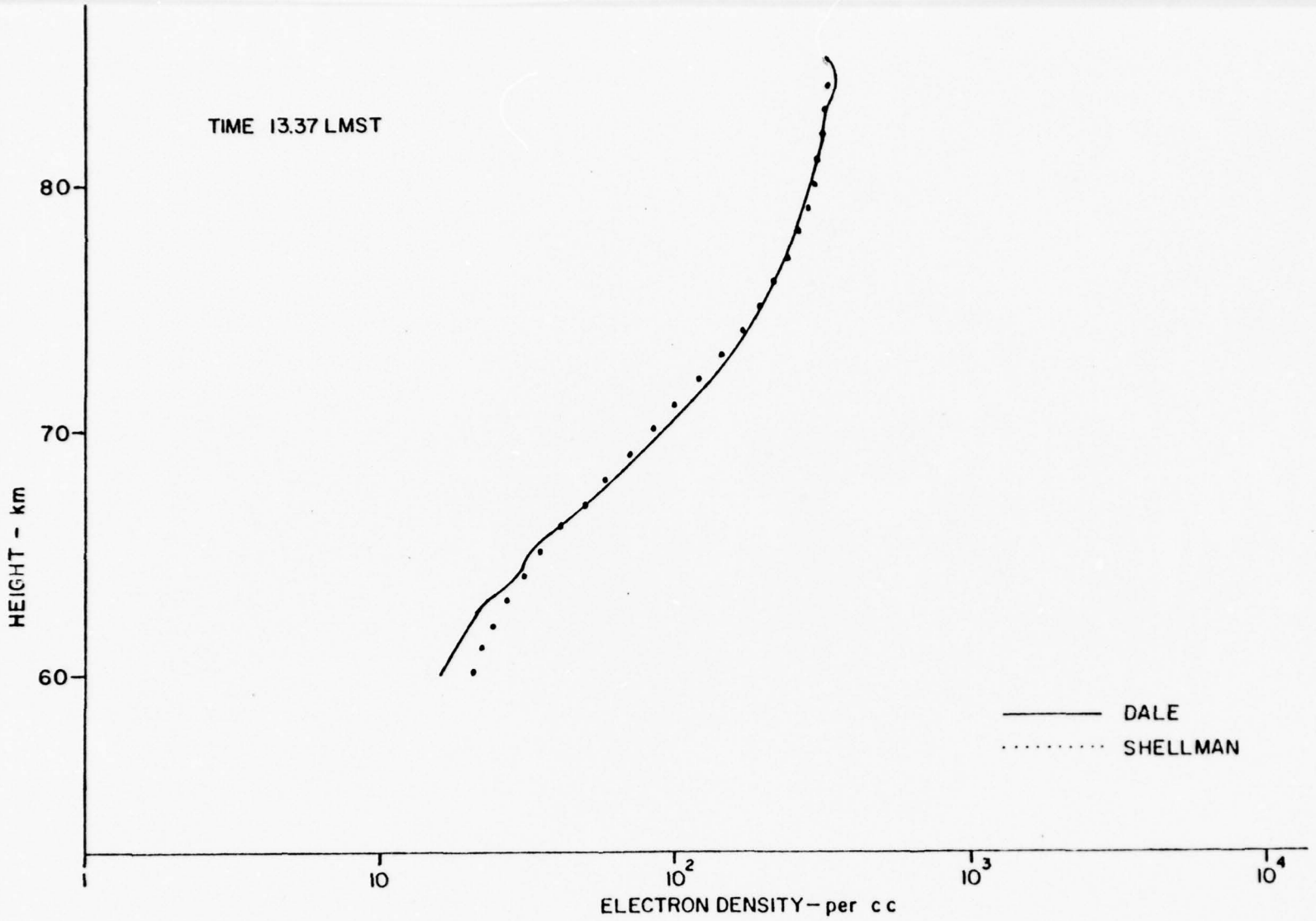

Figure 3.3 Intercomparison of synthesized electron densities

4. Routine Operation for Monitoring D-Region Temporal Variability

As stated earlier in the introduction, this section describes the capability of IRL's digitalized sophisticated wave interaction experimental facilities in monitoring and studying temporal variations in the D-region ionosphere.

The wave interaction data, which are digitally recorded on magnetic tapes covering 28 D-region heights simultaneously once every 300 milliseconds, can be processed in a diversified manner. It is best to describe the processes center around the flow chart shown in Figure 4.1. At present the Penn State Facility is not directly linked to a computer although in principle it can; it has not been necessary for us to do so to meet our scientific objectives. We do still have rather fast "turn-around" with the procedure given in Figure 4.1. A wave interaction data tape is quickly processed at Stage I to give a "quick look" at data profiles; this takes only several minutes after delivering the tapes to Computation Center. Some averaging is done at this stage since during an 8 hour run, for example, there are almost 2.7×10^6 data values for the height range 50 to 90 km. Stage I then gives us an opportunity to examine the quality of data and from our own experience allows us to specify the state of the D-region ionization. A condensing program allows us average data profiles corresponding to time periods of several seconds to several minutes depending upon what D-region feature is being investigated. Minutes would be sufficient for evaluating diurnal features or relativistic electron precipitation events whereas seconds would be needed for X-ray flare events, for instance. Stage II conveniently displays the data in "3-dimensional" format as in Figure 4.2 for the quiet D-region of January 31, 1976. It is evident from Figure 4.2 that there is a diurnal effect as well as irregular behavior in terms of "wave structure" present. Stage II output takes 1-3 hours to obtain dependent

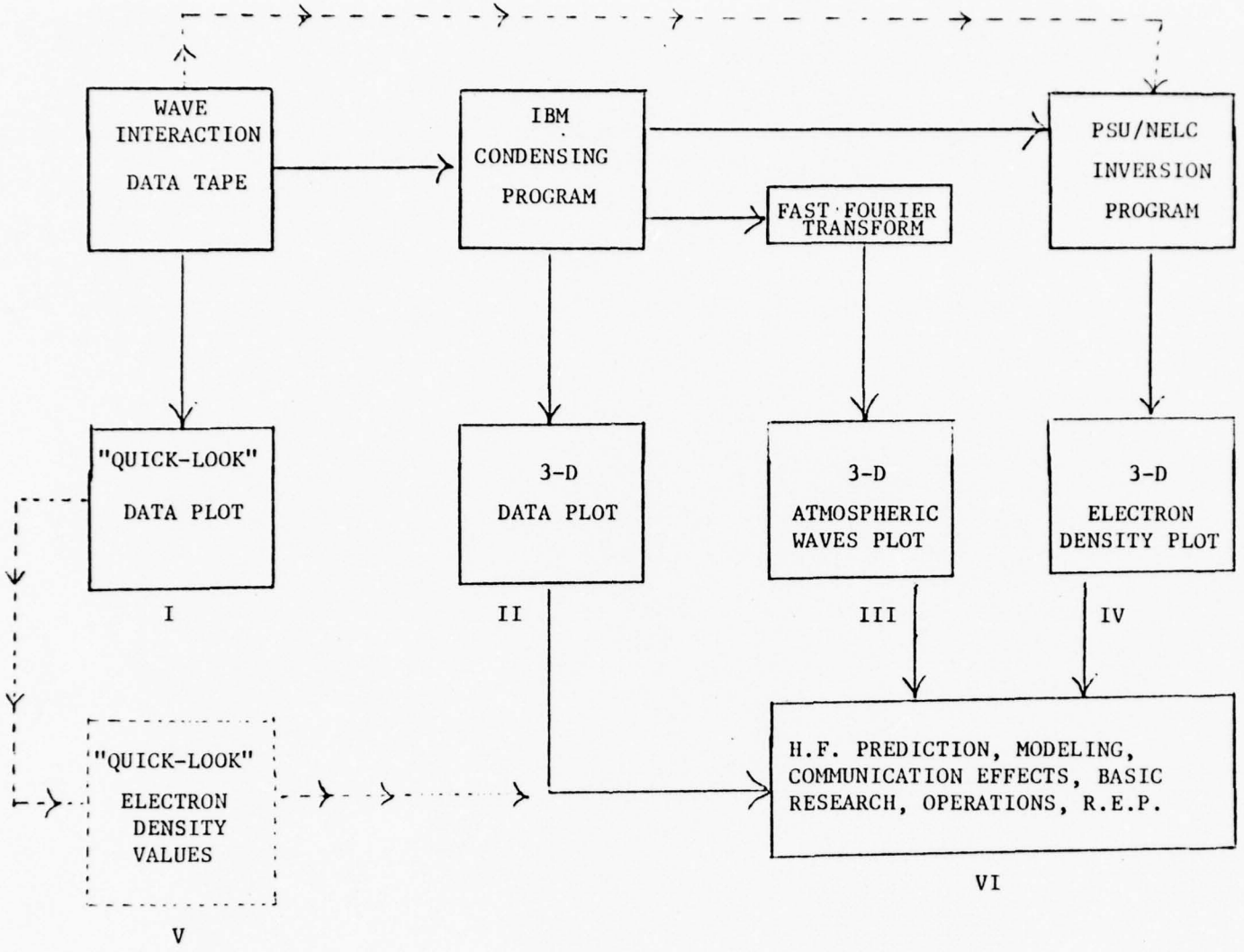

Figure 4.1 Flow Chart of Data Processing Capability

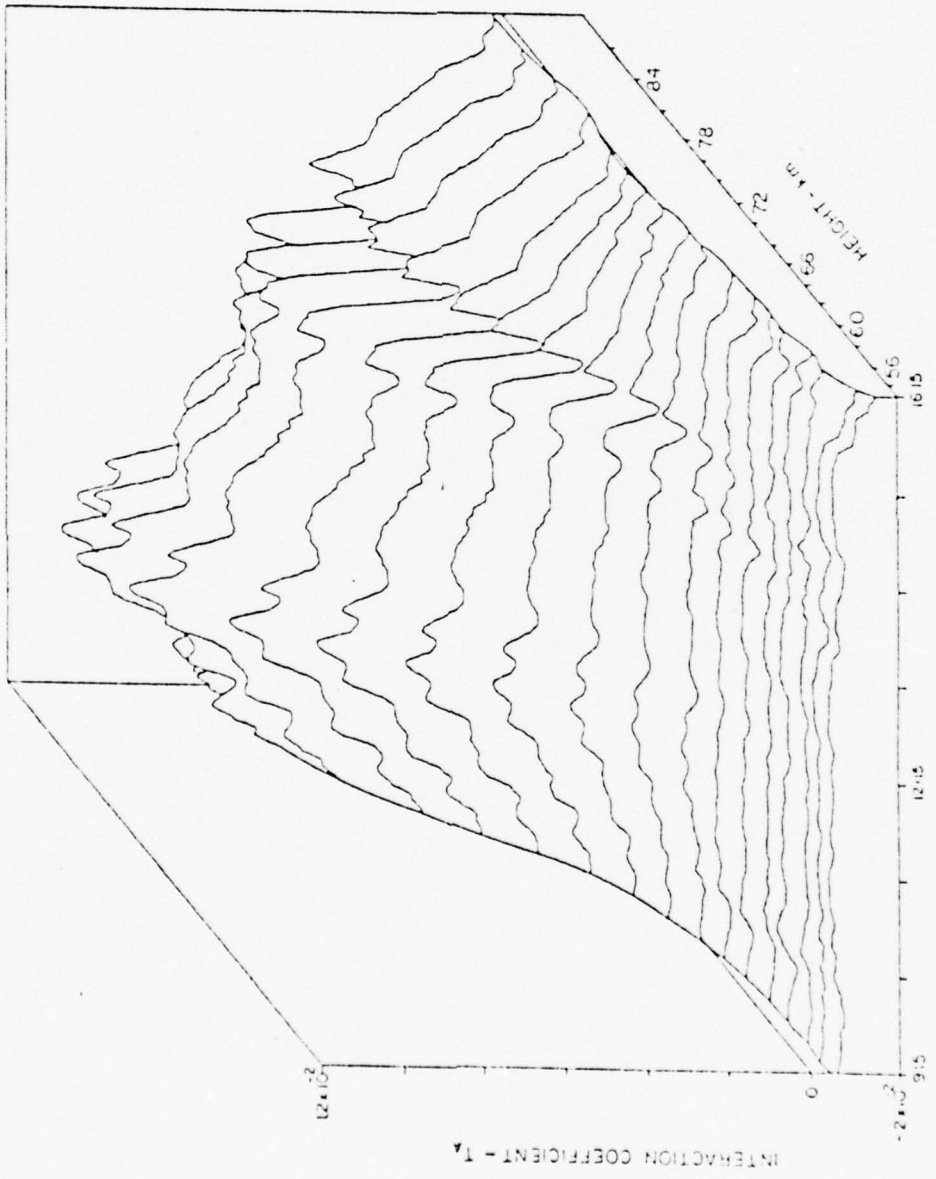

Figure 4.2 Three-dimensional wave interaction data, (quiet day, January 31, 1976, State College)

upon computer availability. If atmospheric wave structure information is required, then the output of the condensing program is put through a fast Fourier transform into Stage III for a display of the spectral data. Figure 4.3 is such a "3-D" presentation corresponding to the data of Figure 4.2. Note, periods of atmospheric waves range from 7 hours to .35 hours with correlation of the peaks with altitude. An output from the condensing program can be transferred to the Dale-Shellman synthesis routine described earlier in Section 3 for generation of electron density profiles versus time. It should be noted that all the results presented in this section were obtained from Dale's synthesis method. All of these stages, of course, contribute to the immense flexibility of the experiment to support a number of programs suggested in Stage VI.

Figure 4.4 shows the diurnal variation of electron densities at various altitudes for the quiet day of January 31, 1976.

Figure 4.5 shows a 3-D display of all-day wave interaction data on March 27, 1976 during the recovery phase of a geomagnetic storm which followed auroral activity. The important features are the extremely increased negative cross-modulation at low heights during the earlier times which indicate production is not solar and probably electron precipitation; lack of a clear diurnal feature as in Figure 4.2 since electron precipitation dominated over solar control. Figure 4.6 displays a few electron density profiles which correspond to larger densities of such disturbed day compared to these of normal quiet conditions.

It is evident from the illustrations given in this section that the all-digitalized wave interaction experimental facilities now possess the time and height resolutions capable of determining temporal variations of electron densities as well as studying wave motions in the D-region ionosphere under normal quiet and disturbed conditions.

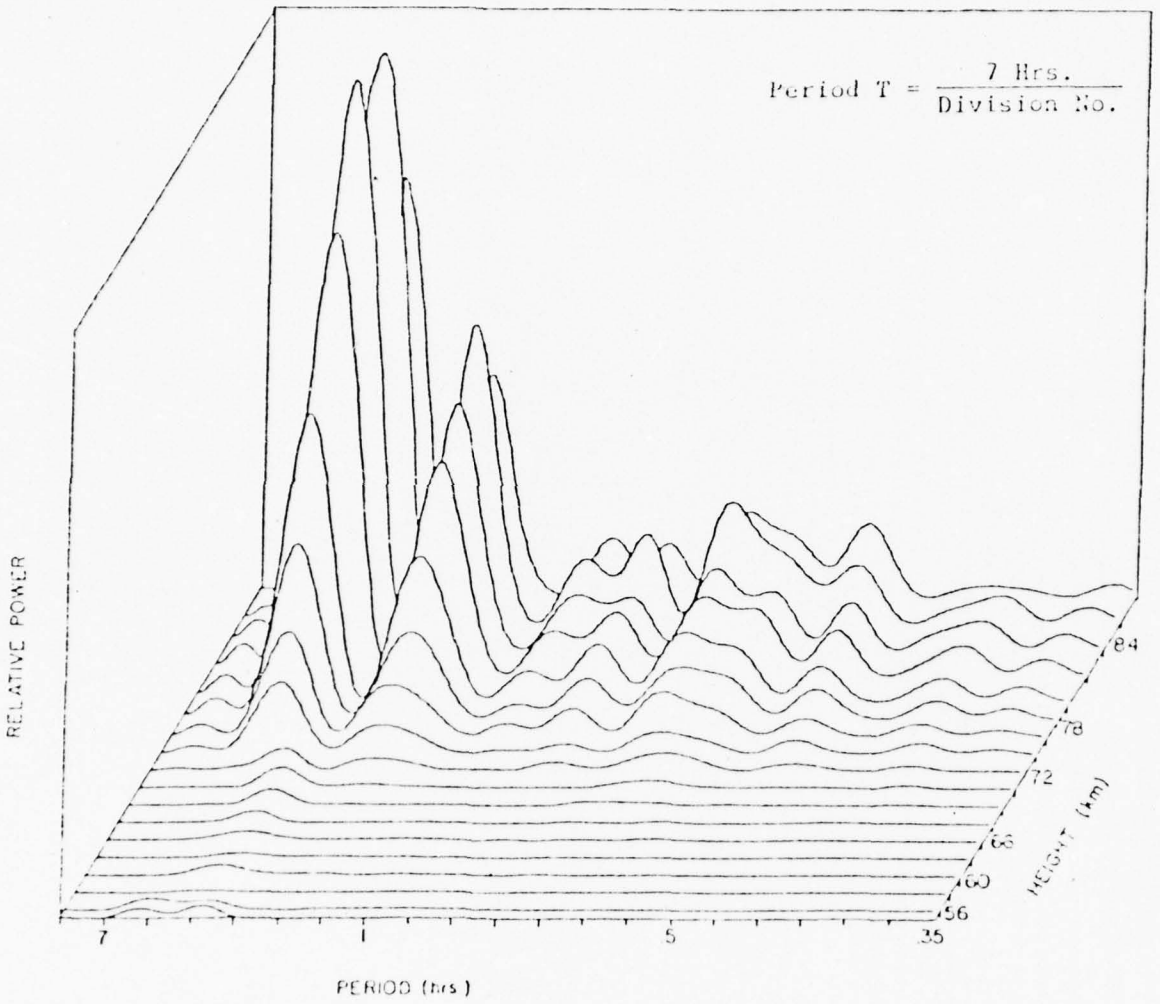

Figure 4.3 Power spectra of three-dimensional data (quiet day, January 31, 1976, State College)

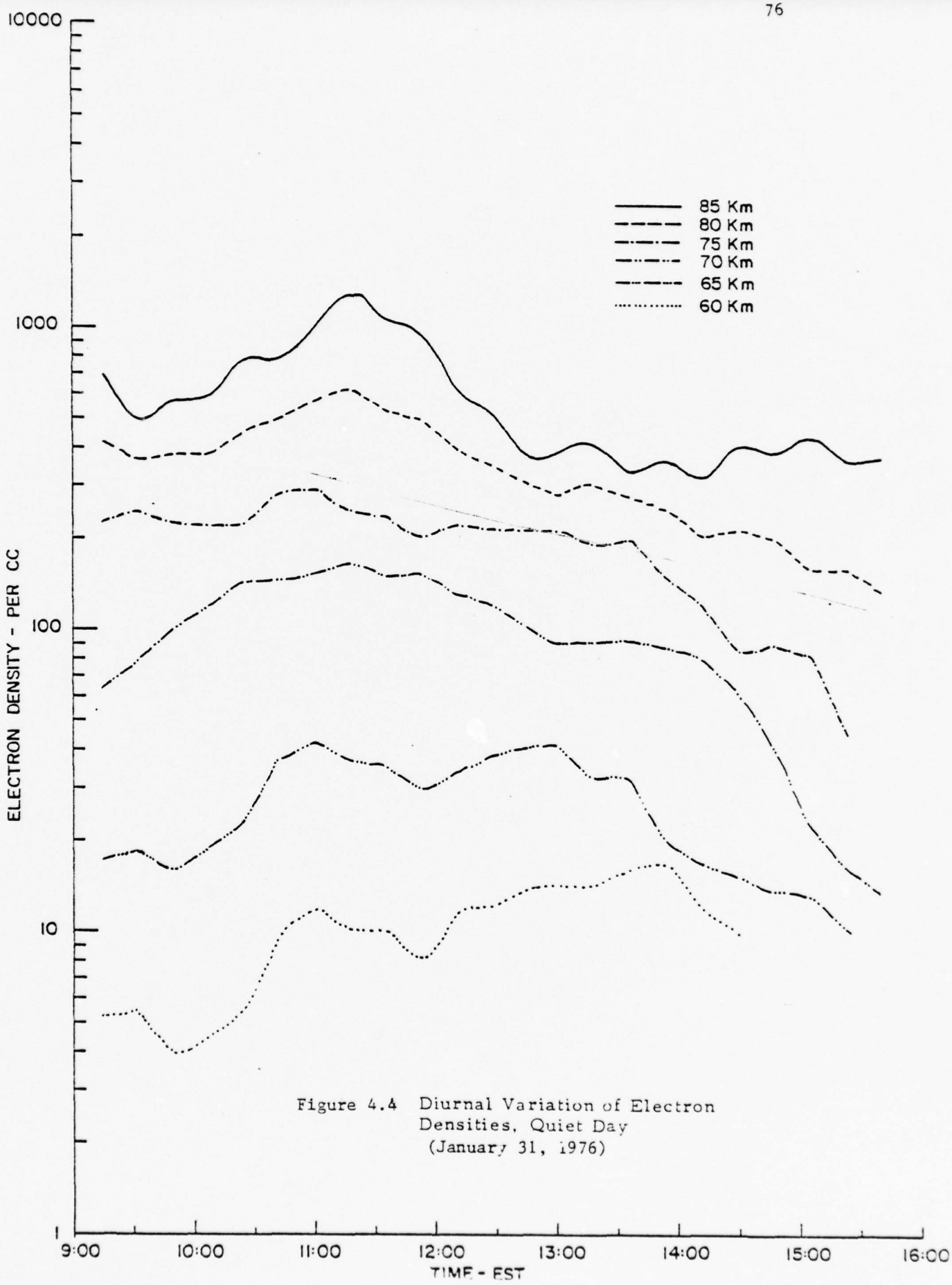

Figure 4.4 Diurnal Variation of Electron Densities, Quiet Day (January 31, 1976)

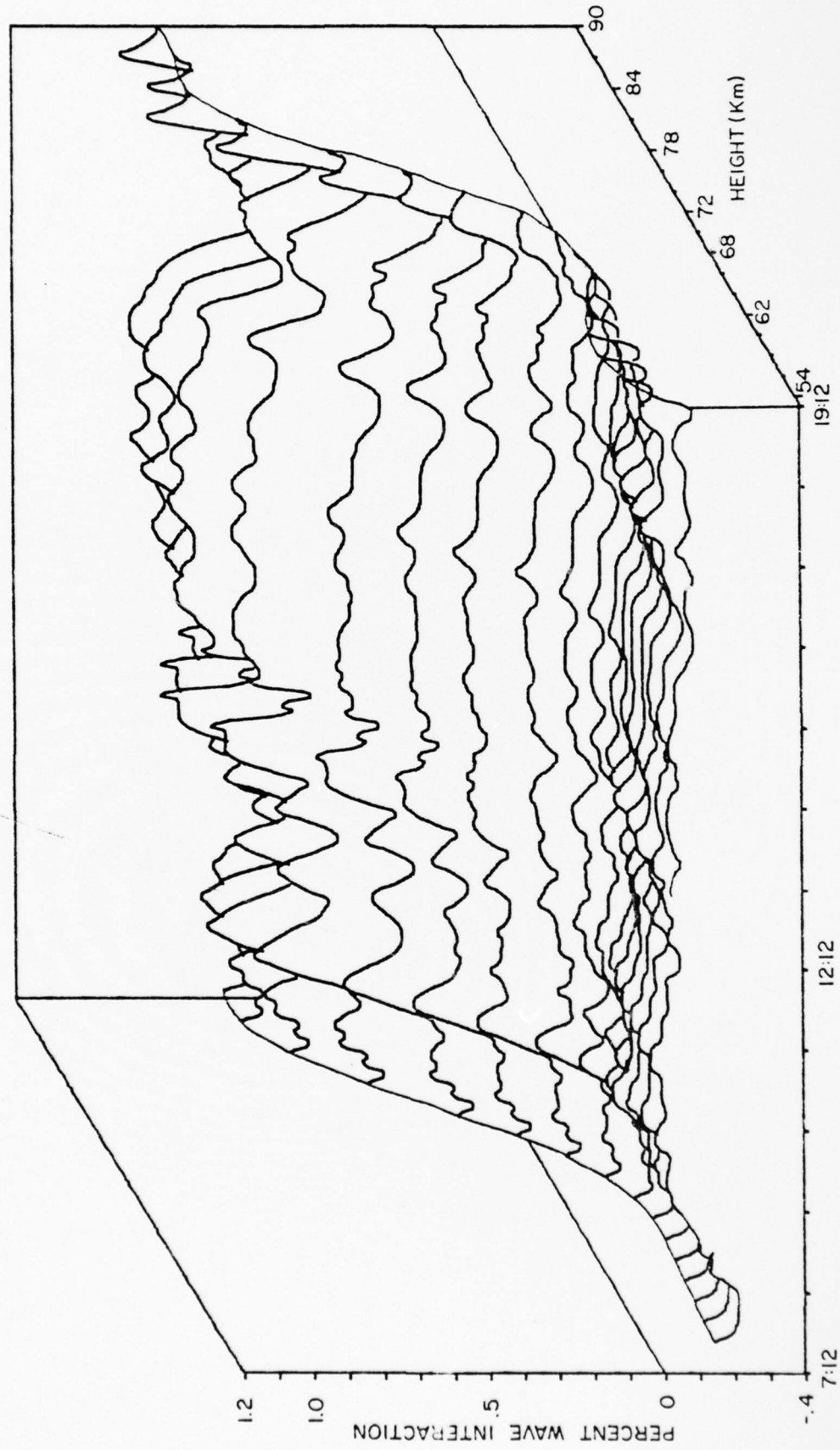

Figure 4.5 Three-dimensional plot of Scotia wave interaction data, electron precipitation event

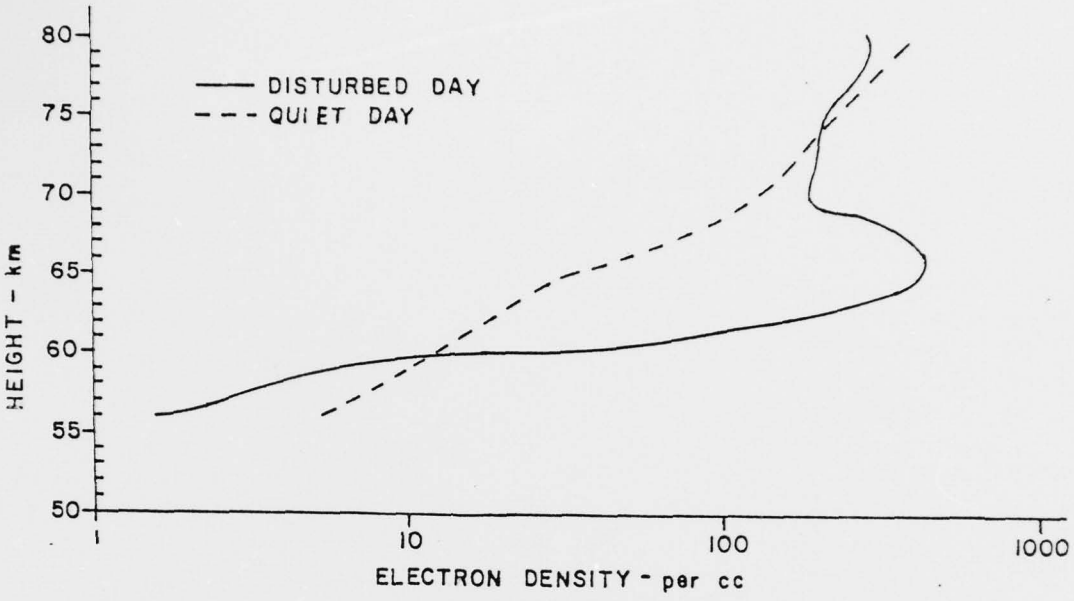

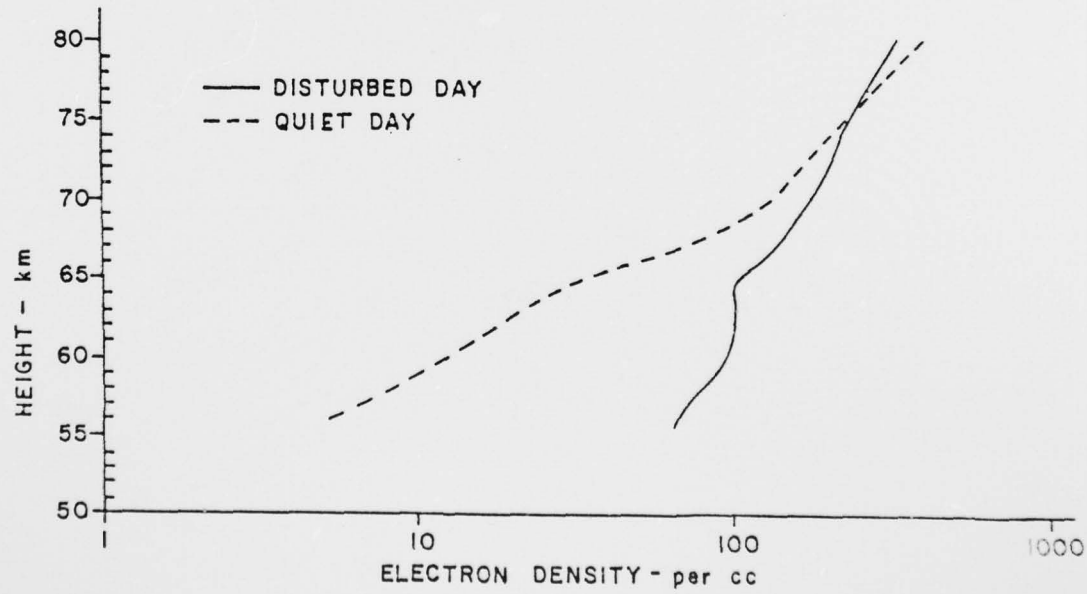

Figure 4.6 Comparison of Disturbed Day Electron Density Profiles (March 27, 1976) with Quiet Day Profiles (January 31, 1976)

Appendix

This appendix contains fifteen additional figures showing the results of intercomparison between the Dale and the Shellman electron density synthesis methods described earlier in Section 3.

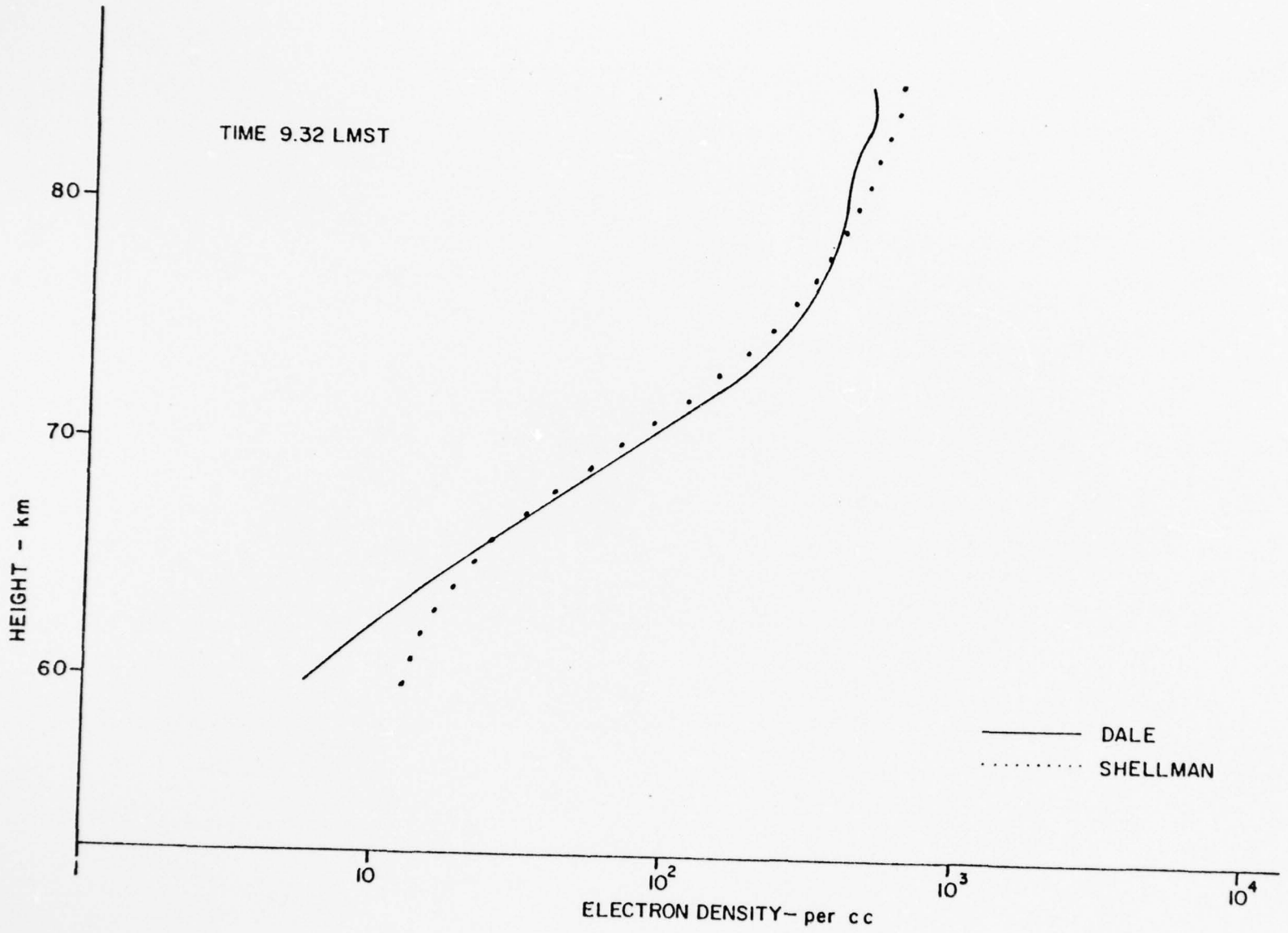
TIME 9.32 LMST
80
70
60
HEIGHT - km
1
10
10^2
10^3
10^4
ELECTRON DENSITY– per cc
DALE
SHELLMAN

FIGURE I-A

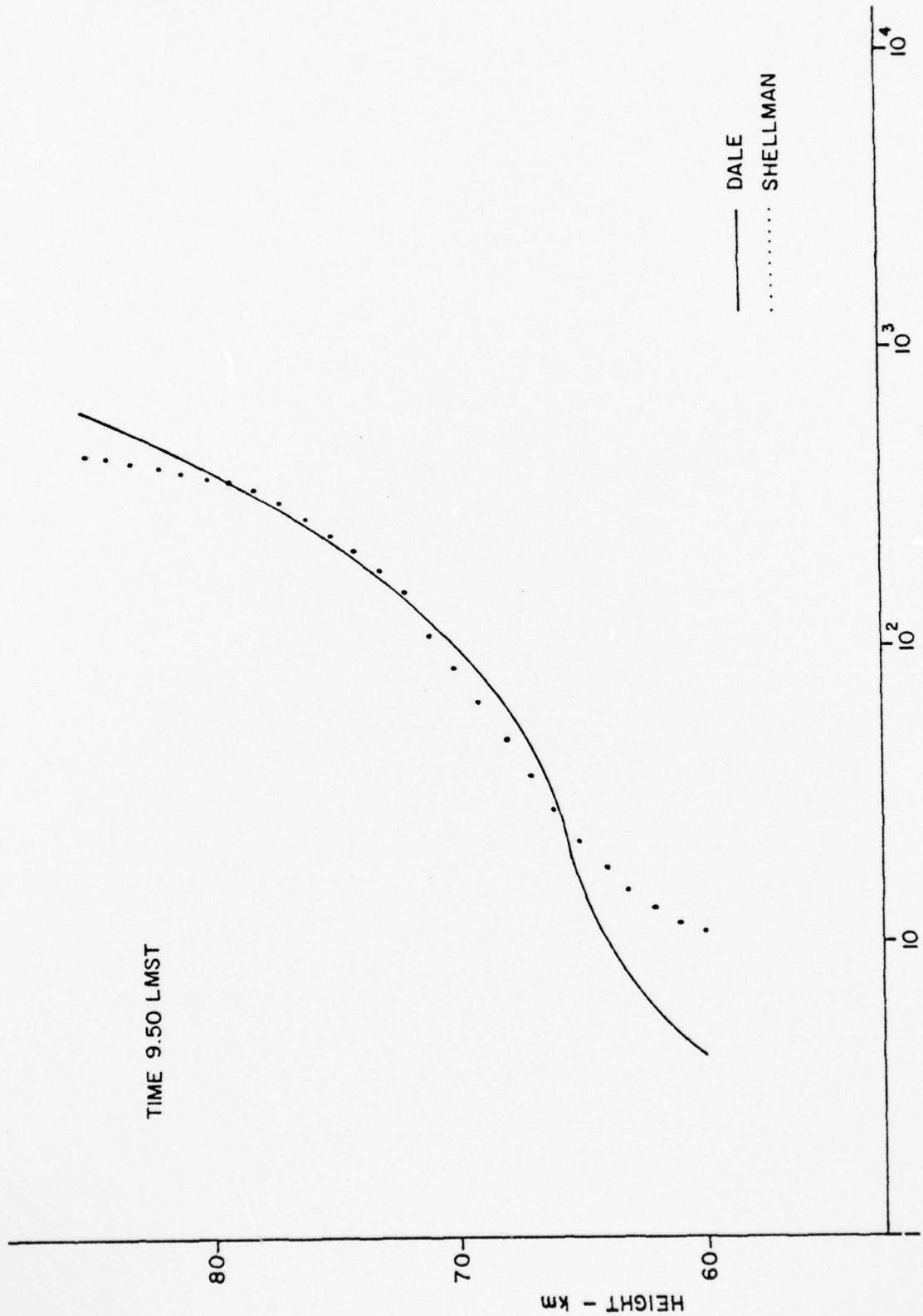
TIME 9.50 LMST
HEIGHT - km
80
70
60
ELECTRON DENSITY- per cc
1
10
10^2
10^3
10^4
DALE
SHELLMAN

FIGURE 2-A

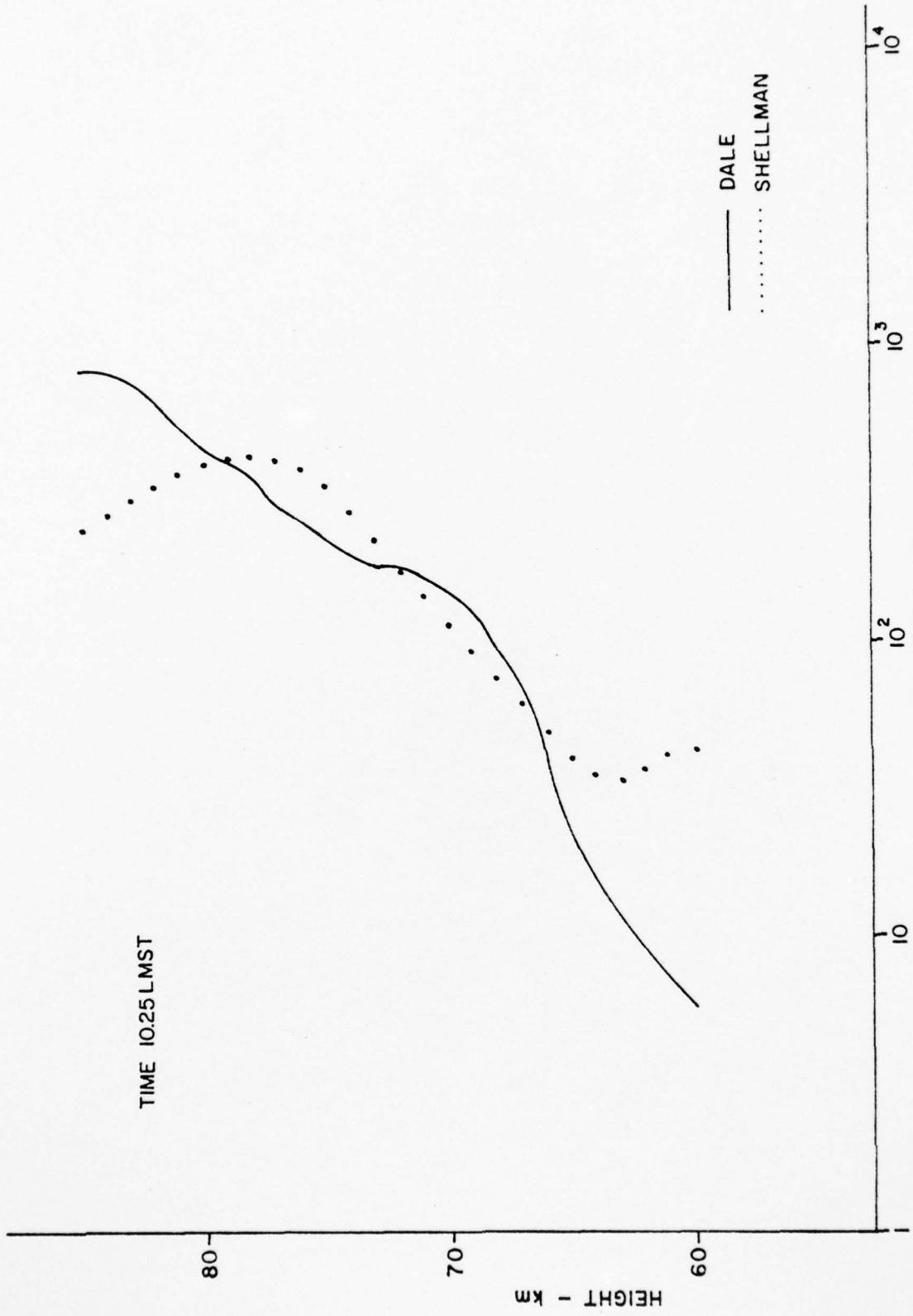
TIME 10.25 LMST
HEIGHT - km
60
70
80
ELECTRON DENSITY - per c c
1
10
10^2
10^3
10^4
DALE
SHELLMAN

FIGURE 3-A

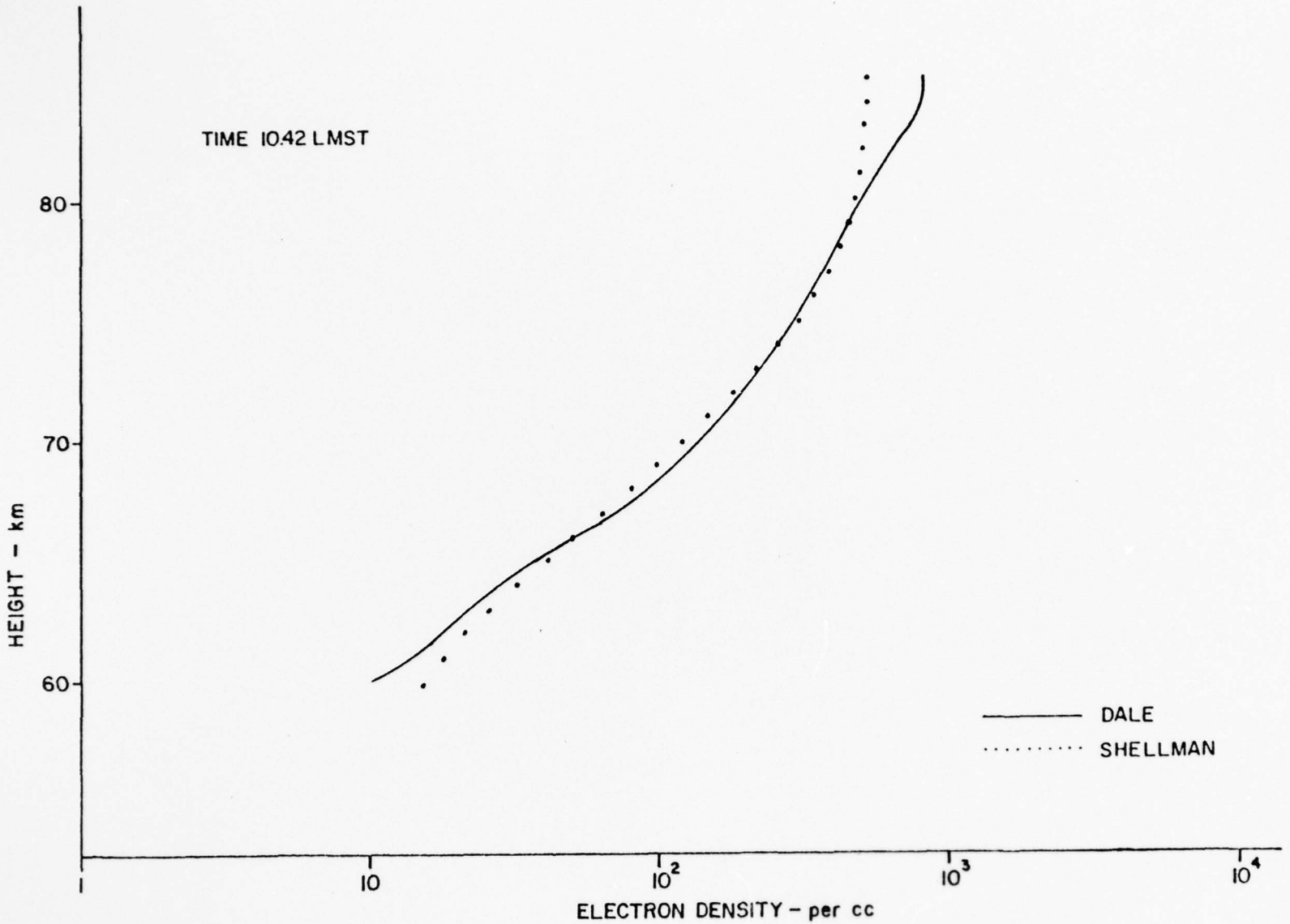
TIME 10.42 LMST
80
70
60
HEIGHT - km
10
10^2
10^3
10^4
ELECTRON DENSITY - per cc
DALE
SHELLMAN

FIGURE 4-A

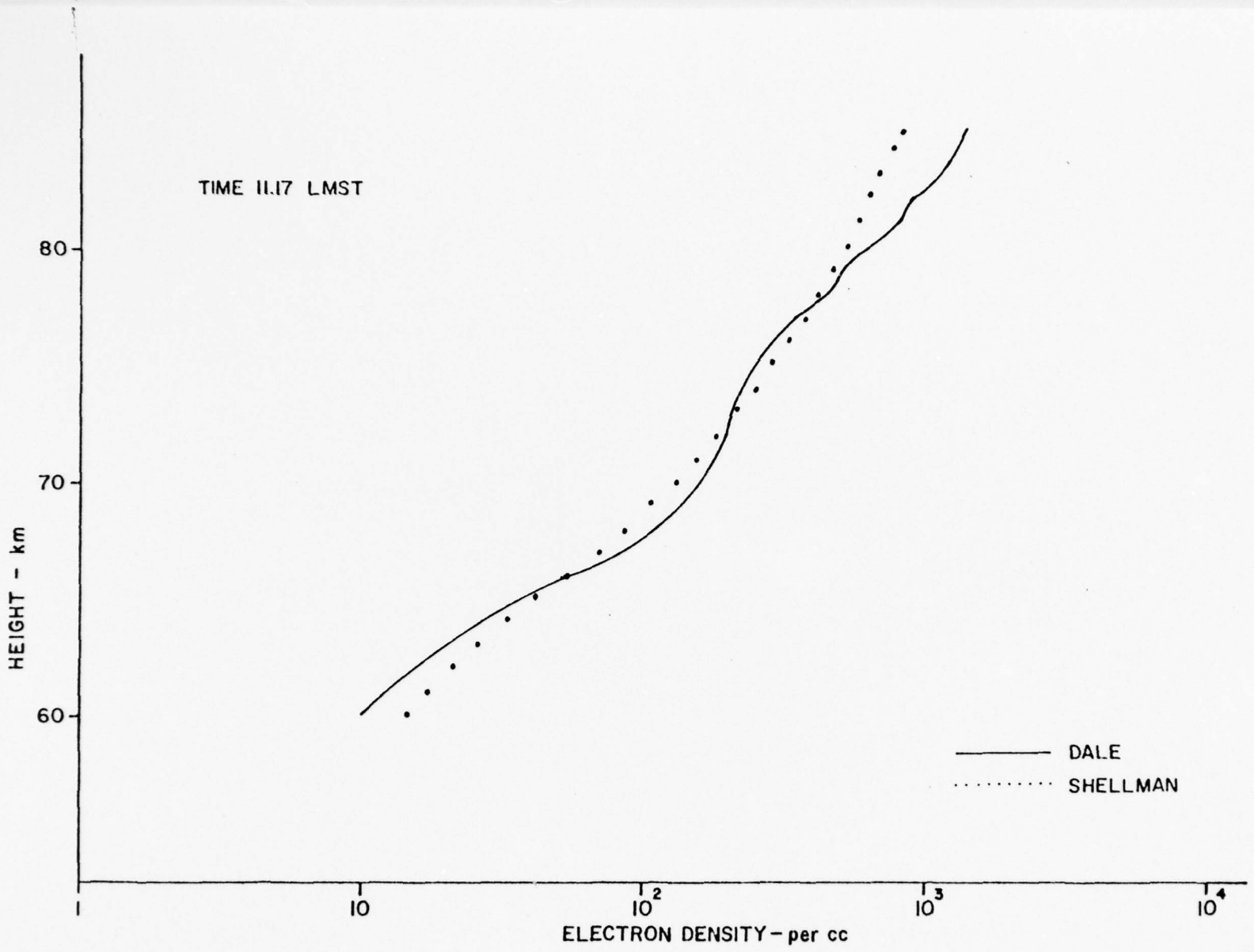
TIME 11.17 LMST
80
70
60
HEIGHT - km
1
10
10^2
10^3
10^4
ELECTRON DENSITY – per cc
DALE
SHELLMAN

FIGURE 5-A

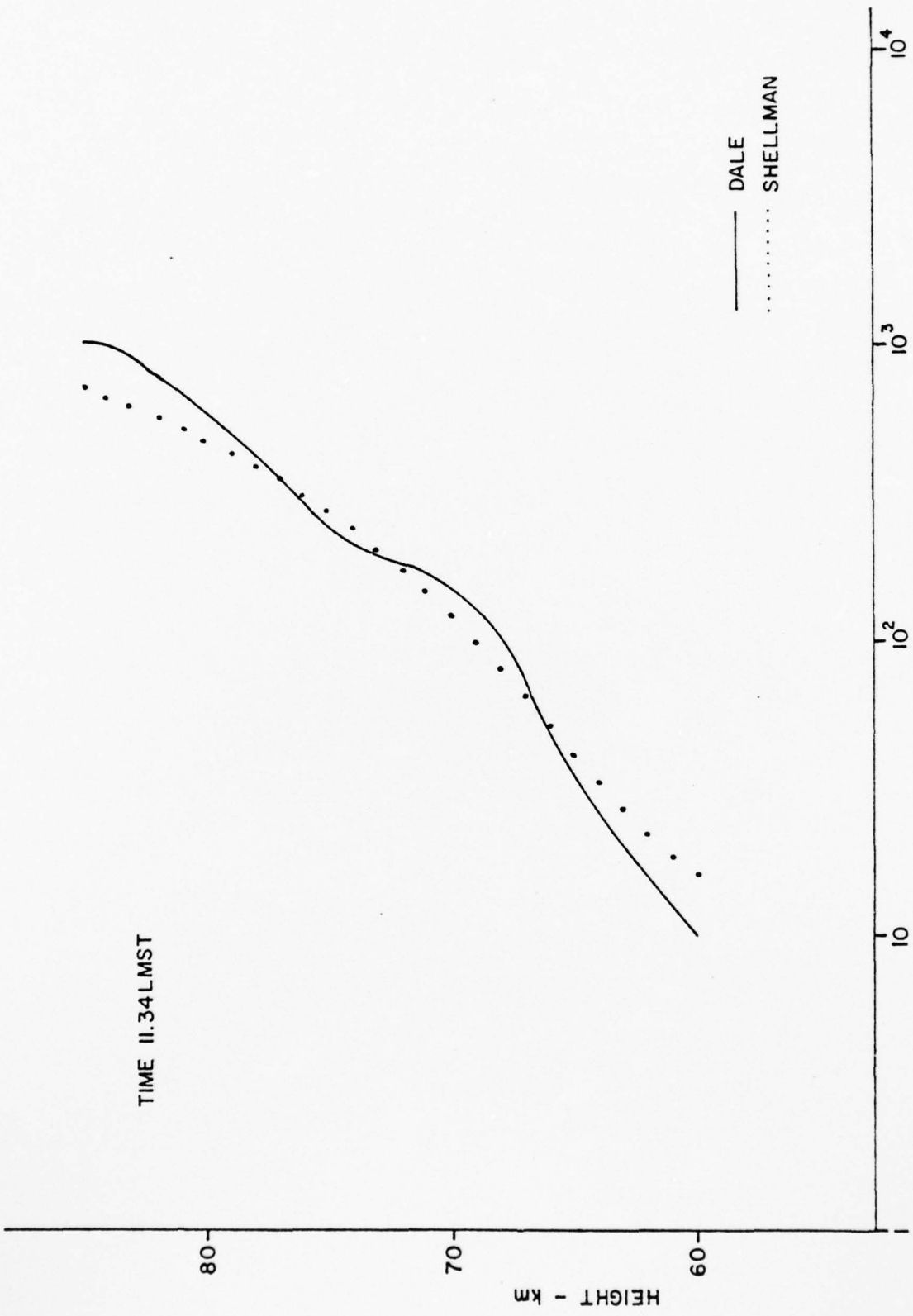
TIME 11.34 LMST
HEIGHT - km
80
70
60
10
10^2
10^3
10^4
ELECTRON DENSITY – per c c
DALE
SHELLMAN

FIGURE 6-A

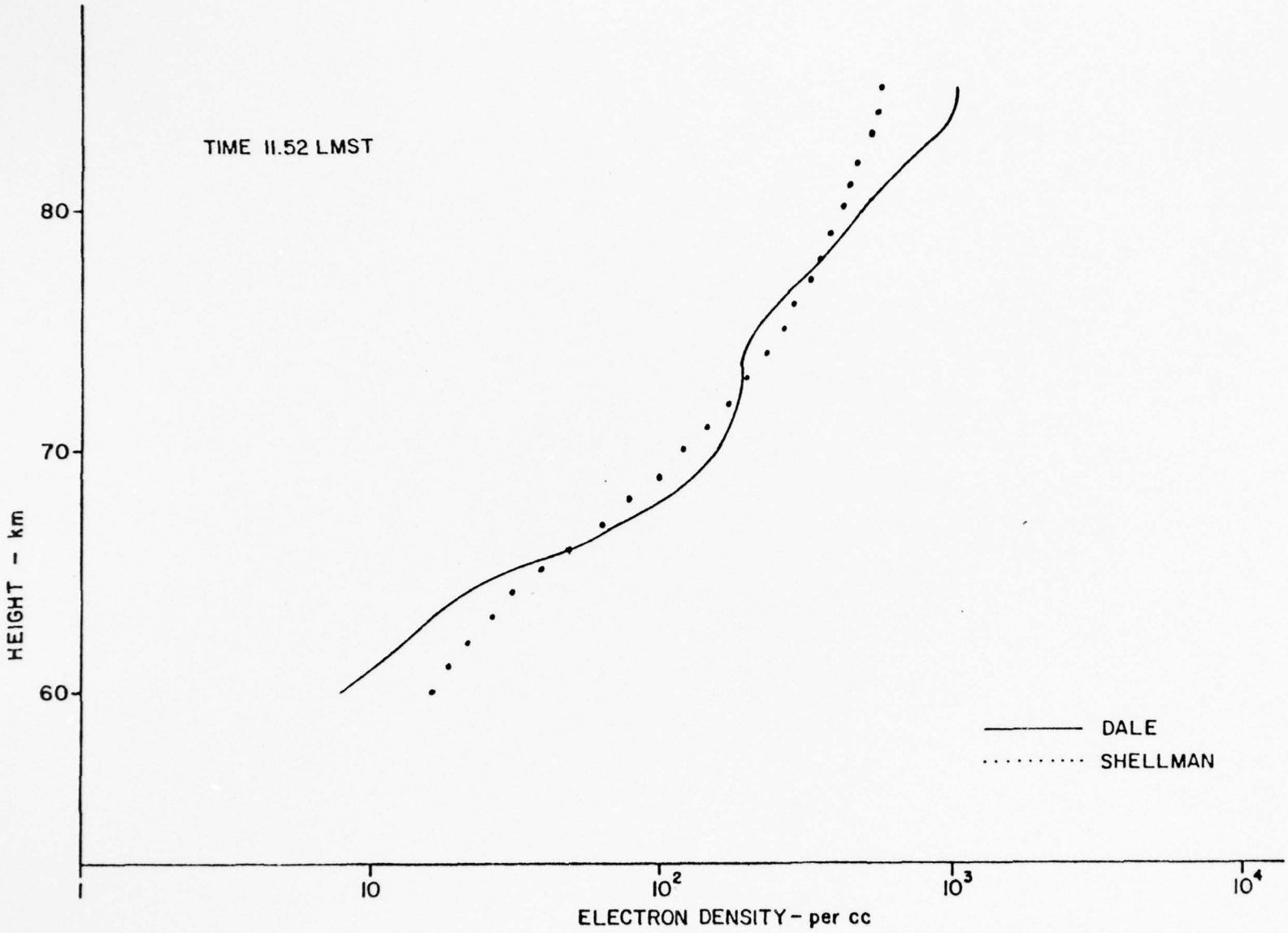
TIME 11.52 LMST
80
70
60
HEIGHT - km
1
10
10^2
10^3
10^4
ELECTRON DENSITY - per cc
DALE
SHELLMAN

FIGURE 7-A

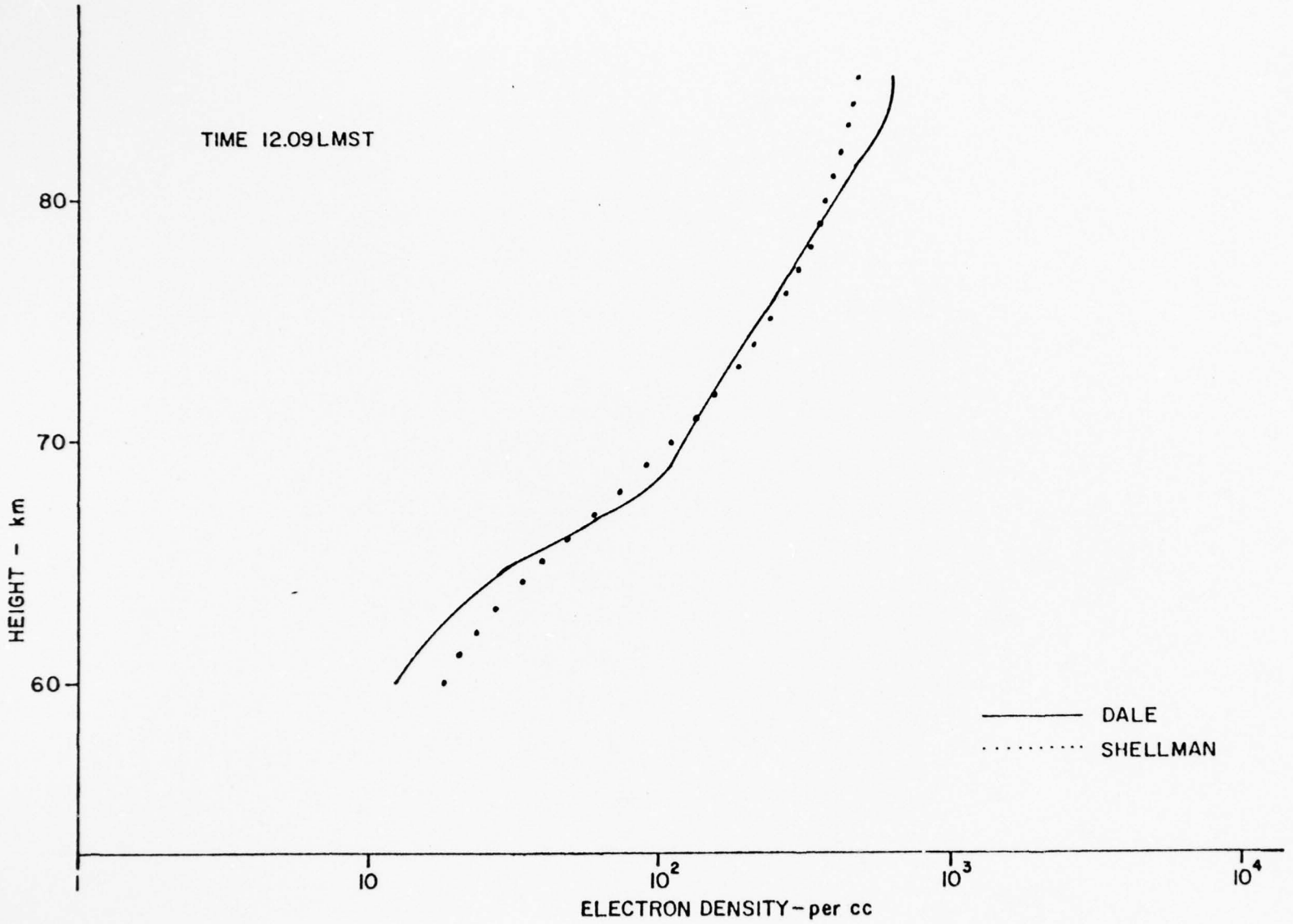
TIME 12.09 LMST
80
70
60
HEIGHT - km
1
10
10^2
10^3
10^4
ELECTRON DENSITY - per cc
DALE
SHELLMAN

FIGURE 8-A

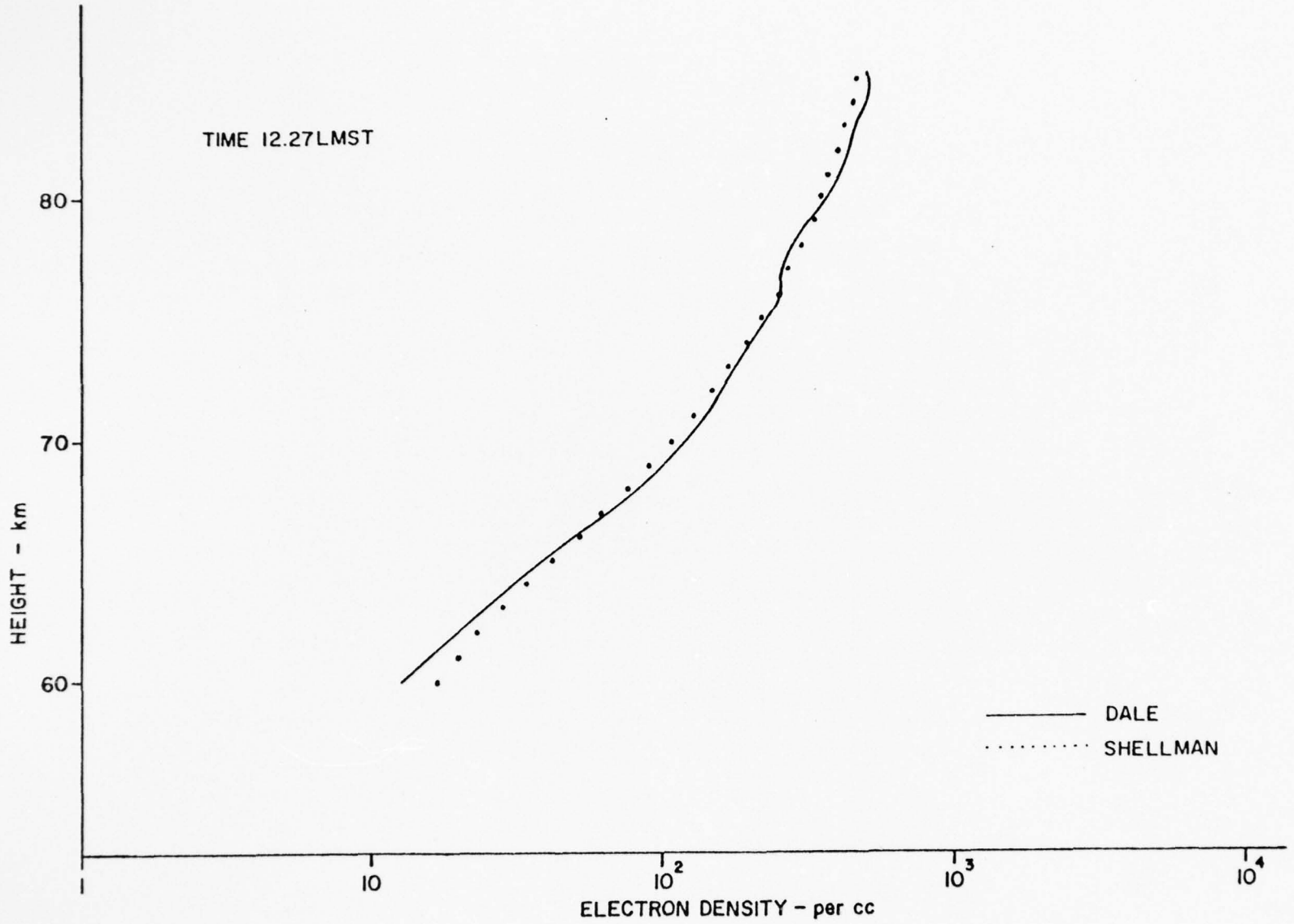
TIME 12.27LMST
80
70
60
HEIGHT - km
1
10
10^2
10^3
10^4
ELECTRON DENSITY - per cc
DALE
SHELLMAN

FIGURE 9-A

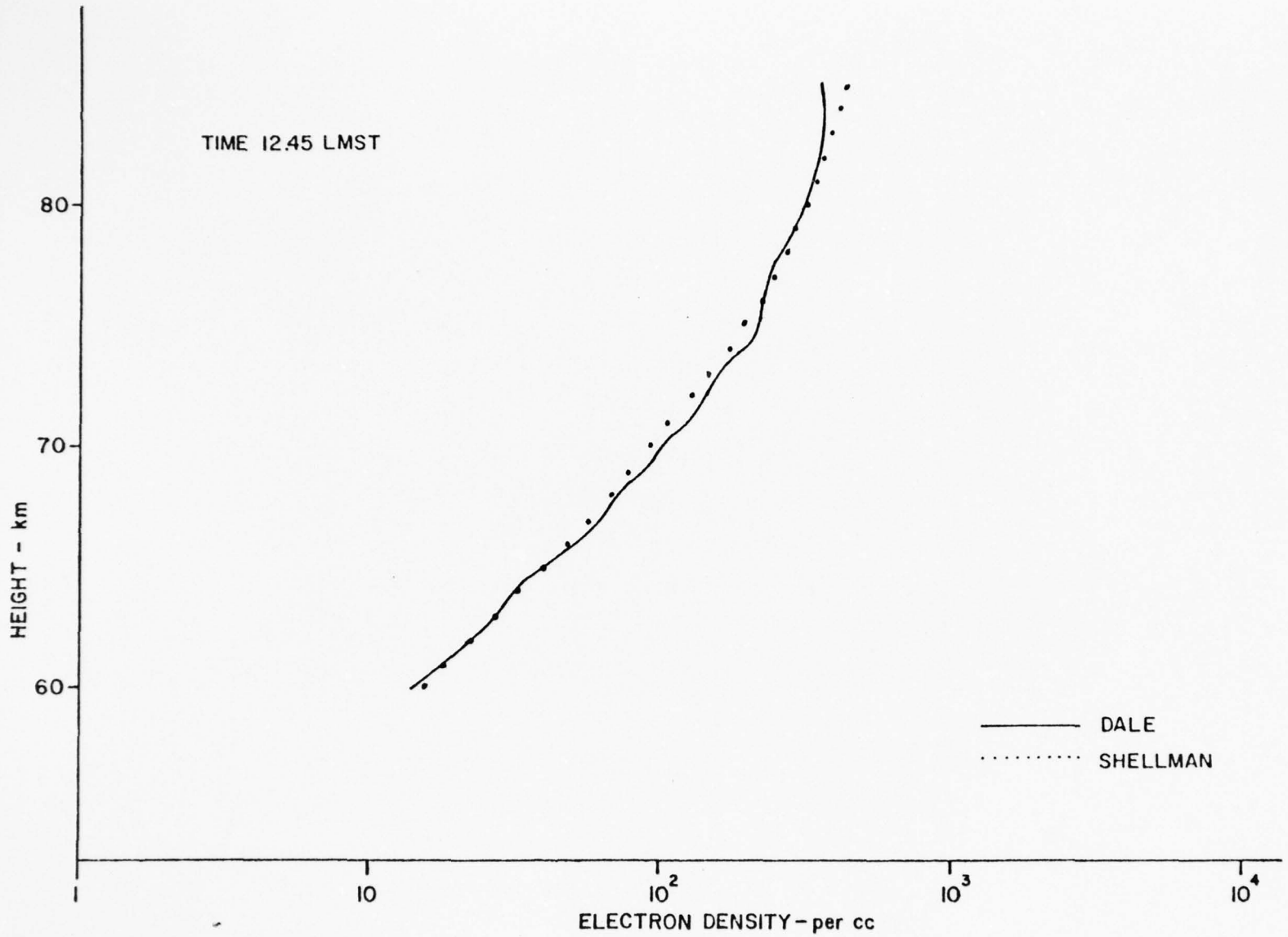
TIME 12.45 LMST
80
70
60
HEIGHT - km
1
10
10^2
10^3
10^4
ELECTRON DENSITY - per cc
DALE
SHELLMAN

FIGURE 10-A

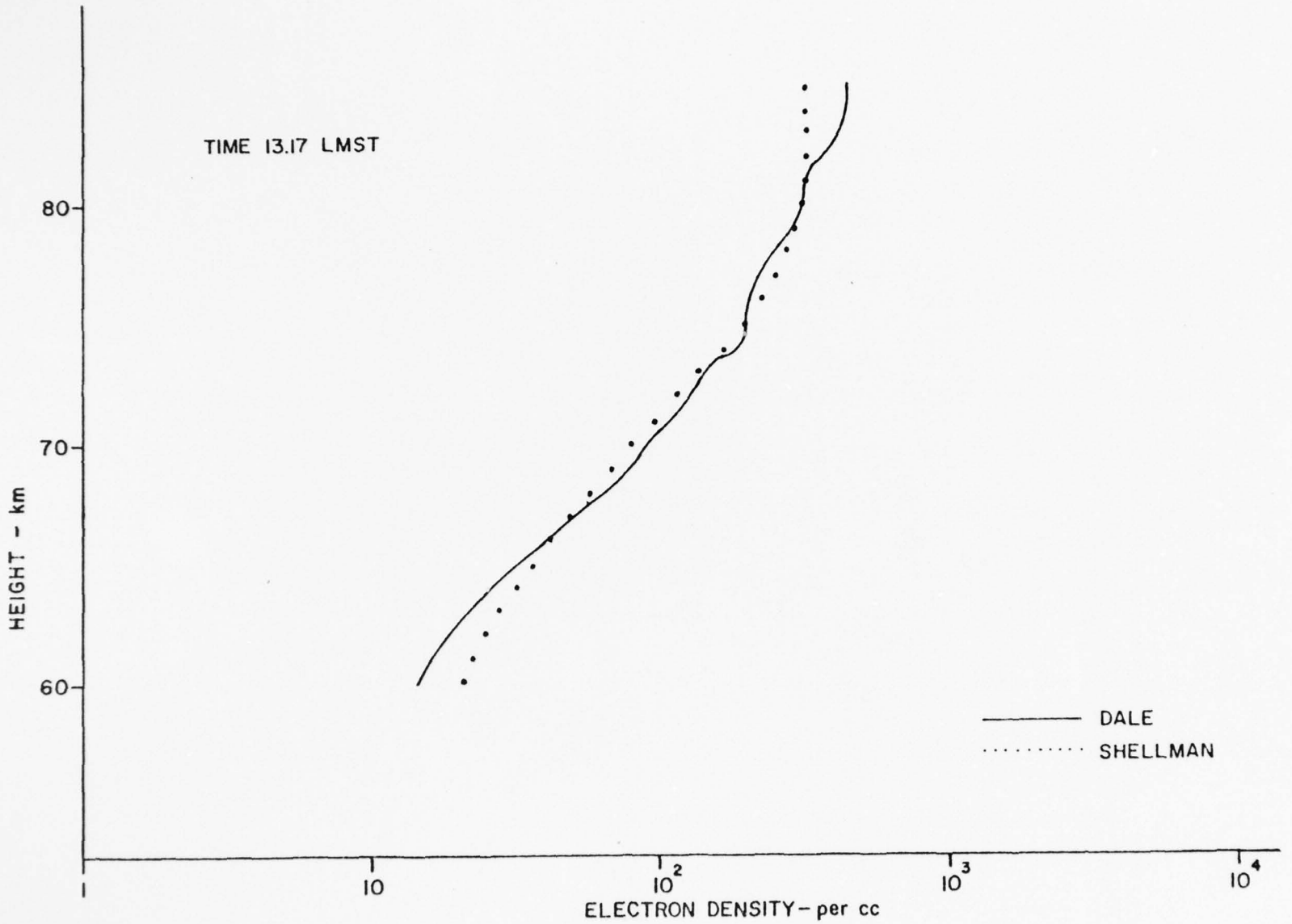
TIME 13.17 LMST
80
70
60
HEIGHT - km
1
10
10^2
10^3
10^4
ELECTRON DENSITY - per cc
DALE
SHELLMAN

FIGURE II-A

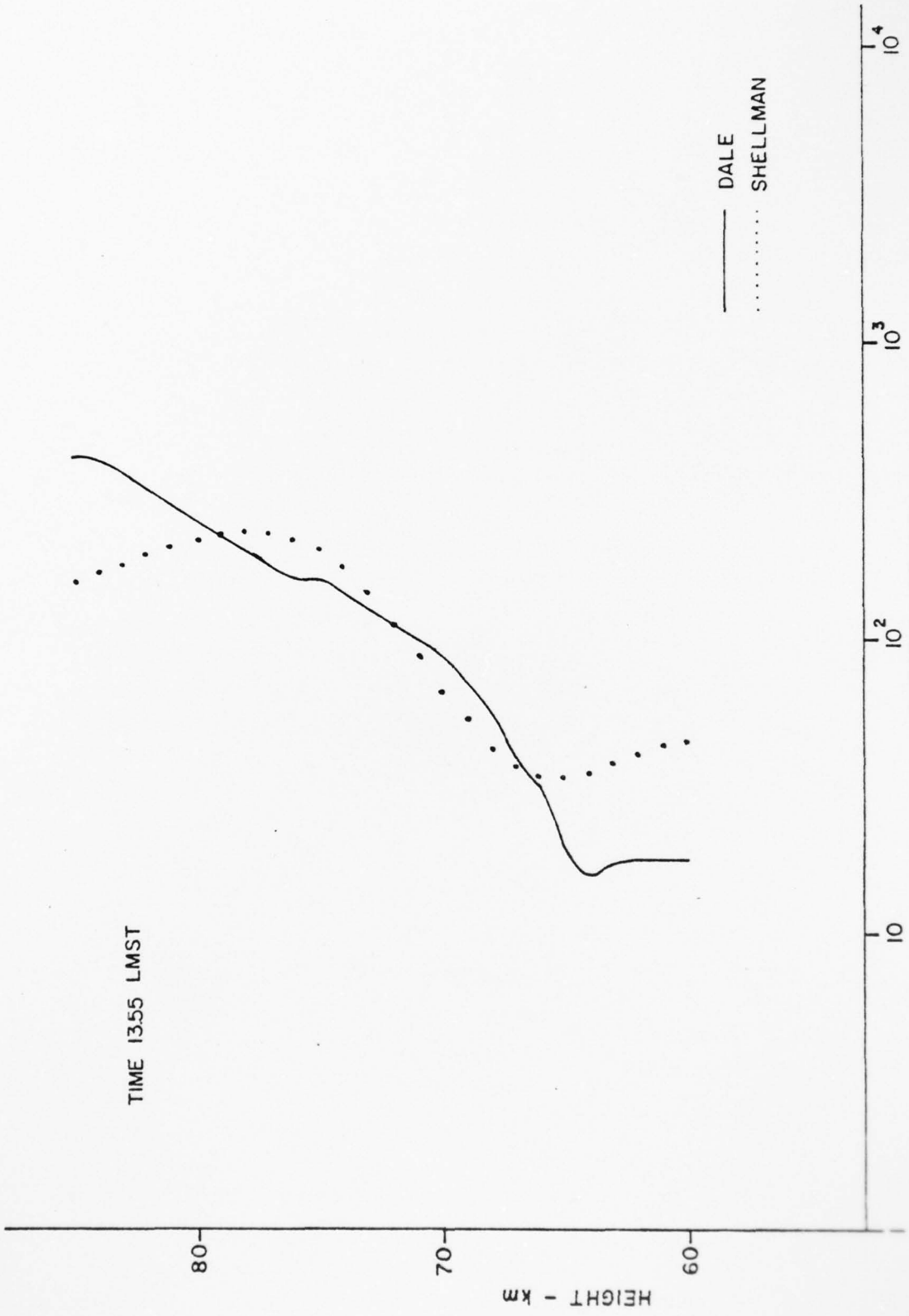
DALE
SHELLMAN
TIME 1355 LMST
HEIGHT - km
80
70
60
10
10^2
10^3
10^4
ELECTRON DENSITY - per cc

FIGURE 12-A

AD-A038 413 PENNSYLVANIA STATE UNIV UNIVERSITY PARK IONOSPHERE R--ETC F/G 4/1
STUDY OF D-REGION IONOSPHERE USING RADIO WAVE INTERACTION TECHN--ETC(U)
FEB 77 H S LEE, A J FERRARO N00014-75-C-0178

UNCLASSIFIED PSU-IRL-FR-77/1 NL

2 OF 2
AD
A038413

END

DATE
FILMED
5 - 77

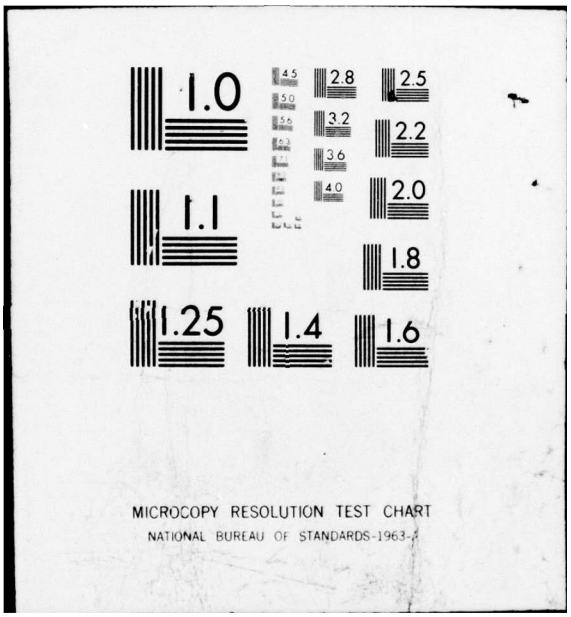
1.0
1.1
1.25
1.4
1.6
1.8
2.0
2.2
2.5
2.8
3.2
3.6
4.0
4.5
5.0
5.6
6.3
7.1
8.0
MICROCOPY RESOLUTION TEST CHART
NATIONAL BUREAU OF STANDARDS-1963-A

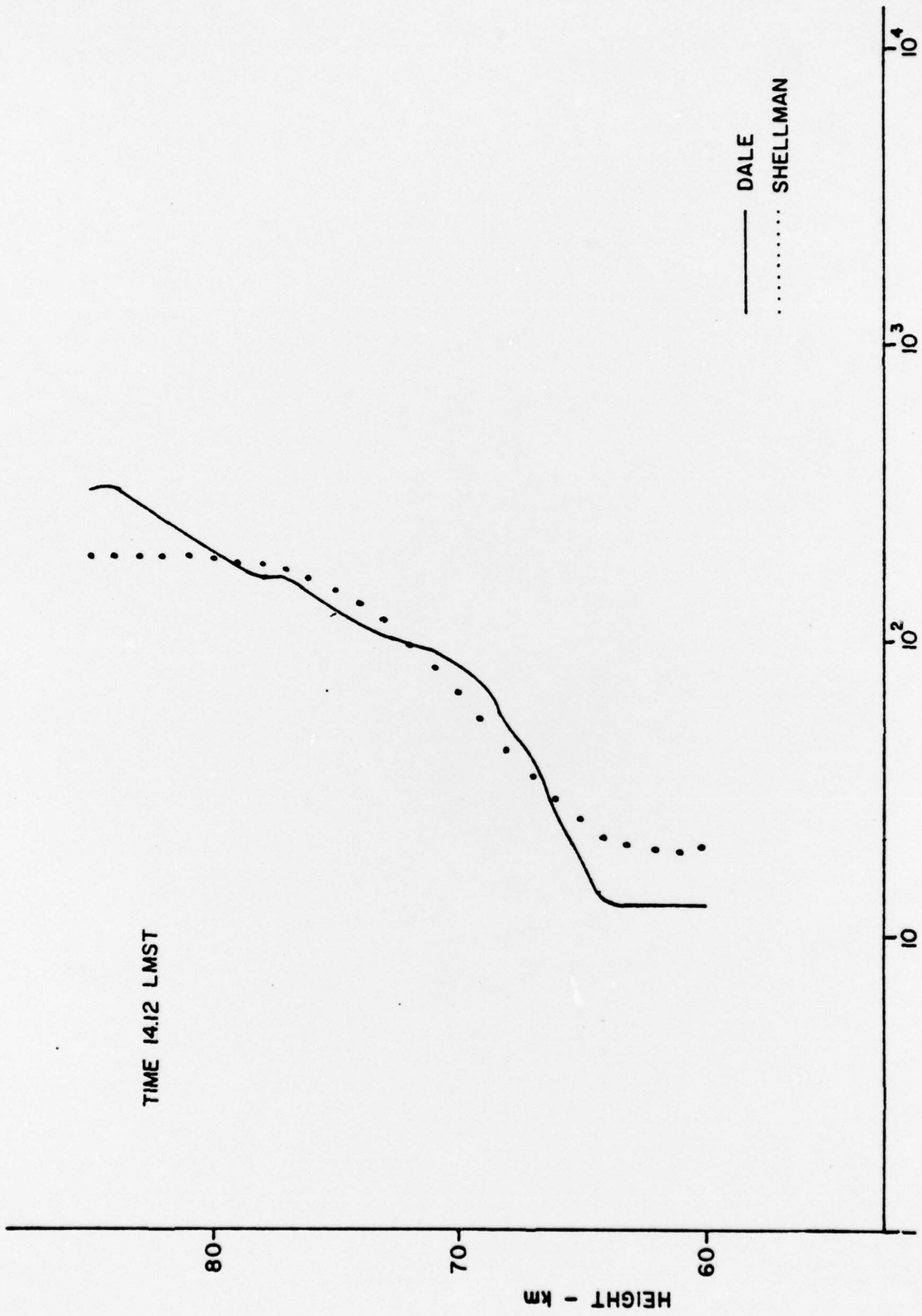
DALE
SHELLMAN
TIME 14.12 LMST
HEIGHT - km
80
70
60
1
10
10^2
10^3
10^4
ELECTRON DENSITY – per c c

FIGURE 13-A

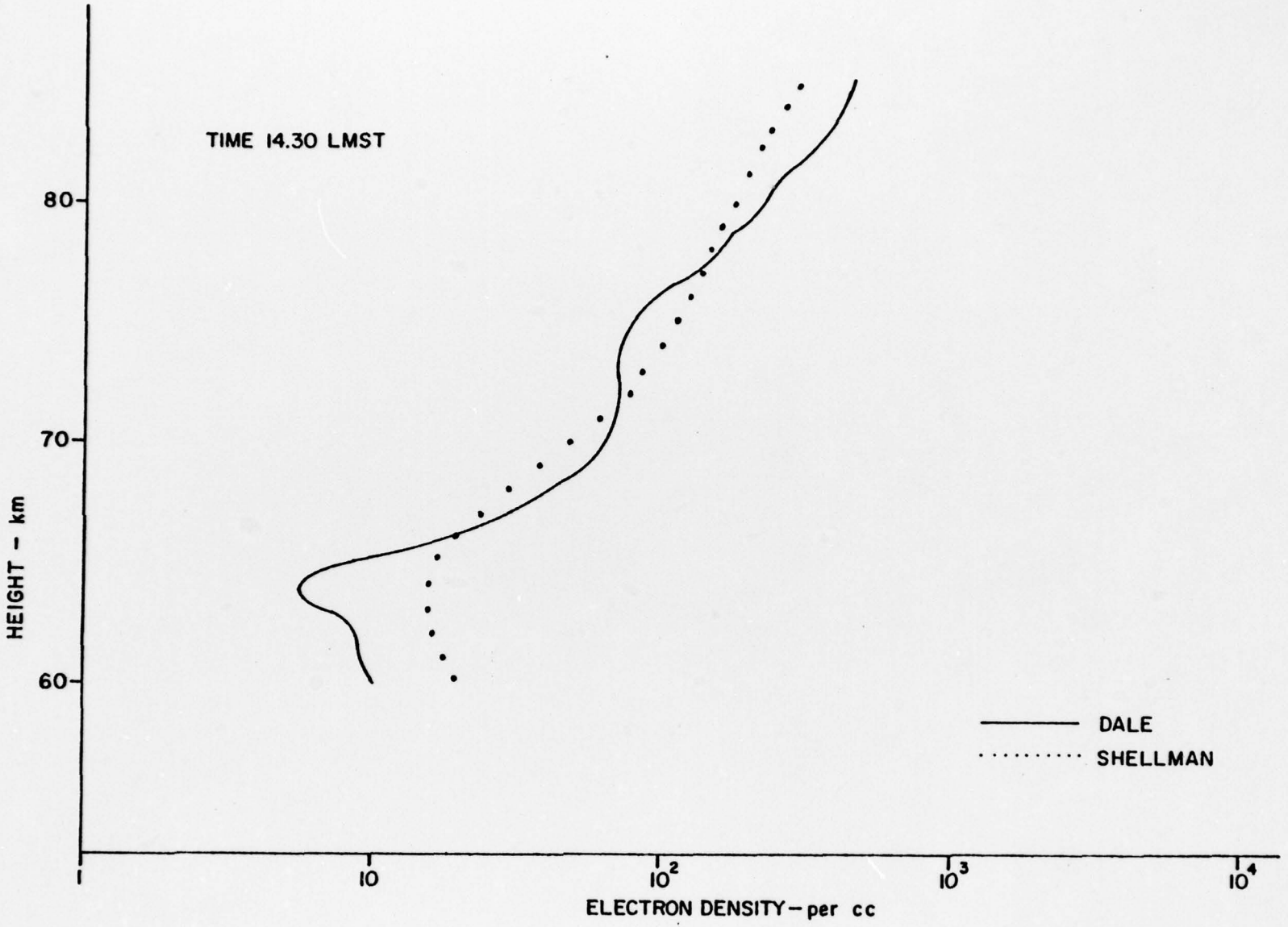
TIME 14.30 LMST
80
70
60
HEIGHT - km
1
10
10^2
10^3
10^4
ELECTRON DENSITY – per cc
DALE
SHELLMAN

FIGURE 14-A

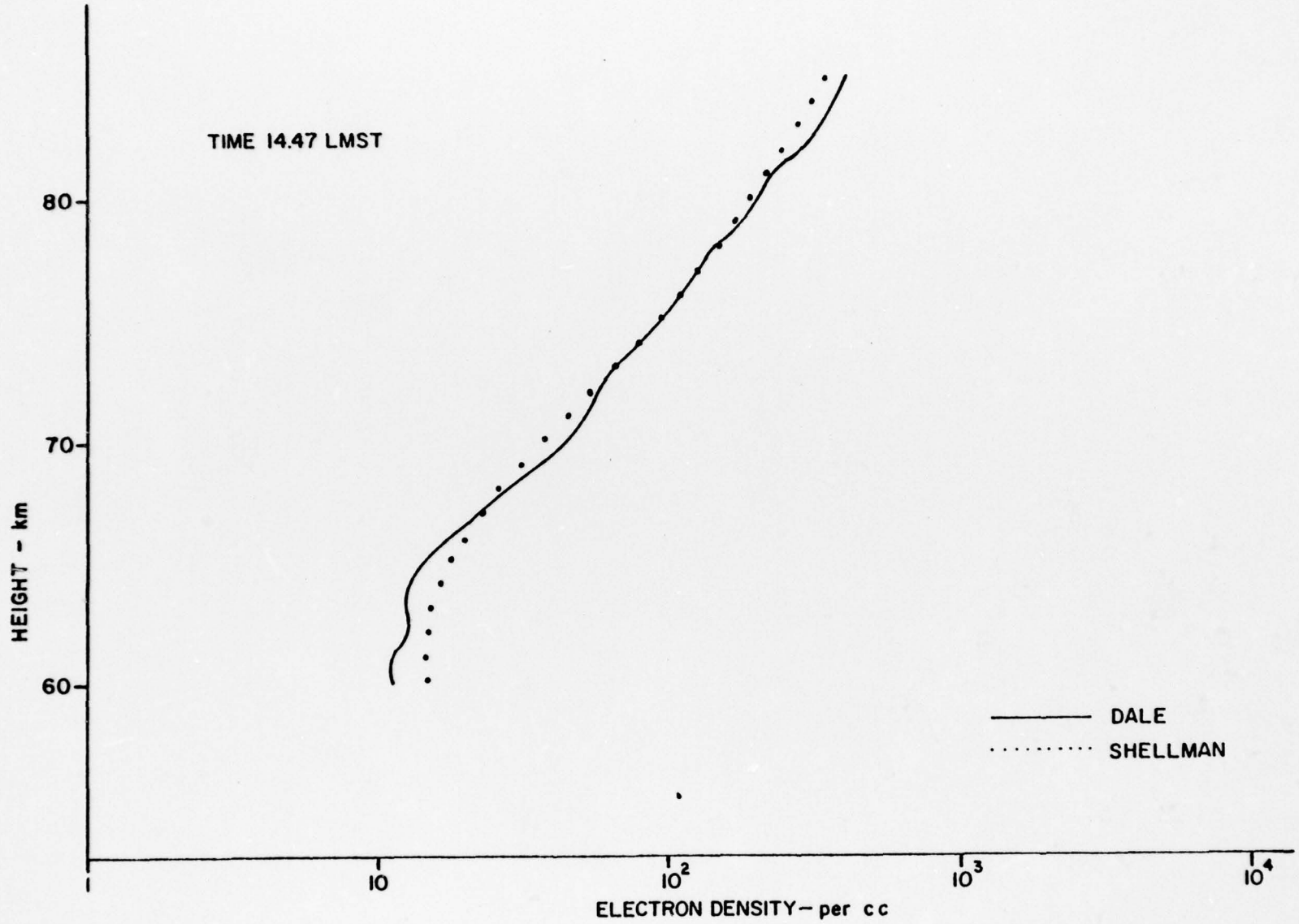
TIME 14.47 LMST
80
70
60
HEIGHT - km
1
10
10^2
10^3
10^4
ELECTRON DENSITY – per c c
DALE
SHELLMAN

FIGURE 15-A

References

Blackman, R. B. and J. W. Tuckey, The measurement of power spectra, Dover Publications, Inc., New York, 1959.

Carlson, A. B., Communication Systems: Air introduction to signals and noise in electrical communication, McGraw-Hill Book Co., New York, 1968.

Dale, S. P., Profile inversion technique for the determination of electron density from wave interaction data, PSU-IRL-SCI-417, Ionosphere Research Laboratory, The Pennsylvania State University, 1973.

Gossard, E. E. and M. R. Paulson, Movement of off-path ionospheric irregularities deduced from short-path VLF measurements, J. Atmos. Terr. Phys., 30, 1795-1807, 1968.

Gossard, E. E. and W. H. Hooke, Waves in the atmosphere, American Elsevier Publishing Co., New York, 1975.

Hines, C. O., Internal atmospheric gravity waves at ionospheric heights, Can. J. Phys., 38, 1441-1480, 1960.

Lance, G. N., Numerical methods for high speed computors, Iliffe, 134-138, London, 1960.

Lee, H. S. and A. J. Ferraro, Winter D-region electron concentration and collision frequency features obtained with high-power interaction measurements, J. Geophys. Res., 74, 1184-1194, 1969.

Marquardt, D. W., An algorithm for least squares estimation of non-linear parameters, J. Soc. Indust. Appl. Math., 11, 431-441, 1963.

Marquardt, D. W., Least squares estimation of non-linear parameters, Share Program Library, 360D-13.6.007, March 1971.

Moursand, D. G. and C. S. Davis, Elementary theory and application of numerical analysis, McGrawOHill Book Co., New York, 1967.

Shellman, C. H., Determination of D-region electron-density distribution from radio propagation data, Naval Electronics Laboratory Technical Report 1856, 1973.

Swanson, K. E., Digitization and automation of the wave interaction and partial reflection experiments at Scotia, M.S. Thesis in Electrical Engineering, The Pennsylvania State University, 1976.

Thome, G., Long period waves generated in the polar ionosphere during the onset of magnetic storms, J. Geophys. Res., 73, 6319-6336, 1968.

Valverde, J. F., Motions of large scale travelling disturbances determined from high frequency backscatter and vertical incidence records, Sci. Report No. 1, Radio Propagation Laboratory, Stanford University, 1958.

Wegstein, J., Algorithm 2 (Rootfinder), Communications of the association for computing machinery, 3, February, 1960.

Weisbrod, S., Investigation of phase interaction as a means for the study of the lower ionosphere, PSU-IRL-SCI-206, Ionosphere Research Laboratory, The Pennsylvania State University, 1964.

DISTRIBUTION LIST FOR THE PENNSYLVANIA STATE UNIVERSITY

Contract No. N00014-75-C-0178

18 February 1977

Director
Defense Advanced Research Projects Agency
Architect Building
1400 Wilson Boulevard
Arlington, VA 22209
1 cy Attn: STO LTC G. T. Pepin

Defense Documentation Center
Cameron Station
Alexandria, VA 22314
12 cy Attn: TC

Director
Defense Nuclear Agency
Washington, D. C. 20305
1 cy Attn: RAAE Dow Evelyn
1 cy Attn: Charles Blank

Director of Defense Research and Engineering
Department of Defense
Washington, D. C. 20301
1 cy Attn: DDS & SS R.S. Ruffine

Office of the Assistant Secretary of the Navy (Research & Development)
Pentagon, Room 4E741
Washington, D. C. 20350
1 cy Attn: Dr. T. P. Quinn

U. S. Army Communications Command
C. E. Services Division
Pentagon, Room 1B269
Washington, D. C. 20310
1 cy Attn: CEAO

Chief of Naval Operations
Navy Department
Washington, D. C. 20350
1 cy Attn: NOP 985

Chief of Naval Research
Navy Department
Arlington, VA 22217
1 cy Attn: Code 461 R. Gracen Joiner
1 cy Attn: Code 427 Henry Mullaney

Commander
Naval Electronics Laboratory Center
San Diego, CA 92152
1 cy Attn: Code 2200 Ilan Rothmuller
1 cy Attn: Code 2200 V. E. Hildebrand

Director
Naval Research Lavoratory
Washington, D. C. 20375
1 cy Attn: Code 5464 John Davis
1 cy Attn: Code 7701 Jack Brown
1 cy Attn: Code 7727 Charles Johnson

Commander
Naval Surface Weapons Center
White Oak, Silver Spring, MD 20910
1 cy Attn: Lee Rudlin

Commander
Naval Electronics Systems Command
Navy Department
Washington, D. C. 20360
1 cy Attn: PME 117T John Doncarlos
1 cy Attn: PME 117-21
1 cy Attn: PME 106 CAPT R. T. Darcy
1 cy Attn: PME 108 CAPT G. Heffernan

AF Geophysics Laboratory, AFSC
Hanscom Air Force Base
Bedford, MA 01730
1 cy Attn: OPR James Ulwick
1 cy Attn: LKB William Swider

Air Force Tactical Applications Center
Patrick AFB, Florida 32925
1 cy Attn: TN

Headquarters
Air Foce Systems Command
Andrews AFB
Washington, D. C. 20331
1 cy Attn: SDR

Department of Commerce
Office of Telecommunications
Institute for Telecommunications Science
Boulder, CO 80302
1 cy Attn: William F. Utlant

Lockheed Missiles and Space Company
3251 Hanover Street
Palo Alto, CA 94304
1 cy Attn: J. B. Reagan
1 cy Attn: Martin Walt

General Electric Company
TEMPO-Center for Advanced Studies
816 State Street
Santa Barbara, CA 93102
1 cy Attn: Warren S. Knapp
1 cy Attn: DASIAC

Pacific-Sierra Research Corporation
1456 Cloverfield Boulevard
Santa Monica, CA 90404
1 cy Attn: E. C. Field

The Pennsylvania State University
Ionosphere Research Laboratory
University Park, PA 16802
1 cy Attn: John S. Nisbet
1 cy Attn: Les Hale
2 cy Attn: A. J. Ferraro/H. S. Lee

The Rand Corporation
1700 Main Street
Santa Monica, CA 90406
1 cy Attn: Cullen Crain

Professor Chalmers F. Sechrist
155 Electrical Engineering Building
University of Illinois
Urbana, IL 61801
1 cy Attn: C. Sechrist

Stanford Research Institute
333 Ravenswood Avenue
Menlo Park, CA 94025
1 cy Attn: Allen M. Peterson
1 cy Attn: Ray L. Leadabrand

Mission Research Corporation
735 State Street
P. O. Drawer 719
Santa Barbara, CA 93102
1 cy Attn: Conrad Longmire